A Study of the Novel C5BTBP-PAN Solid Phase Extractant for the Partitioning of Minor Actinides from High Level Waste

J. Sulakova[*], J. John[*], M. J. Hudson[†], M. R. S. Foreman[†]

* Czech Technical University in Prague, Department of Nuclear Chemistry and Centre for Radiochemistry and Radiation Chemistry, Brehova 7, 115 19 Prague 1, Czech Republic
† School of Chemistry, University of Reading, Whiteknights, RG5 4BD Reading, UK

With respect to the management of spent nuclear fuels, several European countries have chosen the closed fuel cycle involving reprocessing. The nuclear wastes produced by the reprocessing contain the fission products and the minor actinides; they are vitrified and supposed to be deposited in deep geological repositories. Selection of the sites for these repositories must consider the fact that these vitrified wastes contain long-lived radionuclides (LLR), essentially belonging to the family of the actinide elements (An), which induce important radiotoxicity for the long-term. The elimination of these LLR, which are mainly minor actinides (MAn), from the vitrified wastes would significantly decrease the long-term radiotoxicity of these wastes and would simplify the selection of geological sites. After separation, the actinides may be either transmuted into short-lived or stable nuclides by nuclear means or conditioned into stable solid matrices[1].

The 6,6'-bis-(5,6-dipentyl-[1,2,4]triazin-3-yl[2,2']bipyridinyl (C5BTBP) extractant, developed and synthesized at the University of Reading, UK has been recently demonstrated to separate efficiently MAn from the reprocessing waste using liquid–liquid extraction. At the same time very high separation factors between MAn and lanthanides can be achieved in one stage.[2]

At the Czech Technical University in Prague, a novel C5BTBP–PAN solid phase extractant (SPE) was prepared. The beads of the C5BTBP–PAN material were composed of the solid powdered C5BTBP extractant (33 % w/w) and a binding matrix of modified polyacrylonitrile (PAN). For the preparation of the C5BTBP–PAN, a modification of the earlier developed procedure[3] was used.

In an introductory study, the dependences of mass distribution ratios D_g on the nitric acid concentration have been determined for europium(III) and americium(III) for the original C5BTBP–PAN material. The D_g values for europium were below the limit of detection (3.5 mL/g) in all the nitric acid concentration range tested whilst for americium, the D_g values did not exceed the value of ~ 30 mL/g (in 3M HNO_3) and, contrary to the data on the C5BTBP behaviour in liquid-liquid extraction[2], further decreased with increasing nitric acid concentration. The high hydrophobicity of the solid C5BTBP extractant and its low solubility are assumed to be the reasons for these unsuccessful results.

Therefore, the next experiments were directed towards conversion of the C5BTBP–PAN material into a material used in standard extraction chromatography by introducing octanol solvent into the system. Alternatively, addition of pure liquid N,N'-dimethyl-N,N'-dibutyl-tetradecylmalonamide (DMDBTDMA) extractant was tested alone or in conjunction with the octanol.

The performance of these wetted materials was then evaluated by comparing the mass distribution ratios D_g for americium(III) at two nitric acid concentrations (0.01 mol/L and 3 mol/L). The results obtained have shown that the most significant improvement of the performance of the original material can be achieved by wetting it with octanol that dissolves a part of the solid C5BTBP extractant and thus converts the material into a standard extraction chromatography system. However, the overall C5BTBP concentration in this material is much higher than could be achieved by impregnating the support with C5BTBP solution.

Since the difference between the performances of the materials with and without DMDBTDMA was not very significant, the simpler two-component C5BTBP[octanol]–PAN system has been selected for the further studies. For this system, the dependences of mass distribution ratios D_g of Eu(III), Am(III), Pu(IV) and U(VI) on nitric acid concentration were determined. The results obtained are presented in Figure 1.

It can be seen that the C5BTBP[octanol]–PAN material offers the possibility of easy separation of americium from europium in the nitric acid concentration range 0.5–3 mol/L, where a Am/Eu separation factor $SF_{Am/Eu} > 100$ was achieved. No deterioration of the properties of this material was observed after 20 hours of contact with 3M HNO_3. The results obtained also show that the tetravalent actinides [Pu(IV)] are co-extracted with the trivalent ones, while the hexavalent ones are rejected.

In further experiments, the kinetics of uptake of americium by C5BTBP[octanol]–PAN material was followed in detail.

The results obtained are very encouraging, the system has been proposed for further more detailed study.

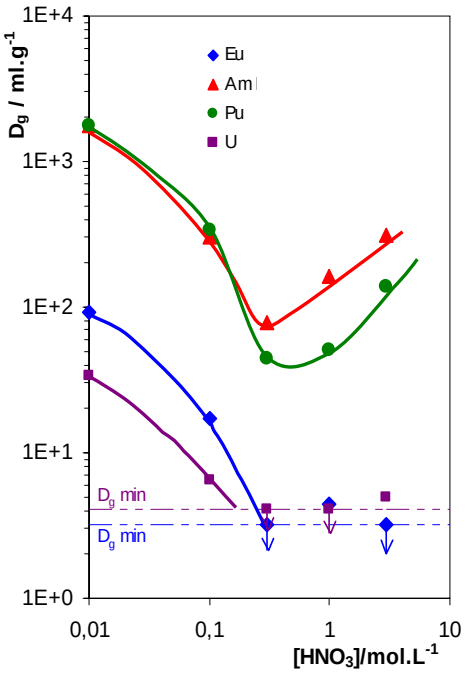

Fig 1: Dependence of mass distribution ratios D_g of Eu(III), Am(III), Pu(IV) and U(VI) on C5BTBP[octanol]–PAN solid extractant on nitric acid concentration.
(V/m = 250 mL/g, 20 hrs of contact)

This research was supported by EC FP6 F16W-CT-2003-508854 project EUROPART and by Czech grant MSM 6840770020. Prof. F. Sebesta is acknowledged for the preparation of the C5BTBP–PAN material.

1 G. R. Choppin, *et al.*, *Chemical Separation in Nuclear Waste Managment. The state of the art and look to the future*. Tallahassee (USA): Florida State University, (2002)

2 M. R. S. Foreman, *et al.*, Solv. Extr. Ion Exch. **23**, (2005)

3 F . Sebesta: Preparation of Granular Forms of Powdered Materials for their Application in Column Packed Beds, In: P. Misaelides, *et al.*, eds.: Natural Microporous Materials in Environmental Technology, Kluwer Academic Publishers, (1999)

Kinetic Model of Actinides and Lanthanides Extraction in None Stationary Conditions

M.A. Afonin, A.A. Kopyrin, A.A. Fomichev

Saint-Petersburg Institute of Technology, 26 Moskovsky av., 190013, Saint-Petersburg, Russia

INTRODUCTION

Separation of similar elements in none steady state conditions are a prospective method to increase elements separation factor. Realisation of the process in non stationary non equilibrium conditions using phenomena of oscillating extraction allows the exploitation of differences in kinetics of ion complexation and extraction rates, using their transport through the boundary area in both directions for elements separation[1]. One of the possible procedures to deviate extraction system from equilibrium is oscillatory changing of the temperature of the extractors. However, the influence of oscillatory temperature changing in the extractor(s) is not described in the literature.

EXPERIMENTAL

The influence of periodical oscillations of the temperature on extraction and stripping processes in the extraction systems is studied. Two extraction system with tri-n-butyl phosphate (TBP) were investigated, №1: 6M $NaNO_3$ – $Nd(NO_3)_3$ – $Pr(NO_3)_3$ – TBP – kerosene and №2: $[Nd(NO_3)_3 \cdot 3TBP]$ – $[Pr(NO_3)_3 \cdot 3TBP]$ – kerosene – 0.1M HNO_3. The setup flow sheet (fig. 1.) is described as following: the emulsion is pumped from thermostatic extractors 16, 17 to centrifugal separators 5, 6 through the turbidimeters 11, 12 by peristaltic pump 10. After separation from the separator 5 the organic phase flows to the extractor 17 and from the separator 6 the organic phase flows to spectrophotometer 8 for analysis and it flows to the extractor 16, passing through both aqueous phases organic phase forms bulk liquid membrane. After spectrophotometers 7, 9 the aqueous phases come back to their corresponding extractors. Data acquisition of pH, red/ox potential of the aqua phase, temperature and emulsion turbidity are performed with frequency above 1 Hz using the DAQ board in computer 18 and specially designed software. Diode-array spectrophotometers are used to obtained spectra every 6-15 seconds. By deconvolution of each spectrum, using specially designed software concentration of several elements can be obtained.

RESULTS AND DISCUSSION

Dependence of rate constants of extraction on temperature according to Arrhenius equation has been included into existing mathematical model of none stationary membrane extraction. The values of activation energy and Arrhenius pre-exponential factor for the rate constants of extraction and stripping reactions of Pr and Nd were calculated from experimental temporal dependencies of metal concentration and temperature by solving reverse kinetics problem using proposed mathematical model and software package. The difference between the activation energy of extraction and the activation energy of stripping of Pr, and Nd from 6 Mol/l $NaNO_3$ by TBP in the temperature range 293-329 K were -25±3 kJ/Mol and -30±3 kJ/Mol respectively. The

rate constants of Pr and Nd extraction and stripping in 6 M $NaNO_3$ and 0.1 M HNO_3 were also calculated.

The series of experiments with influence of periodical oscillations of the temperature on the extraction system for separation of rare earth elements using bulk liquid membrane between two extractors are performed. The mathematical model describes experimental data adequately.

On the basis of the extraction and stripping rate constants and corresponding activation energies the optimization of the extraction process of separation of rare earth elements by liquid membrane under the influence of periodical oscillation of the temperature is carried out. The optimal conditions of separation by liquid membrane were found: frequency and amplitude of thermal oscillations, effective boundary area and liquid membrane flow rate.

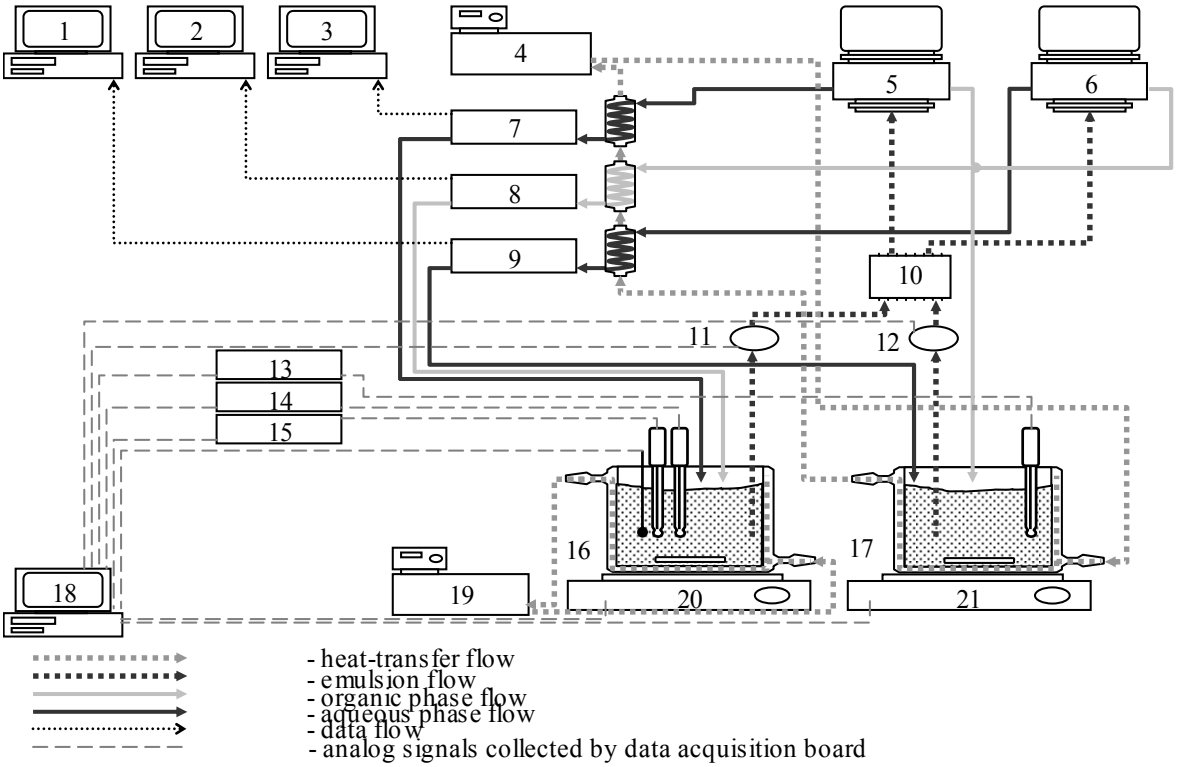

Fig 1: Experimental setup: 1-3, 18 computers; 4, 19 – thermostats; 5, 6 – centrifugal separators EC-33 NIKIMT; 7, 8, 9 – spectrophotometers SF 2000 OKB Spectrum; 10 – peristaltic pump; 11, 12 – turbidimeters; 13 –pH-meter; 14, 15 potentiometers; 16, 17 – extractors; 20, 21 – magnetic stirrers

Acknowledgements. This work was supported by the U.S. Department of Energy, Office of Basic Energy Sciences, under grant RUC2-20011-ST-04 administered by the Civilian Research and Development Foundation..

1 M. A. Afonin, et all, J. of Alloys and Compds, **374**, 426 (2004).

Electrochemical behaviour and dissolution of UC in acidic media.

A. Maslennikov[*], B. Fourest[†], Ph. Moisy[§],V. Sladkov[†], M. Lecomte[§]

[*] A.N. FRUMKIN Institute of Physical Chemistry and Electrochemistry, RAS, Moscow, Russia
[†] Institute of Nuclear Physics, University Paris-XI, F-91406 Orsay Cedex, France
[§] CEA, Research Center VALRHO, BP 17171, 30207 Bagnols-sur-Cèze Cedex, France

AIM OF THE STUDY

Uranium-based carbides cause a renewed interest as possible fuels for the future high temperature gas cooled reactors (HTGR). Since the minor actinides (MA) and most of long-lived fission products (FP) could be incinerated in HTGR, its reprocessing process should be strongly simplified. Certain aqueous flowsheets for the HTGR fuel reprocessing preview the actinides (An) and FP separation already at the step of the fuel dissolution. In order to develop the dissolution process, providing feasible and effective reprocessing, the knowledge of the fundamental redox properties of actinides and fission products carbides in aqueous solutions is essential.

The present work is aimed to study UC electrochemical behavior in 0.1 – 4.0 M $HClO_4$. The boundaries of UC passivation, and transpassivation, as well as charge transfer resistance (R_{ct}), double layer capacitance (C_{DL}) and conditional charge transfer rate constants (k^o_{ct}) and their changes with solution acidity and applied potential were determined.

METHOD AND MAIN RESULTS

UC spherical ingot (Ø = 4 mm) was prepared by arc melting, pressed into a Teflon tip and connected to an EDI101T rotating disk electrode (RDE) assembly (Radiometer). This assembly served as working electrode in a three-electrode system comprising also an Hg/Hg_2Cl_2 reference electrode (SCE) and a Pt wire counter electrode. Cyclic voltammetry (CV), electrochemical impedance spectroscopy (EIS) and multistep potential sweep coulometry (MPSC) were applied while carrying out the study.

CV and MPSC curves in 0.1- 4.0 M $HClO_4$, presented in Fig. 1, give general information about the electrode reactions occurring at the UC electrode. In the interval of potentials from open circuit potential ($E_{i=0}$) to +400 mV/SCE, a slow anodic reaction with a rate increasing with the H^+ concentration is observed. The Nyquist plots associated with this reaction (Fig. 2) represent straight lines with a slope increasing from 0.1 to 0.58 with the increase of H^+ concentrations. The latter observation indicates that in this region of potentials the UC oxidation is diffusion controlled. The slopes of Z_i-Z_r curves, less than 1, show that the diffusion in the double layer is complicated by the surface film formation.

The increase of anodic reaction rate is observed in the range of potentials from 400 to 700 mV/SCE (Fig. 1). This increase is much greater in 1.0 M $HClO_4$, than in 0.1 M $HClO_4$ (Fig. 1), and is practically independent on $HClO_4$ concentration with a further increase to 4.0 M. The Nyquist plots for these potential values (Fig. 2) contain a semi-circular part indicating the increase of charge transfer limitations to the kinetics of the UC oxidation.

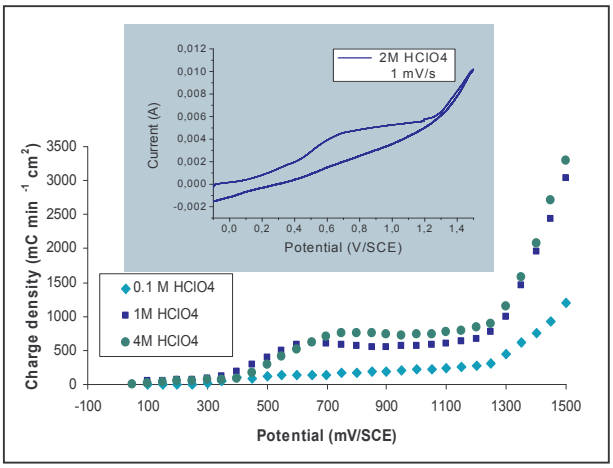

Fig.1: MPSC and LV (inset) curves at a UC sphere electrode (S = 0.145 cm^2) in $HClO_4$ solutions of different concentrations.

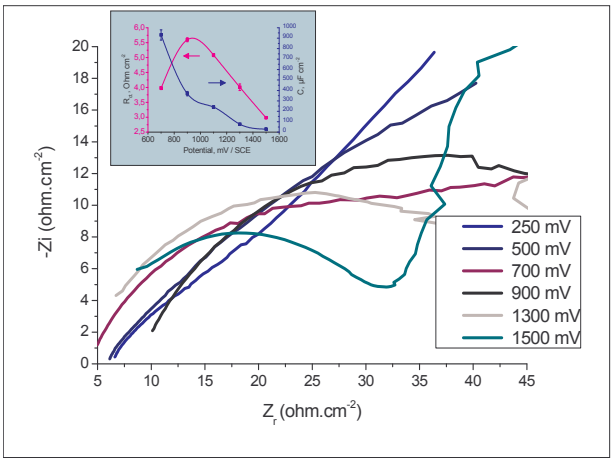

Fig. 2: EIS Nyquist plots of UC sphere electrode (S = 0.145 cm^2) in 2M $HClO_4$ and calculated Rct, CDL values (inset) as a function of the applied potential.

The plateau of the anodic current in the potential range from 700 to 1100 mV/SCE, may be associated with the formation of a pseudopassive film on the UC surface. The oxidation rate in this potential region is limited by the electron transfer (Fig. 2), R_{ct} achieving its maximum at 900 mV/SCE. The formation of the passive film is proved by the decrease of C_{DL} with the increase of the applied potential (Fig. 2, inset).

At potential values exceeding 1100 mV/SCE, the transfer of UC electrode to a transpassive state, characterized by a drastic increase of the anodic current (Fig. 1), is observed. Corresponding Nyquist plots indicate a R_{ct} decrease, while the C_{DL} values decrease only slightly in the range of potentials 1100 - 1500 mV /SCE, indicating no further growth of the passive film thickness.

The k_{ct} values are found to increase from $(2.69 \pm 0.17)\cdot10^2$ to $(1.12 \pm 0.02)\cdot10^4$ s^{-1} with the increase of the UC potential from 700 to 1500 mV/SCE. The fitting of the obtained values with the equation $k_{ct} = k^o_{ct}\cdot\exp[-\alpha nF/RT(E-E^o)$ provides $k^o_{ct} = 7.9 \pm 1.8$ s^{-1} and shows that the electrochemical reaction is strongly irreversible ($\alpha n = 0.119$).

CONCLUSION

LV, MPSC and EIS measurements at the UC electrode in 0.1 – 4.0 M $HClO_4$ demonstrated that UC charge transfer controlled oxidation becomes possible at E > 449 mV/SCE resulting in the formation of a pseudopassive film at the electrode surface. UC is transferred to a transpassive state at the potentials exceeding 1100 mV/SCE. The UC electrochemical dissolution rate in the transpassive region may achieve 50 mg cm^{-2} h^{-1} according to MPSC data.

Spectroelectrochemical Studies of Actinides in Ionic Melts

C. A. Sharrad[*], H. Kinoshita[*], I. May[*], I. B. Polovov[†], J. M. Charnock[§], C. Hennig[‡], A. C. Scheinost[‡] and B. Kralj[#]

*Centre of Radiochemistry Research, School of Chemistry, Oxford Road, Manchester, M13 9PL, U.K.
[†] Department of Rare Metals, Ural State Technical University – 14 Mira Street, UPI, Ekaterinburg, 620002, Russia.
[§] CCLRC Daresbury Laboratory, Daresbury, Warrington, Cheshire, WA4 4AD, U.K.
[‡] Forschungszentrum Rossendorf, Institute of Radiochemistry, P. O. Box 510119, 01314 Dresden, Germany.
[#] Nexia Solutions, B13022, Sellafield, Seascale, Cumbria, CA20 1PG, U.K.

INTRODUCTION

Ionic melt technologies, at both high and room temperature, have been considered for a range of applications in the nuclear industry,[1,2] including the electrolytic separation of uranium from irradiated nuclear fuel and plutonium purification for military applications. Many of these processes are relatively poorly understood from a fundamental chemical viewpoint due to the harsh chemical environment, from the very high melting points of some of the salts used to radiological hazards.

Several groups, including ours, have investigated *in situ* actinide speciation in ionic melts using a variety of spectroscopic techniques including electronic absorption spectroscopy (EAS), Raman spectroscopy and X-ray absorption spectroscopy (XAS).[3-5] Our previous molten salt XAS experiments were performed using chemically generated U species, with measurements made in transmission mode.[5] However, our main interest is the linking of our understanding of actinide speciation in ionic melt systems with electrochemical properties, including the industrially relevant processes of anodic dissolution and cathodic deposition. The air and moisture sensitivity of these systems, and the thermal resistivity required, renders the development of a spectroelectrochemical cell more challenging than for conventional systems.

RESULTS

We wish to report studies into the speciation of uranium in oxidation states III, IV, V and VI in high temperature alkali chloride salts and room temperature ionic liquids using spectroelectrochemical techniques (EAS and XAS). In doing so we have developed a cell-furnace system (Figure 1) to probe electrolytically generated uranium species in high temperature melts. This has allowed us to perform the first *in situ* XAS spectroelectrochemical studies of uranium in high temperature melts. Anodic dissolution of uranium metal and cathodic reduction of U(IV) to U(III) in LiCl-KCl eutectic at 450 ^{o}C were probed using the X-ray absorption near edge structure (XANES) region of the XAS experiments (Figure 2). The U L_{III}-edge position is observed to shift to more negative values as the cathodic reduction of U(IV) to U(III) proceeds but a relatively pure U(III) melt was only obtained by anodic dissolution of uranium metal. Modelling of the extended X-ray absorption fine structure (EXAFS) of the U(III)

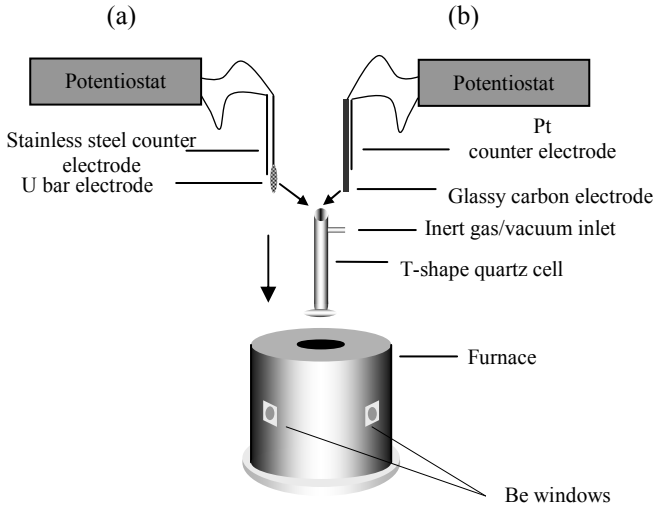

Fig. 1 Schematic diagram of the experimental apparatus used for *in situ* EXAFS spectroelectrochemistry on U species in high temperature melts using (a) anodic dissolution and (b) cathodic reduction processes.

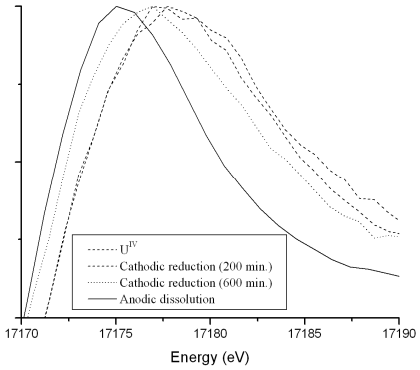

Fig. 2 U L_{III}-edge XAS spectra of uranium cathodic reduction ($U^{IV} \rightarrow U^{III}$) and anodic dissolution (U metal $\rightarrow U^{III}$) in LiCl-KCl at 450 ^{o}C.

spectrum was able to obtain a U-Cl distance of 2.83±0.02 Å, typical for the +III oxidation state, with six chlorine atoms surrounding the uranium atom.

Investigations into $\{UO_2\}^+$ species in the room temperature ionic liquid (RTIL), trimethylbutylammonium bistriflimide ($Me_3BuN^+TFSI^-$), have been conducted through the electrolytic reduction of $UO_2(TFSI)_2$ in the RTIL. EAS indicated the slow disproportionation of $\{UO_2\}^+$ to $\{UO_2\}^{2+}$ and U(IV). XAS studies have been conducted using a specially designed electrochemical cell.[6]

Finally, the first EAS spectroelectrochemical studies of ^{237}Np in high temperature chloride melts have also been undertaken with the cathodic reduction of Np(IV) to Np(III) in LiCl-KCl eutectic (450 ^{o}C) studied.

CONCLUSIONS

The *in situ* speciation of electrochemically generated actinide species in ionic melts has been achieved using EAS and XAS techniques. This can lead to a better understanding of electrolytic methods for actinide separation processes in such media.

We would like to thank Nexia Solutions for financial support, INTAS for a fellowship for I. B. P., and CCLRC and ESRF for the provision of synchrotron radiation facilities.

1 D. G. Lovering, Ed. *Molten Salt Technology*, Plenum, New York, (1982); R. J. Gale and D. G. Lovering, Eds. *Molten Salt Techniques*, Plenum, New York, 1984.

2 V. A. Cocalia, K. E. Gutowski and R. D. Rogers, Coord. Chem. Rev. in press.

3 V. A. Volkovich, A. I. Bhatt, I. May, T. R. Griffiths and R. C. Thied, J. Nucl. Sci. Technol. **Suppl. 3,** 595 (2002); V. A. Volkovich, T. R. Griffiths, D. J. Fray and R. C. Thied, Phys. Chem. Chem. Phys. **2,** 3871 (2000).

4 G. M. Photiadis and G. N. Papatheodorou, J. Chem. Soc., Dalton Trans. 3541(1999).

5 A. I. Bhatt, E. F. Kerdaniel, H. Kinoshita, F. R. Livens, I. May, I. B. Polovov, C. A. Sharrad, V. A. Volkovich, J. M. Charnock and R. G. Lewin, Inorg. Chem. **42,** 2 (2005); V. A. Volkovich, I. May, J. M. Charnock, Rasplavy **2,** 76 (2004).

6 C. Hennig, J. Tutschuku, A. Rossberg, G. Bernhard and A. C. Scheinost, Inorg. Chem. **44,** 6655 (2005).

Effect of Hydrogen on Dissolution of the Spent Fuel Matrix and UO_2 pellets doped with Plutonium : A Threshold Phenomenon?

C. Jégou, B. Muzeau, V. Broudic
Commissariat à l'Énergie Atomique (CEA/Valrhô), DTCD/SECM/LMPA
BP 17171, 30207 Bagnols-sur-Cèze Cedex, France

INTRODUCTION

The option of direct disposal of spent nuclear fuel in a deep geological formation raises the need to investigate the long-term behavior of the UO_2 matrix in aqueous media subjected to $\alpha\beta\gamma$ radiation. Molecular hydrogen, produced as a result of the anoxic corrosion of iron container, appears to be capable of inhibiting oxidizing dissolution of the spent UO_2 fuel matrix due to water radiolysis in a α and/or $\beta\gamma$ radiation field[1], although the mechanisms behind this phenomenon have not been clearly identified. The effect of molecular hydrogen on radiolytic decomposition of pure water subjected to a mixed radiation field combining high-LET charged α particles and low-LET $\beta\gamma$ radiation has nevertheless been investigated in relation with radiolysis problems in nuclear reactor primary systems[2]. This work has demonstrated that molecular hydrogen was capable of reducing the concentration of oxidizing species in the medium through a radical chain reaction. This chain reaction occurs in the presence of hydrogen with a sufficient radical concentration, which requires low-LET radiation and assumes that the molecular species such as O_2 and H_2O_2 likely to stop the chain reaction are not in excess, i.e. when the high-LET radiation is not too intense. The competition between these phenomena results in a threshold effect above which water decomposition is observed. The objective of this study is to determine to what extent the spent fuel UO_2/water interface inherently subjected to a mixed $\alpha\beta\gamma$ radiation field reacts according to similar mechanisms in the presence of hydrogen, and whether a threshold effect may be applicable.

EXPERIMENTAL PROCEDURE

An aqueous solution initially containing 8×10^{-5} mol/L hydrogen (Ar + 4% H_2 at 2.5 bars, with no hydrogen renewal during the experiment) was irradiated for 14 days by a 260 Ci cobalt (^{60}Co) source. The γ dose rate in the homogeneous solution determined by Fricke dosimetry was 650 Gy/h. Various materials containing UO_2 were placed in the experimental reactor to vary the intensity of the α radiation field at the UO_2/water reaction interface. The H_2O_2 concentration in the homogeneous solution was determined by chemiluminescence[3] after 14 days of irradiation. The materials used consisted of spent fuel fragments (UO_2 with a burnup of 60 GWd/t_{HM}), UO_2 pellets doped with different ^{238}Pu concentrations to vary the alpha radiation intensity at the reaction interface, and Simfuel pellets (6 at%)[4]. The Simfuel did not supply a significant self-irradiation field but—with some reservations—its chemistry was comparable to that of the spent fuel. The alpha irradiation fields corresponding to these materials are summarized in Table I.

EXPERIMENTAL RESULTS AND DISCUSSION

Two H_2O_2 concentrations were determined experimentally in the homogeneous solution depending on the materials used (Table I). For the materials having the most intense alpha irradiation fields a concentration of $2 (\pm 0.2) \times 10^{-7}$ mol/L was measured after 14 days, compared with

$3 (\pm 0.5) \times 10^{-8}$ mol/L for the materials with the lowest alpha irradiation fields. The Chemsimul kinetic code[5] was used for radiolysis calculations to assess the H_2O_2 concentrations in the homogeneous solution irradiated by a 650 Gy/h cobalt source versus the initial hydrogen concentration. The calculations revealed a threshold (Fig. 1) depending on the hydrogen concentration. Based on these calculations, initially adding 8×10^{-5} mol/L of hydrogen to the homogeneous solution should result in the onset of steady-state conditions near 3×10^{-8} mol/L (Fig. 1) in the homogeneous solution for all experiments. This calculated concentration is in full agreement with the experimental results for the materials with the lowest alpha irradiation field. For the materials with an intense alpha irradiation field, an experimental value of 2×10^{-7} mol/L was obtained. This value is consistent with the calculated value obtained in absence of a substantial effect of hydrogen on the production of oxidants (i.e. low hydrogen concentrations). The results clearly show that in a high-intensity alpha irradiation field at the UO_2/water interface the initial hydrogen concentration in comparison with the molecular species formed under alpha radiation is probably not sufficient to sustain the chain reaction .

Table I. Alpha dose rate at the reaction interface for the test materials and H_2O_2 concentrations in the homogeneous solution

Material	α dose rate (Gy/h)	$[H_2O_2]$ (mol/L)
Spent fuel	1600	$2 (\pm 0.2) \times 10^{-7}$ mol/L
^{238}Pu-doped UO_2	1100	$2 (\pm 0.5) \times 10^{-7}$ mol/L
^{238}Pu-doped UO_2	110	$3 (\pm 0.5) \times 10^{-8}$ mol/L
Simfuel	< 0.01	$3 (\pm 0.5) \times 10^{-8}$ mol/L

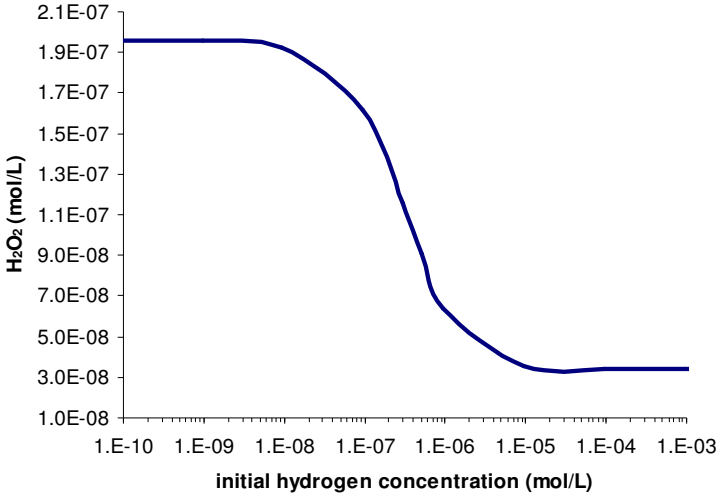

Fig. 1. Model of H_2O_2 concentration in the homogeneous solution versus the initial hydrogen concentration (650 Gy/h for 14 days)

1 K. Spahiu, L. Werme, U-B. Eklund, The influence of near field hydrogen on actinide solubilities and spent fuel leaching, *Radiochim. Acta* 88 (2000) 507-511.

2 B. Pastina, Ph.D Thesis, Université Paris-Sud, Paris, France, 1997; no. 4862.

3 V. Broudic, B. Muzeau, C. Jégou, M. Bonnal, A. Gavazzi, C. Marques, Application of chemiluminescence to the study of alpha, beta and gamma radiolysis of water. *Atalante 2004* international conference, June 21-24, 2004: Nîmes, France. P2-11.

4 P.G. Lucuta, R.A. Verrall, Hj. Matzke and B.J. Palmer. *Journal of Nuclear Materials* 178 (1991) 48-60.

5 P. Kirkegaard and E. Bjergbakke, *CHEMSIMUL, A program package for numerical simulation of chemical reaction systems*. November 20, 1998. Riso National Laboratory DK-4000 Roskilde Denmark (1998).

Engineering-Scale Distillation of Cadmium for Actinide Recovery

B.R. Westphal, J.C. Price, and D. Vaden

Idaho National Laboratory, Idaho Falls ID 83415 USA

BACKGROUND

The electrometallurgical treatment of Experimental Breeder Reactor-II (EBR-II) spent nuclear fuel at the Idaho National Laboratory (INL) comprises a set of operations designed to recover actinides from radioactive fission products and place the fission products into acceptable waste forms [1]. A glass-bonded ceramic waste form and a stainless steel-based metallic waste form are the two types of high-level waste forms being qualified for disposal in a geological repository [2]. Two actinide products are recovered during the spent fuel treatment process; a primarily uranium product and a plutonium-uranium product. The low enriched uranium products recovered from spent fuel treatment are currently being stored pending a decision by the Department of Energy on final disposition. To date, several plutonium-uranium products have been produced and are the subject of this paper.

Treatment of the EBR-II spent fuel is performed in the Fuel Conditioning Facility (FCF), a shielded hot-cell environment located at the Materials and Fuels Complex of the INL. The treatment program was initiated in June 1996 and continues presently on the balance of the spent fuel. Batch operations on the spent fuel include a chopping step, electrorefining, cathode processing, and casting. The electrorefiner and cathode processor are the primary recovery steps for the actinide products. During electrorefining, fuel is anodically dissolved in a LiCl-KCl eutectic salt such that the transport of actinides as cathode material is feasible. In addition to the LiCl-KCl, other chloride species are present in the electrorefiner salt due to the oxidation of fission products, bond sodium, and actinides present in the spent fuel. Once transported, uranium cathode products are collected and further processed by a vacuum distillation operation for the removal of the adhering salts. The plutonium-uranium products are produced by utilizing a liquid cadmium cathode for electrorefining and then removing the cadmium by distillation. Both distillation operations are performed in the same piece of equipment, the cathode processor, to produce consolidated actinide ingots.

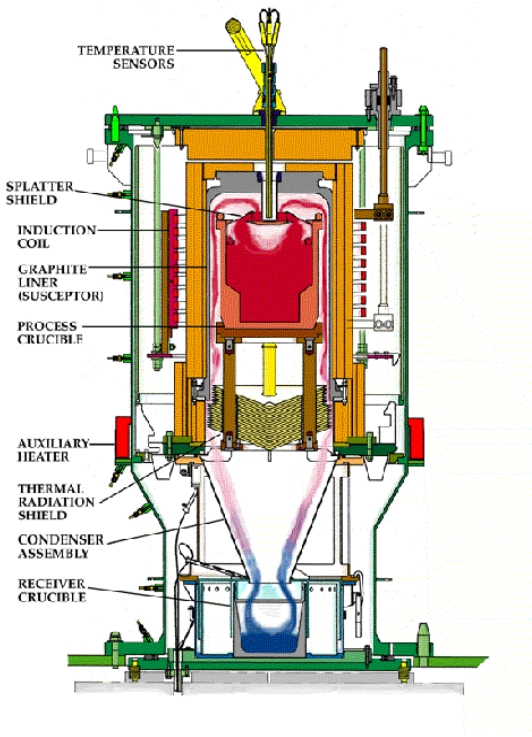

Fig 1. Schematic of Cathode Processor

EXPERIMENTAL

The cathode processor (Fig. 1) is an induction-heated furnace capable of temperatures to 1400^{o}C and

pressures less than 0.1 Torr. The furnace region contains a passively cooled induction coil and a graphite furnace liner that acts as the susceptor to heat the process materials. Separation of the chloride salts and cadmium from the actinide products in the cathode processor is accomplished by reducing the internal pressure to approximately 1 Torr and heating to at least 1200°C to consolidate the actinide products. A more detailed description of the cathode processor and its general operation is given elsewhere [3].

Of the four experiments performed at the cathode processor for cadmium distillation, three have been with plutonium-uranium products from the electrorefiner. The first test in the cathode processor utilized surrogate materials to confirm operating parameters developed during qualification testing. For cadmium distillation, the process conditions consist of evacuating the cathode processor vessel to 1 Torr, isolation of the vacuum system from the vessel to prevent the migration of cadmium vapor, heating to 700°C at 8 kW, and then heating to a maximum temperature of 1200°C at 15 kW. The reduced power level controls the rate of cadmium distillation initially while the 700°C temperature is considered high enough to achieve thermal decomposition of any plutonium-cadmium compounds. The overall run time (from induction power start to finish) for the four cadmium distillation experiments averaged less than nine hours per run. The three consolidated plutonium-uranium ingots are then processed in the casting furnace where samples are taken for chemical analyses. Due to facility safeguard issues, dilution with depleted uranium is necessary for the plutonium-uranium products. Additionally, the actinide product ingots are returned to the electrorefiner salt to enable continued testing.

RESULTS

For the four cadmium experiments performed in the cathode processor, at least 25 kg of cadmium was distilled and greater than 99 wt.% was recovered for reuse. An average cadmium distillation rate of 0.41 g/min/cm^2 was determined which compares favorably with previous investigators. The final plutonium-uranium products for three experiments contained levels of cadmium below the detection limits of analytical chemistry; typically 50 ppm. Similar to cadmium, negligible amounts of rare earth impurities were detected in the samples taken following casting. Additional sampling was performed following cathode processing on the cadmium and process waste streams and their analyses will also be reported. In conclusion, a successful separation of cadmium from actinide products was achieved at the engineering-scale to support further research efforts in actinide recovery.

The authors would like to acknowledge the cathode processor designers, FCF operations support, and analytical laboratory personnel for their contributions to the testing program. Work supported by the U.S. Department of Energy, Office of Nuclear Energy, Science, and Technology, under DOE-NE Idaho Operations Office Contract DE-AC07-05ID14517.

1 K.M. Goff, K.L. Howden, G.M. Teske, and T.A. Johnson, "Pyrochemical Treatment of Spent Nuclear Fuel", Proc. Global 2005, (Tsukuba, Japan: AESJ, 2005).

2 K. Marsden et al., "Process and Equipment Qualification of the Ceramic and Metal Waste Forms for Spent Fuel Treatment", Proc. Global 2005, (Tsukuba, Japan: AESJ, 2005).

3 A.R. Brunsvold, P.D. Roach, and B.R. Westphal, "Design and Development of a Cathode Processor for Electrometallurgical Treatment of Spent Nuclear Fuel," Proc. Eighth Int. Conf. Nucl. Eng. (ICONE), (New York, NY: ASME, 2000).

The LLNL Heavy Element Facility -- Facility Management, Authorization Basis, and Readiness Assessment Lessons Learned in the Heavy Element Facility (B251) Transition from Category 2 Nuclear Facility to Radiological Facility

Mark Mitchell*, Brian Anderson, Erik Brown, Leonard Gray
*Lawrence Livermore National Laboratory, Livermore CA 94552 USA
UCRL-ABS-218323

This presentation discusses Facility Management, Readiness Assessment, and Authorization Basis experience gained during the Risk Reduction Program (RRP). These lessons can help facilitate similar activities at other sites, including facilities restarting operations or new facilities starting new operations. The RRP successfully downgraded the Heavy Element Facility (B251) from a Category II Nuclear Facility to a Radiological Facility. Leading up to this major achievement were significant safety accomplishments, completing objectives on time and on budget, achieving the November 2003 Milestone for reducing Inventory to 20% of the initial inventory, and reducing Inventory to < 0.03 ^{241}Am-equivalent curies by the April 2005 Milestone.

B251 was constructed at LLNL to provide research areas for conducting experiments in radiochemistry using transuranic elements. B251 capabilities once included the preparation of tracer sets associated with the underground testing of nuclear devices and basic research devoted to a better understanding of the chemical and nuclear behavior of the transuranic elements. Facility safety and experimental systems were deteriorating with age, even with preventative maintenance. A variation of seismic standards were used in a design that encompassed eight building increments constructed over a period of 26 years. The RRP was created to mitigate the risk of dispersal of radioactive material during an earthquake by removing the radioactive materials inventory and glove box contamination. The cost to bring the facility into compliance with the current requirements was quite high, and simply maintaining B251 as a Category 2 nuclear facility posed serious cost considerations under a changing regulatory environment. LLNL adopted the goal of reaching Radiological Facility status.

To support the RRP, B251 transitioned from a standby to fully operational, Category 2 Nuclear Facility, compliant with current regulations. A work control process was developed, Authorization Basis Documents were created, work plans were written, off-normal drills practiced, a large number of USQ reviews were conducted, and a type II Readiness Assessment (RA) was conducted to start up operations. Subsequent RA's focused on specific operations. Finally, a four-step process was followed to reach Radiological Status: 1) Inventory Reduction and D&D activities reduced the inventory and radiological contamination of the facility below the Category 3 threshold (DOE-STD-1027), 2) Radiological Safety Basis Document (SBD aka HAR) was approved by NNSA, 3) the inventory control system was in place, and 4) verification by NNSA of radiological status was completed.

Key to this success is the RRP philosophy in a schedule driven paradigm.

- *"Expect the unexpected and confirm the expected"*
- Recognize when you reach the point of diminishing returns,
- Develop robust processes that anticipate and can handle surprises,
- Plan, plan, and re-plan *"Measure twice, cut once"*

This presentation will discuss:

- History of the Heavy Element Facility, B251
- Risk Reduction Program
  - Objectives
  - Accomplishments
- Lessons Learned
  - Transitioning from Standby to Operating Facility
  - Robust processes that "*Expect the Unexpected*"
  - Authorization Basis Strategies
  - Facility Infrastructure Strategies
  - Readiness Assessment (RA) Strategies
  - Operational Strategies
- Conclusions

Staff from multiple organizations played significant roles in downgrading B251 from Nuclear Category 2 to Radiological

Impressive safety accomplishment
No one had decontaminated facilities with this level and variety of high specific activity isotopes (e.g. ^{244}Cm, ^{238}Pu)
Dramatic cost savings, $250 million under current regulations

Reference: Mark Mitchell et al, *The LLNL Heavy Element Facility -- Facility Management and Authorization Basis Lessons Learned in D&D Environment: Transition from Category II Nuclear Facility to Radiological Facility*, UCRL-PRES-213765, Proceedings of the 2005 Tri-Lab Conference, Monterey, CA, September 2005.

Photochemical Oxidation of Oxalate, Urea, and Hydroxylammonium in Pu-238 Process Streams

K. Long, D. Ford, G. Jarvinen

Los Alamos National Laboratory, Los Alamos NM 87544 USA

For over forty years, NASA has relied on plutonium-238 in Radioisotope Thermoelectric Generator (RTG) units and Radioisotope Heater Units (RHUs) to provide power and heat for many space missions including Transit, Pioneer, Viking, Voyager, Galileo, Ulysses and Cassini. RHUs provide heat to keep key components warm in extremely cold environments found on planets, moons, or in deep space. RTGs convert heat generated from the radioactive decay of plutonium-238 into electricity using a thermocouple. Plutonium-238 has proven to be an excellent heat source for deep space missions because of its high thermal power density, useful lifetime, minimal shielding requirements, and oxide stability.

At Los Alamos, a plutonium-238 scrap recovery system has been built at Technical Area 55 (TA-55) and will be operational in the near future. This glovebox facility will purify Pu-238 from scrap material and residues from past production operations to provide RTGs and RHUs for additional NASA missions. The scrap material is balled-milled to give a mean particle size < 5 microns and then dissolved in a mixture of nitric acid and hydrofluoric acid. The plutonium solution is purified using an ion exchange column, if necessary, or it is sent directly to oxalate precipitation. During the oxalate precipitation step, urea is added to scavenge nitrite, hydroxylamine nitrate is added to adjust the valence of plutonium to Pu(III), and oxalic acid is added to precipitate plutonium as $Pu_2(C_2O_4)_3$. The plutonium oxalate is isolated and calcined in a gas stream containing oxygen-16 enriched water vapor to produce the PuO_2 used in the RTGs and RHUs. The filtrate after oxalate precipitation still contains a significant amount of Pu-238, most of which is precipitated by addition of sodium hydroxide to give a pH of 10-13. An ultrafiltration process with water-soluble chelating polymers is used to selectively bind with most of the remaining plutonium in the solution, reducing the alpha radioactivity to meet regulatory

discard limits. The hydroxide precipitation and the polymer filtration process are both more efficient at removing plutonium if the oxalate is not present to compete with hydroxide or the water-soluble polymer for the plutonium. We are investigating using UV irradiation to oxidize the oxalate (along with urea and hydroxylamine nitrate) before the hydroxide precipitation or ultrafiltration operations.

Surrogate solutions comprised of oxalic acid, urea, and hydroxylamine nitrate in a nitric acid have been used for experimentation. The test solutions were placed in a glass reactor containing a water-cooled quartz immersion well. A 1200-watt or 2000-watt mercury vapor lamp was used to irradiate the solution and compressed air or argon was used to continuously sparge the solution. The oxidation rates of oxalic acid and urea were measured throughout each irradiation period by monitoring the total organic carbon content of the solutions. The concentrations of oxalate, hydroxylammonium, ammonium, and nitrate were monitored by ion chromatography. A number of variables, including concentrations of oxalic acid, urea and hydroxylamine, type of sparge gas, and additions of iron as an oxidation catalyst were studied to help optimize the processing conditions. Figure 1 gives an example of the time dependence of the concentration of the solution constituents during irradiation. An overview of the irradiation test results to date will be presented.

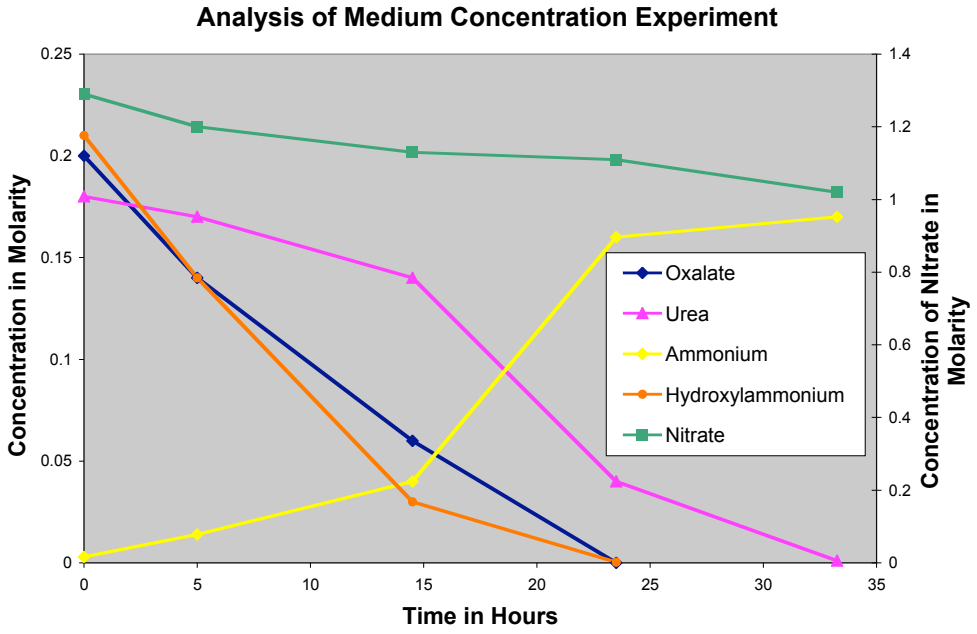

Figure 1. Time dependence of the concentration of solution constituents during irradiation.

Diffusion Behavior of Actinide and Lanthanide Elements in Molten Salt for Reductive Extraction

D Yamada[1], T. Murai[1], K. Moritani[1], T. Sasaki[1], I. Takagi[1], H. Moriyama[1], K. Kinoshita[2], H, Yamana[3]

[1] Department of Nuclear Engineering, Kyoto University, Yoshida, Sakyo-ku, Kyoto 606-8501
[2] Central Research Institute of Electric Power Industry, Tokyo 201-8511
[3] Research Reactor Institute, Kyoto University, Kumatori, Osaka 590-0494

INTORODUCTION

In recent years, there has been a renewed interest for new nuclear fuel cycles or new nuclear waste management strategies, especially for efficient transmutation of long-lived radionuclides in order to minimize the radiological toxicity of nuclear wastes. Reductive extraction process, which has been developed for reprocessing molten salt reactor fuels, is expected to be more useful for separation and recovery of transuranic elements. Up to date extensive studies have been performed concerning the thermodynamics of reductive extraction.[1,2] However little is still known about the kinetics. For the development of reductive extraction process the rate of extraction of actinide and lanthanide elements in a two-phase system of molten LiCl-KCl eutectic salt and liquid cadmium was measured at 723-873K in our previous study.[3] The mass transfer coefficients were found to be as high as expected. In some cases, however, it was found that the rate of reductive extraction was possibly affected by the solubility limits of the solute elements in the metal phase.

For comparison, in the present study, the diffusion coefficients of actinide and lanthanide elements were measured as a function of temperature in LiCl-KCl for reductive extraction. By combining the present results with the previous ones on the rate of extraction, the extraction mechanism and the system performance will be discussed for further development of the extraction system.

EXPERIMENTAL

Diffusion coefficients were measured by a capillary method.[4] All the chemicals were of reagent grade obtained from Nacalai Tesque, Inc., and the radioactive tracers were produced by neutron irradiation of metal specimens. All experiments used high-purity reagents and were performed in a glove box under argon atmosphere containing <0.5ppm of O_2 and <0.2ppm of H_2O.

In the measurement, a quartz capillary tube of an i.d. of 0.2 or 0.3mm and a length of about 50mm sealed from one end was used. The open end of the evacuated capillary was immersed into molten LiCl-KCl containing the radioactive tracers in order to allow the liquid to rise up. The capillary filled with the LiCl-KCl was then immersed into a pure LiCl-KCl. The temperature of the system was controlled within ±0.5K. After a known diffusion time, the capillary was removed, allowed to cool, and cut into several sections. The concentration profile of each

radioactive tracer was determined by a direct γ-ray spectrometry. No significant differences were observed for the capillaries of 0.2 and 0.3mm, and it was concluded that thermal convection was not important source of uncertainty.

RESULTS

In Fig. 1, the diffusion coefficients of solute elements in LiCl-KCl are plotted as a function of inverse temperature and compared with literature values for La[5] and U[6]. Similar temperature dependences are found for all the elements, although some differences are observed possibly due to the different interactions of solute elements with the solvent and due to different sizes of the diffusing species. The obtained results are discussed for the kinetics of reductive extraction process.

1 T. Inoue, M. Sakata, H. Miyasiro, A. Sasahara and T. Matsumura, *J. Nucl. Technol.* **93** (1991) 206.
2 K. Kinoshita, T. Inoue, S. P. Fusselman, D. L. Grimmett, J. J. Roy, R. L. Gay, C. L. Krueger, C. R. Nabelek and T. S. Storvick, *J. Nucl. Sci. Technol.* **36** (1999) 189.
3 H. Moriyama, D. Yamada, K. Moritani, T. Sasaki, I. Takagi, K. Kinoshita, and H. Yamana, *J. Alloys and Compounds* **408-412** (2006) 1003.
4 H. Moriyama, K. Moritani and Y. Ito, *J. Chem. Eng. Data* **39** (1994) 147.
5 M. V. Smirnov, Yu. N. Krasnov, V. E. Komarov and V. N. Alekseev, *Electrochem. Molten Solid Electrolytes*, **6**, 47, (1968).
6 S. A. Kuznetsov, H. Hayashi, K. Minato and M. Gaune-Escard, *J. Nucl. Mater.* 344 (2005) 169.

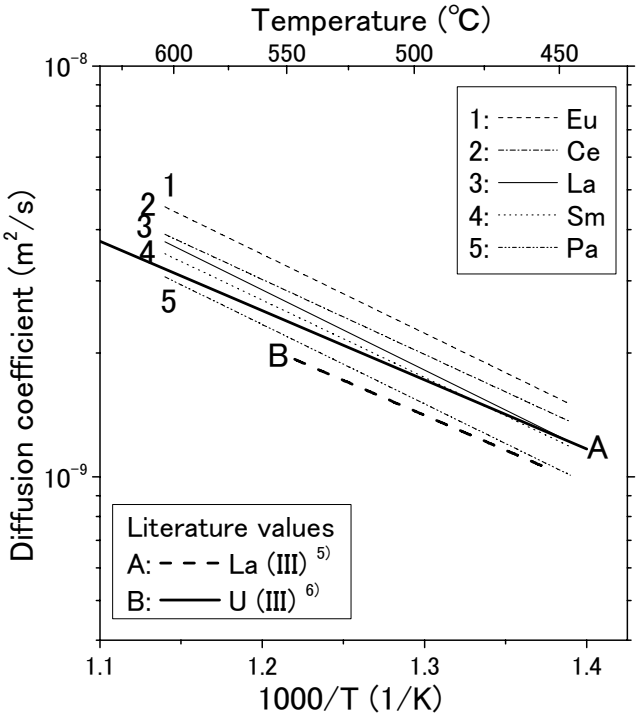

Fig. 1. Diffusion coefficients of actinide and lanthanide Elements in LiCl-KCl.

Plutonium and americium ceramic matrices: Structure and resistance to self-irradiation damage

R. Belin[*], J. Cambedouzou[*], D. Bregiroux[*†], P. Valenza[*] and F. Audubert[*].

* Commissariat à l'Energie Atomique - CEA Cadarache - DEN/DEC/SPUA - 13108 Saint-Paul-lez-Durance, FRANCE
† Laboratoire Science des Procédés Céramiques et de Traitements de Surface - UMR 6638 - 123 avenue Albert Thomas - 87060 Limoges, FRANCE

INTRODUCTION

Management of minor actinides (MAs) is one of the main concerns of the nuclear industry. The proposed strategies have to take into account large volumes, strong activities and political issues. Both once-through transmutation and direct long-term storage are viable options. In any case, matrices have to handle long-term containment. It is well known that a potential alpha-decay induced amorphization of the material causes an increase of several orders of magnitude of lixiviation. Thus, a better understanding of resistance to self-irradiation damage is of major importance. In that prospect, we have performed comparative studies on pyrochlores and monazites ceramic oxides, respectively prominent candidates for once-through transmutation and long-term immobilization. Plutonium and americium compounds were synthesized, their structures characterized by XRD and compared. Finally, the evolution of the americium compounds under the effect of self-irradiation was followed and discussed.

SYNTHESIS AND XRD CHARACTERIZATION

All compounds were prepared on the scale of a few milligrams and AmO_2 was handled in a special glove-box equipped with biological protections. $Pu_2Zr_2O_7$ and $Am_2Zr_2O_7$ pyrochlores were prepared starting from polycrystalline PuO_2 or AmO_2 and ZrO_2. Both compounds were ground/mixed with the appropriate ratios and fired in a Mo crucible under a reducing atmosphere (Ar/5% H_2) at 1673 K for 55 hours, the process repeated twice. The following monazites were prepared: $PuPO_4$, $(Pu^{+3}Pu^{+4})_{1-x}Ca_xPO_4$ and $AmPO_4$. These samples are not representative of the considered material for storage as, based upon observations on mineral monazite [1], the actinide incorporation ratio will not exceed 10wt%. Nevertheless, pure actinide monazites allow a plain comparison with the pyrochlores. The compounds were made by solid-state reaction between PuO_2 or AmO_2 and $NH_4H_2PO_4$ (and CaO for $PuCaPO_4$) at 1400°C for 2 hours and the entire process repeated. Both plutonium monazites were synthesized under air and argon, whereas $AmPO_4$ synthesis was only carried out under argon. X-ray samples were prepared according to a procedure previously described [2]. The pyrochlore structure was investigated in detail by the Rietveld method, which allowed us to refine the 48f oxygen position. This parameter is critical for the structural stability of the compound. Regarding monazites, the effect of the atmosphere and the incorporation of tetravalent plutonium in the structure were studied.

RESISTANCE TO SELF-IRRADIATION DAMAGE

The effects of alpha irradiation on the structure were followed as a function of time for $Am_2Zr_2O_7$ and $AmPO_4$. It was found that the pyrochlore structure progressively disappeared to the benefit of a fluorite-type solid solution in correlation with the alpha dose-rate, as shown by the fading of superstructure peaks marked by * (see Fig. 1). The stability of the pyrochlore phase versus the fluorite phase has been examined. Interestingly, the compound shows a significant resistance to radiation damage as no amorphization is observed even after 400 days ($2.13x10^{25}$ α-decay/m^3).

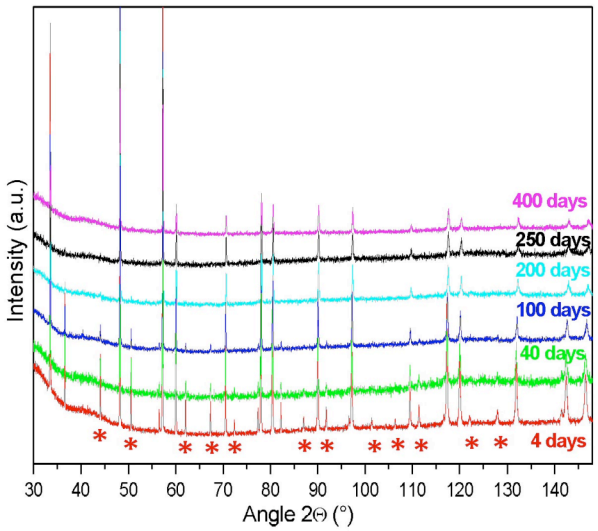

Fig.1: Evolution of X-ray patterns for $Am_2Zr_2O_7$ as a function of time.

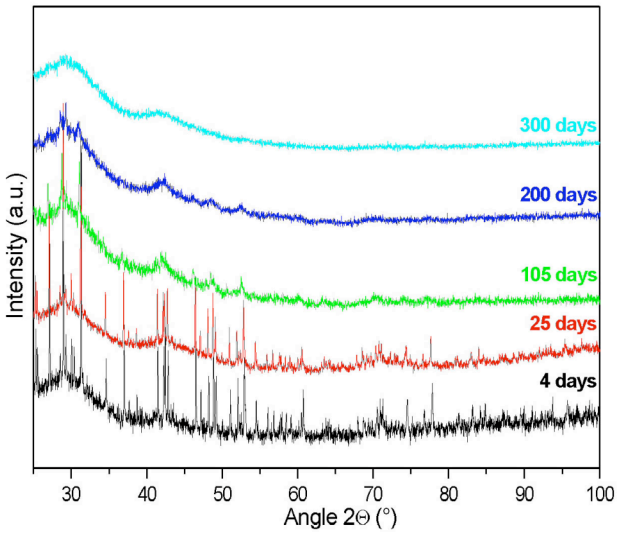

Fig.2: Evolution of X-ray patterns for $AmPO_4$ as a function of time.

On a reverse fashion, $AmPO_4$ shows a complete amorphization after 300 days and a dose of $1.65x10^{25}$ α-decay/m^3 as no more diffraction peak is observed (see Fig. 2). This result is in agreement with Burakov who found that ^{238}Pu doped $PuPO_4$ turns amorphous for an equivalent dose [3]. Resistance to amorphization can be seen as the structure's ability to regain the initial crystalline state following the damage. Bonds ionicity - the competition between the short-range covalent and long-range ionic forces - is considered as an important factor to understand this behavior [4,5].

In the presentation we shall give a precise description of $Am_2Zr_2O_7$ and $AmPO_4$ structures and, by comparing their electronic density maps, discuss how the type of interatomic forces involved is relevant for resistance to amorphization.

1 L. A. Boatner and B. C. Sales, Monazite. In Radioactive Waste Forms for the future (ed. W. Lutze and R.C. Ewing), 495-564. Elsevier (1988)

2 R. C. Belin *et al.*, J. Appl. Cryst. 37, 1034-1037 (2004)

3 B.E. Burakov *et al.*, Mater. Res. Soc. Symp. Proc. 824, 219-224 (2004)

4 K. Trachenko, J. Phys.: Condens. Matter 16, R1491-R1515 (2004)

5 H. M. Naguib and R. Kelly, Radiat. Eff. 25, 1-12 (1975)

Leaching of Plutonium and Americium from Perovskite-Based Ceramics

Merkushkin[*], A.O., Ochkin[*], A.V., Rovniy[+], S.I., Bobylev[+], A.I. Stefanovsky[*+], S.V.
*University of Chemical Technology, Miusskaya sq,9, Moscow 125047 RUSSIA
[+]FSUE PA "Mayak", Lenin st., 31, Ozersk, Chalyabinsk reg. 456780 RUSSIA
*[+] SIA Radon, 7th Rostovskii lane 2/14, Moscow 119121 RUSSIA

Introduction

Perovskite, ideally $CaTiO_3$, is orthorhombic structure phase (space group P_{nma}) capable to form continuous solid solutions with lanthanide aluminates, $LnAlO_3$ and ferrites $LnFeO_3$.[1] General formula of such modified perovskites is $M^IM^{II}O_3$, where M^I and M^{II} are eight- and six-coordinated cations with ionic radii about 0.10 nm and 0.06 nm, respectively. Thus, the perovskite structure compounds are promising host phases for trivalent rare earths, actinides, such as Am and Cm, and iron group elements (corrosion products) of high level waste (HLW) as well as gallium. In our previous works we have demonstrated low leachability of trivalent actinides and lanthanides from perovskite ceramics.[2-4] On the next stage of the work we studied leaching of Pu, Am and Cm from the perovskite-based ceramics doped with actual actinide-bearing HLW. Some preliminary data were published in ref.[3]

Experimental

Two oxide mixtures with specified formulations 0.2 $La_2O_3 \cdot Al_2O_3$ and 0.4 $La_2O_3 \cdot Fe_2O_3$ were milled, mechanically activated and homogenized in a planetary mill. The precursors obtained were soaked with radioactive solution containing Pu, Am, Cm, and Pm, dried at 150 ^{0}C, and calcined at 750 ^{0}C for 30 min. The batches were compacted in pellets ~7 mm in diameter and ~5 mm in height under a pressure of 300 MPa, heat treated in a resistive furnace in an Ar atmosphere to either 1300 ^{0}C (ferrite ceramic) or 1400 ^{0}C (aluminate ceramic) kept at this temperature for 5 hours followed by cooling to a room temperature in turned-off furnace. Total Pu, Am, and Cm concentrations in the pellets were 13, 0.336, and 0.002 mg/g, respectively.

The ceramics were examined by X-ray diffraction. Open porisity and relative density were measured using standard procedures. Specific surface area was measured using a BET method. Leach measurements were performed using a MCC-5 Soxhlet test[5] for 10 days at a temperature close to 100 ^{0}C (boiling water). Activities of individual radionuclides were measured by α-, β-, and γ-spectrometry. Leach rates of radionuclides were calculated by eq. (1)[6]: $w = (A \times m) / (A_0 \times S \times t)$ (1), where w - leach rate, g/(cm^2× day), A - activity of the radionuclide in leachate, s^{-1}, t – leaching time, days, A_0 – initial activity of the radionuclide in the sample, s, S – surface area, cm^2, m – sample mass, g. The data obtained were treated using an eq. (2): $w = a_1 \times exp(-b \times t) + a_2$ (2), where a_1 is a leach rate of radionuclide from relatively highly soluble minor phases, a_2 is "equilibrium" leach rate from the major host phase, and b is constant depended on test conditions.

Results

As follows from XRD data the aluminate ceramic is composed of major perovskite type phase (ideally $LaAlO_3$) and minor β-alumina (ideally $LaAl_{11}O_{18}$). The ferrite ceramic consists of predominant perovskite structure phase (ideally $LaFeO_3$) and minor partially reacted hematite ($Fe_{1-x}La_xO_3$). These data are consistent well with the data obtained for samples containing HLW surrogate.[3,4] The open porosity, theoretical and relative density values for the ceramics 0.2 $La_2O_3 \cdot Al_2O_3$ were found to be 28%, 4.75 g/cm^3, and 75% of theoretical value, respectively. The same values for the 0.4 $La_2O_3 \cdot Fe_2O_3$ ceramic were 0.3%, 6.10 g/cm^3, and 85% of theoretical value, respectively. Thus aluminate ceramic is much more porous than the ferrite one. As a result at similar geometric surface areas (14.06 and 10.44 cm^2) their actual surface areas measured by

BET-method are strongly different (~28100 and <1000 cm^2).

Leach rates (a_2) of individual radionuclides from the monolithic ceramic samples are given in Table. For the aluminate ceramic leach rates calculated using geometric surface area are higher than those measured by the BET-method by on average a factor of 2000 because leaching takes place from both outer surface of the sample and inner surface of its open pores. Pu and Am leach rates from the aluminate ceramic with surface area measured by the BET-method were found to be almost the same as those from the aluminate ceramic doped with trace amounts of radionuclides.[3]

Table. Leach rates of radionuclides, in g/(cm^2×day), from monolithic ceramic samples.

Radionuclide	0.2 $La_2O_3 \cdot Al_2O_3$		0.4 $La_2O_3 \cdot Fe_2O_3$
	S_{geom} = 14.06 cm^2	S_{BET} = 28100 cm^2	S_{geom} = 10.44 cm^2
^{239}Pu	5.8×10^{-7}	2.9×10^{-10}	6.1×10^{-8}
^{241}Am	4.2×10^{-8}	2.1×10^{-11}	2.0×10^{-8}
^{244}Cm	3.1×10^{-8}	1.6×10^{-11}	2.8×10^{-8}
^{147}Pm	2.2×10^{-8}	1.1×10^{-11}	6.7×10^{-8}

Pu and Am leach rates from the ferrite ceramic calculated by geometric surface area are higher than those found for the ceramic doped with radionuclide tracers where surface area was measured by the BET-method by approximately 10 times. It may be suggested that this difference is due to porosity of the samples used in the given work and should disappear in the case of the samples with zero open porosity. Leach rate of ^{244}Cm has approximately the same level as ^{241}Am. Pu exhibits higher leach rate from the aluminate ceramic as compared with that of Am and Cm by about one order of magnitude probably due to occurrence of some Pu in a tetravalent form.

Leach rate of ^{147}Pm as a matrix constituent allows to make some conclusions on long-term stability of the matrix. Using density values (ρ, g/cm^3) corrosion rates (R, cm/day) of the aluminate and ferrite matrices calculated by eq.: $R = w/\rho$ (3) are 5.2×10^{-9} and 1.1×10^{-8} cm/day, respectively. This corresponds to average matrix corrosion depth of 1.9 mm and 4.0 mm, respectively, providing for mechanical integrity even under incidental conditions when repository is flooded with water.

Discussion

According to a HLW partitioning concept HLW a long-lived REE/An fraction must be separated from a short-lived Cs/Sr fraction to be converted in ceramic and glass waste forms, respectively. The REE/An fraction contains major rare earths and minor actinides (Am, Cm, and traces of residual Pu). Because actinides are the most dangerous HLW constituents requiring their storage for a period of up to half of billion years it is expedient to separate them and process into ceramic waste form with high chemical durability and radiation resistance. The components of this An fraction - Am, Cm, residual Pu and lanthanides are mainly trivalent and the perovskite structure phases seem to be the most suitable hosts for these elements.

References

1. Phase Diagrams of High-Fusible Oxide Systems (Russ.), Nauka, Leningrad, 5 (1985-1991).
2. Ochkin, A.V., Chizhevskaya, S.V., Archakova, N.E. et al. Mat. Res. Soc. Symp. Proc. 757, 303-308 (2003).
3. Merkushkin, A., Ochkin, A., Rovniy, S., Stefanovsky, S. In: Proc. 35^{iemes} Journees des Actinides, Baden, Austria, April 23-26, 2005. Abstract P-27, CD-ROM.
4. Merkushkin, A., Ochkin, A., Rovniy, S., Stefanovsky, S. In: Proc. 35^{iemes} Journees des Actinides, Baden, Austria, April 23-26, 2005. Abstract P-28, CD-ROM.
5. Nuclear Waste Materials Handbook (Test Methods), DOE Technical Information Center, Washington, DC. Report DOE/TIC-11400 (1981).
6. Chemical Durability and Related Properties of Solidified High-Level Waste Forms, Technical Reports Series No.257, IAEA, Vienna (1985).

SHS method for immobilization of plutonium-containing waste

Levakov Eu.V., Postnikov A.Yu.

(RFNC - VNIIEF, Russia, Sarov)

Glagovskyi E.M., Kuprin A.V., Bogdanov A.I., Pelevin L.P.

(VNIINM, Russia, Moscow)

The main results of work in the area of technology development for immobilization of highly active waste (HAW) and, in particular plutonium-containing ones into mineral-like array compounds using the method of self-spreading high-temperature synthesis (SHS) are presented.

The choice of mineral-like arrays for HAW immobilization is proved. According to the results of thermodynamic calculations the availability of systems' formation based on zirconolite, pyrochlorine and other mineral-like compounds under SHS mode has been shown. The conditions influencing on both characteristics of SHS systems combustion and quality of obtained materials have been studied to optimize the technological parameters of SHS mineral-like arrays.

Base technological modes for SHS compacting of arrays based on pyrochlorine containing HAW simulators have been tested.

It is shown that the parameters of hydrothermal stability of arrays formed by SHS methods are similar to the same ones in arrays got by the method of cold compacting- sintering. Based on the experimentally got results the stands for immobilization of HAW simulators by SHS have been created.

An Improved Method To Dissolve Alloyed Plutonium Residues

L. Pescayre, C. Passot, D. Cardonna, H. Chollet
CEA/DAM, Centre d'Etude de Valduc – 21120 IS SUR TILLE – France

INTRODUCTION

The activities of the Valduc nuclear centre generate various plutonium metal residues which do not meet the required purity specifications to be directly reused. A nitric acid based process enables the recovery of the majority of the plutonium scrap in a purified form since the seventies. It consists in four main stages:

- Direct dissolution of the metal in NH_2SO_3H,
- Transformation in plutonium nitrate,
- Purification,
- Conversion into plutonium dioxide and metal.

However this process is not efficient or not safe for alloyed plutonium residues (alloyed elements> 15 wt %). A new method has been developed for four years to dissolve it. The first step is an oxidation of the metal. The second step is an aqueous dissolution in a mixture of HNO_3/HF (10 N/0.05N). The purpose is to develop a procedure and equipment for efficiently recovering the residues: complete burning (no metal remaining), good kinetics and recovery yield > 80%.

EXPERIMENTAL PROCEDURE

The first apparatus, which leads to the production of oxide, consists in a large horizontal muffle oven (Figure 1). A gas line feeds a mixture of oxygen (15% O_2) and argon into the furnace. The flow is measured before entering the glove box (45 l/h). The water vapour concentration varies between 0 and 14 000 vpm. The temperature is maintained at 550°C for 2 hours. The sample is placed in a "stainless steel/tantalum/stainless steel" cell (Figure 2).

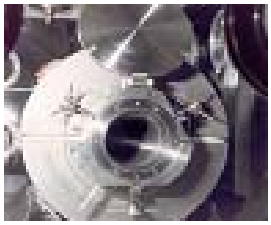

Fig 1: Horizontal Furnace

Fig 2: Pu alloyed sample

Fig 3: Vessel used for dissolution

The second apparatus consists in a stainless steel (Uranus B6) vessel surrounded by an electric resistance (Figure 3). A wet cooling component is present on the top of the vessel head. The HNO_3/HF mixture is thermostated at 70°C for 2*6 hours with a coated thermometer and agitated with a mechanical stirrer.

MAIN RESULTS

As noted in many works before, the rate of corrosion of alloyed plutonium increases substantially with moisture. For a water vapour concentration of 14000 vpm, the burning rate is about 20 g/h/cm^2. A greater rate could be performing with a mechanical system which breaks the protective dioxide layer. A general trend is that the burning rate is not very sensitive to the impurities present in the metal.

The observed increase of the sample weight is that expected for a complete oxidation to PuO_2. X-ray diffraction on one of the product exactly shows the pattern and lattice constants of c.f.c. PuO_2.

It seems there is no residual plutonium metal. However metallic grains or droplets appear inside the product (Figure 4). They are extracted from the plutonium oxide and spread with a blade on the surface of the container. SEM analysis shows that they are alloyed elements that segregated during the combustion because of good resistance to oxidation (Figure 5).

Fig 4: Burning product

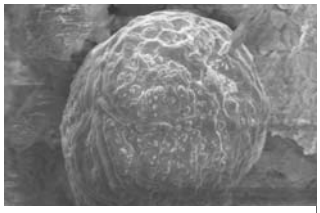

Fig 5: Alloyed element (SEM)

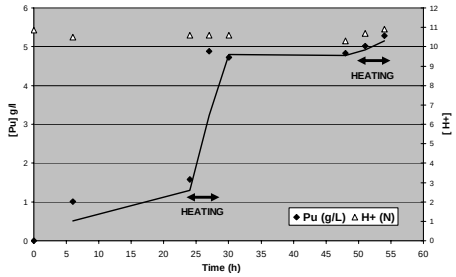

Fig 6: [Pu] during dissolution

Plutonium powder dissolution is efficient. The yield is higher than 97 %. The dissolution kinetic results from the burning temperature, the HF concentration and the dissolution temperature (Figure 6). The plutonium content of the residual undissolved powder was estimated by gamma counting. After rinsing, the insoluble solid residue contains less than 2g of plutonium for about 150g of impure oxide to be dissolved.

CONCLUSION - PERSPECTIVE

In order to recycle alloyed plutonium residues, an improved method has been successfully tested. The recovery yield is higher than 97 %.

New furnace device is in progress to improve the burning kinetic. A mechanical system will break the protective dioxide layer.

High Temperature Behaviour of Irradiated Mixed Nitride Fuel during Post Heating Tests

I. Sato*, K. Tanaka, T. Hirosawa, S. Miwa, K. Tanaka

*Japan Atomic Energy Agency, 4002 Narita-cho, Oarai-machi, 311-1393 IBARAKI, JAPAN

INTRODUCTION

In the Feasibility Study on Commercialized Fast Reactor Cycle System in Japan (F/S), a uranium-plutonium mixed nitride fuel with good thermal properties was selected as a candidate fuel form[1] with which conceptual design studies have been performed. Fast reactor design candidates suitable for the nitride fuel include middle and small size reactor cores using a coolant of Pb-Bi alloy and pellet type fuel. In a safety study for these concept reactors, it is quite important to recognize the behaviour of the nitride fuel under abnormal fuel temperatures such as in core damage accidents (CDAs). This is because a large amount of fission gases could remain in the nitride fuel due to the lower irradiation temperature experienced as compared to that for oxide fuel and these gases might be rapidly released as the temperature rose during CDAs. Moreover, if the temperature exceeds 2000℃, decomposition (the nitride fuel changes to metals and nitrogen gas) of the nitride fuel may occur[2], which can complicate the fission gas release behaviour. However, hardly any fission gas release data from irradiated mixed nitride fuel under abnormal temperature conditions have been obtained. The same holds for the decomposition behaviour.

JAEA is studied the applicability of nitride fuel for fast reactors by heating tests using uranium-plutonium mixed nitride fuels irradiated in the experimental fast reactor, "JOYO." In this work, the fission gas release and the decomposition behaviours were evaluated for the safety study of a Pb-Bi cooled fast reactor. The gas release behaviour and metallographic observations during and after the tests are shown and discussed.

Table 1: Characteristics and irradiation conditions of the uranium-plutonium nitride fuel pellet

N/M	1.00
Diameter	7.28 mm
Pu /(Pu+U)	18.6 wt%
U235 enrichment	19.6 wt%
Density	84.8 %T.D.
Burn up	Approx. 4 at%
Max fuel temperature	Approx. 1700℃

EXPERIMENTAL PROCEDURE

The characteristics and irradiation conditions of nitride fuel pellet are shown in Table 1. Results for other post irradiation examinations (PIEs) for this fuel pellet have been given in the literature[3]. A pellet was removed from the fuel pin and the cladding was cut away to get the test specimens. The test specimens were heated in an induction heating furnace in an atmosphere of flowing high-purity Ar. The heating tests were designated Nifti-1 and Nifti-2 (Nifti: Nitride fuel heating test after irradiation). In Nifti-1, the temperature was slowly elevated to the maximum of 2400 ℃ to allow observation of the fission gas release and decomposition behaviour in detail. In Nifti-2, a relatively rapid heating rate (approx. 20K/s) was applied from 1700 ℃ (equivalent

to the centre line temperature under irradiation) to 2500 ℃, which simulated a transient timescale, "slow TOP." During the tests, the released gases were analysed in-site by gas mass spectrometry, and then the concentrations of released gases were evaluated depending on the heating temperature. Details of analysis systems have been given in the literature[4]. After these heating tests, metallographic observations and EPMA for these specimens were carried out to get microstructures and elemental distributions.

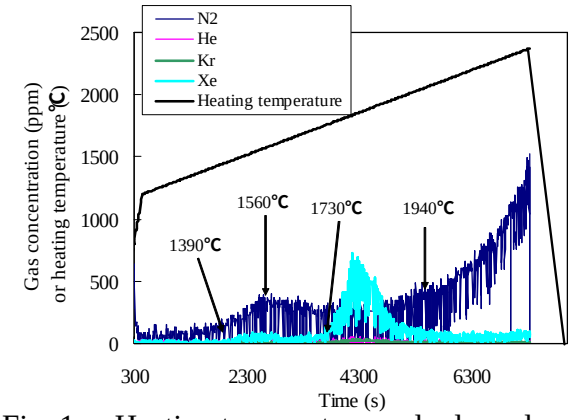

Fig. 1: Heating temperature and released gas concentration histories during Nifti-1.

RESULTS AND DISCUSSION

In Nifti-1, a concentration profile of fission gases and nitrogen in the carrier gas was obtained as shown in Fig. 1. The fission gas release starts around the heating temperature of 1730 ℃. Although the heating temperature is sufficiently high compared to the normal fuel temperature, a few dozen percent of fission gases remain in the fuel after the heating test from results of the other gas quantitative analysis. Concerning the relationship between the fission gas release and nitrogen release by the decomposition, the main nitrogen release starts around 1900 ℃, but is not dependent on the fission gas release. Fig. 2 shows the metallographic images of a specimen before and after Nifti-1. The quite small pores existing before the heating test could connect with each other and grow by heating to become larger ones. Therefore, the fuel density before heating (approx. 13 g/cm^3) is 9 g/cm^3 which is smaller than the coolant density (10 g/cm^3). The fuel pellet could float above the coolant during CDA with cladding melting. However, in the Nifti-2 specimen, there are still small pores after heating. This implies that the pore size and number depend on the heating rate applied in each test.

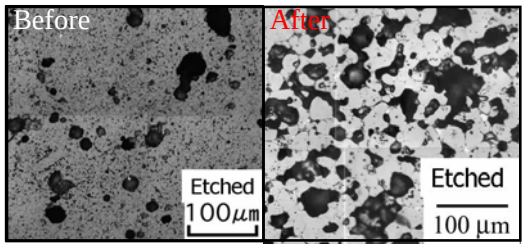

Fig. 2: Metallographic images obtained before and after Nifti-1.

EPMA for the Nifti-1 specimen shows some inclusions containing Pu and Rh without U. This indicates that Pu preferentially except U can precipitate along with the decomposition.

Acknowledgements

The authors are grateful to Dr. Ikken Sato for suggestions and discussions about this work. They also wish thank the technical staff members, Mr. T. Ishida and Mr. S. Sekine.

1 M. Konomura, et al., JNC report, JNC TN9400 2004-035 (2004) [in Japanese].
2 K. Richter and C. Sari, J. Nucl. Mater. **184** (1991) 167.
3 K. Tanaka, K. Maeda, K. Katsuyama et al., J. Nucl. Mater. **327** (2004) 77 .
4. I. Sato, T. Nakagiri, T. Hirosawa, et al. J. Nucl. Sci. Technol. **40** (2003) 104.

Oxygen Chemical Diffusion in Hypostoichiometric MOX

M. Kato[*], K. Morimoto[*], T. Tamura[†], T. Sunaoshi[†], K. Konashi[† †], M. Kashimura[*]

[*]Nuclear Fuel Cycle Engineering Laboratories, Japan Atomic Energy Agency, 4-33 Muramatsu, Tokai-Mura, Ibaraki 319-1194, JAPAN
[†]Inspection Development Company, 4-33 Muramatsu, Tokai-Mura, Ibaraki 319-1194, JAPAN
[† †]Tohoku University, 2145-1313 Narita-cho, Oarai-machi, Ibaraki 311-1313, JAPAN

INTRODUCTION

Plutonium and uranium mixed oxide (MOX) has been developed to use as the fuel for fast reactors. The oxygen to metal ratio (O/M) of the MOX fuel is an important parameter to control fuel and cladding chemical interaction. The oxygen potential and the oxygen diffusion coefficient of MOX are essential data to understand oxygen behaviour in MOX. The oxygen potentials of MOX were measured previously with good accuracy as a function of O/M and temperatures[1]. In the present work, the oxygen chemical diffusion coefficients in $(Pu_{0.2}U_{0.8})O_{2-x}$ and $(Pu_{0.3}U_{0.7})O_{2-x}$ were investigated using a thermo gravimetric technique.

EXPERIMENTAL

Two kinds of MOX powder with 20%Pu and 30%Pu contents were prepared by a direct microwave heating denitration process. Each powder type was pressed and sintered into needle-like samples, which were about 1.4mm in diameter and 5.7-7.2mm in length, weighed about 120mg and had 87.8-92.9%TD.

Measurements of the changing rate of O/M ratio were carried out by thermal gravimetry and differential thermal analysis (TG-DTA) at temperatures of 1250, 1300 and 1350˚C. Details of the apparatus were reported previously[1]. The oxygen partial pressure in the atmosphere was controlled rapidly by changing hydrogen content in the atmosphere and the change of sample weight was measured as a function of time.

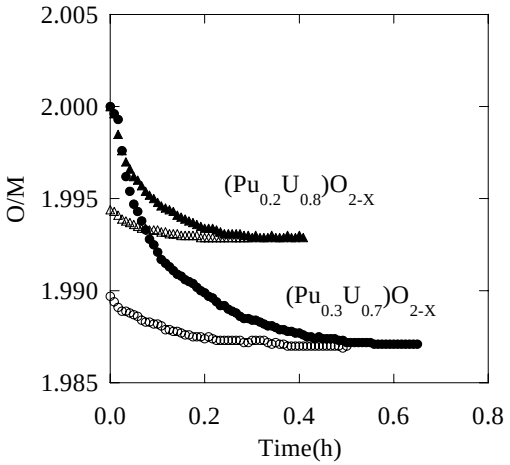

Fig.1 Kinetics of reduction process of $(Pu_{0.2}U_{0.8})O_{2-x}$ and $(Pu_{0.3}U_{0.7})O_{2-x}$ at 1300°C as a function time.

RESULTS AND DISCUSSION

Figure 1 shows measurement results of the reduction process in the range of hypostoichiometric composition. The average concentration $\overline{c}$ of an infinite cylinder sample of radius r_0 is given by Eq. (1) when the change is dominated by chemical diffusion[2].

$$F = \frac{\overline{c} - c_f}{c_i - c_f} = \sum_{\nu=1}^{\infty} \frac{4}{\xi_\nu^2} \exp\left(-\frac{\xi_\nu^2 \tilde{D} t}{r_0^2} \right) \qquad (1)$$

Here c_i, c_f, t and ξ_v are the initial concentration, the final concentration, time and the roots of the equation $J_0(x)=0$, respectively, where $J_0(x)$ is the Bessel-function of zero order. The measurement results were analyzed using Eq. (1), since the infinite cylinder is a good approximation for the needle-like samples. Eq. (1) represents the curves of the reduction processes very well. The oxygen chemical diffusion coefficients D of hypostoichiometric MOX with 20%Pu and 30%Pu are estimated to be 3.2×10^{-6}cm^2/s and 1.6×10^{-6}cm^2/s, respectively, from the results of reduction curves at 1300ºC.

The oxygen chemical diffusion coefficients of $(Pu_{0.2}U_{0.8})O_{2-x}$ and $(Pu_{0.3}U_{0.7})O_{2-x}$ are expressed by the following equations.

$$\ln \tilde{D} = \left(-\frac{68.4\times10^3}{RT} \right) + \ln(5.486\times10^{-4}) \quad \text{for } (Pu_{0.2}U_{0.8})O_{2-x} \quad (2)$$

$$\ln \tilde{D} = \left(-\frac{116.1\times10^3}{RT} \right) + \ln(1.16\times10^{-2}) \quad \text{for } (Pu_{0.3}U_{0.7})O_{2-x} \quad (3)$$

Figure 2 shows the oxygen chemical diffusion coefficients calculated by Eqs. (2) and (3) using the experimental values as a function of 1/T. The oxygen chemical diffusion coefficient in $(Pu_{0.2}U_{0.8})O_{2-x}$ is larger than that in $(Pu_{0.3}U_{0.7})O_{2-x}$. Data from other works are also plotted in the figure[3-5]. The results of this work are smaller than the literature data which were obtained from measurement results of oxidation of $(Pu_{0.2}U_{0.8})O_{2-x}$.

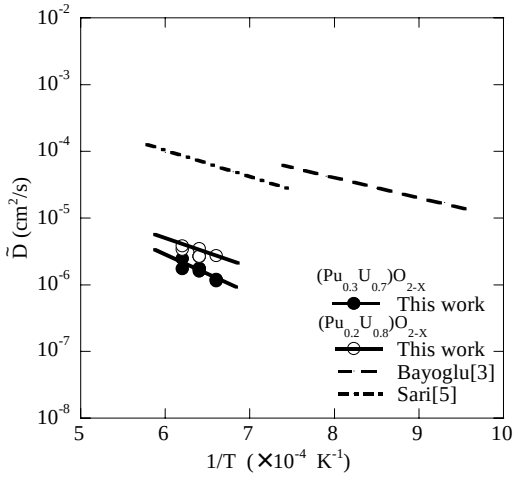

Fig.2 Oxygen chemical diffusion coefficients plotted in an Arrhenius diagram.

CONCLUSION

The kinetics of the reduction processes of $(Pu_{0.2}U_{0.8})O_{2-x}$ and $(Pu_{0.3}U_{0.7})O_{2-x}$ were measured by TG-DTA. The oxygen chemical diffusion coefficients were estimated from the reduction curves. It was concluded that the oxygen chemical diffusion coefficient in $(Pu_{0.3}U_{0.7})O_{2-x}$ was smaller than that of $(Pu_{0.2}U_{0.8})O_{2-x}$.

REFERENCES

1 M. Kato, et al., Journal of Nuclear Materials, 344, 235, (2005)
2 W. Jost, Diffusion in solid, liquids, gases, Academic press, (1960)
3 A. S. Bayoglu, Solid State Ionics, 12, 53, (1984).
4 F. D'annucci and C. Sari, Journal of Nuclear Materials, 68, 357, (1977)
5 C. Sari, Journal of Nuclear Materials, 78, 425, (1978)

The oxidation rate of $(U_{0.7}Pu_{0.3})O_{2-x}$ with two fcc phases

K. Suzuki*, M. Kato*, T. Tamura†, S. Aono*, M. Kashimura*
*Nuclear Fuel Cycle Engineering Laboratories, Japan Atomic Energy Agency, 4-33 Muramatsu, Tokai-Mura, Ibaraki 319-1194, JAPAN
† Inspection Development Company, 4-33 Muramatsu, Tokai-Mura, Ibaraki 319-1194, JAPAN

INTRODUCTION

It has been reported that sintered MOX pellets of hypostoichiometric composition were oxidized at room temperature in an atmosphere of inert gas and air[1, 2]. The region of two fcc phases exists at room temperature in the $(Pu,U)O_{2-X}$ with Pu content of greater than 20%.[3, 4] In this study, using a thermogravimetric technique, we investigated the oxidation rate of $(Pu_{0.3}U_{0.7})O_{2-X}$ with two fcc phases to contribute to understanding of the oxidation behavior.

EXPERIMENTAL

The sintered pellets of $(U_{0.7}Pu_{0.3})O_{2-X}$ were prepared by a mechanical blending method and were sliced into disc-like samples with about 1 mm thickness and 85-93% theoretical density. The samples were annealed under appropriate conditions to adjust the ratio of oxygen to metal (O/M) to 1.95-1.97[5]. The oxidation rate of the samples were measured using thermal gravity and differential thermal analysis (TG-DTA) at 60, 125 and 150ºC in an atmosphere of air, N_2 and air/N_2 gas mixture with moisture content of 1 - 700ppm. The X-ray diffraction patterns of samples were analyzed before and after the TG-DTA.

RESULTS AND DISCUSSION

Figure 1 shows kinetics of the isothermal oxidation reaction in air as a function of time and temperatures. In the isothermal oxidation, under 150ºC, the O/M of sample did not exceed 2.00 and the oxidation rate increased with an increase of temperature. In the results of X-ray diffraction measurement, the amount of fcc phase with O/M≈2.00 was observed to increase by the oxidation of sample. It was reported that the $(Pu_{0.3}U_{0.7})O_{2-X}$ exists as two fcc phases at room temperature and the O/M ratios of the two fcc phases are estimated to be O/M=1.85 and 1.985, respectively [3,4]. Therefore, we think that the oxidation of $(Pu_{0.3}U_{0.7})O_{2-X}$ with two fcc phases is explained by diffusion of the higher O/M phase formed on the surface.

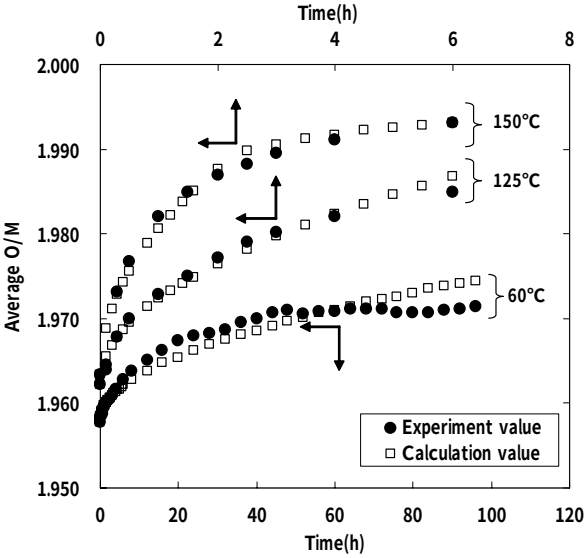

Fig.1 Kinetics of the oxidation reaction in air plotted as a function of time and temperatures

Jost[6] treated diffusion in a system

consisting of two phases as shown in Fig.2. The distribution of O/M is expressed by following equation as a function of x-direction

$$O/M_x = O/M_s - B \cdot erf\left(\frac{x}{2\sqrt{\tilde{D}t}}\right),$$

for $0 < x < \xi$ $\cdots$ (1)

$O/M_x = O/M_i$, for $x \geq \xi$.

Here O/M_x= O/M at x, O/M_s= O/M at sample surface, O/M_i= initial O/M, B= arbitrary constant, t= time, $\tilde{D}$ =oxygen chemical diffusion coefficient and ξ = discontinuous point of O/M distribution. The average O/M ratio of the sample was calculated using equation (1) as shown in Fig.1. We see the calculation results are good agreement with measurement results.

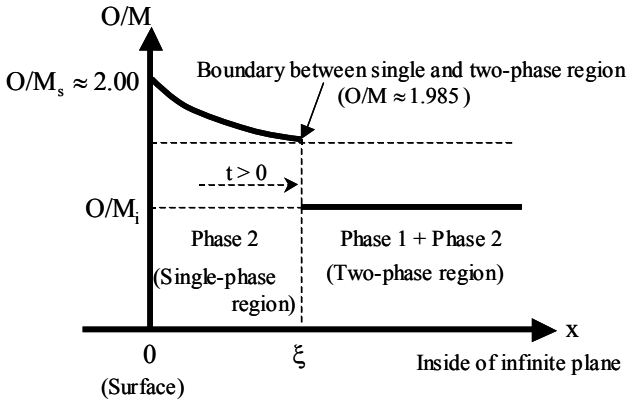

Fig.2 Diffusion into the two-phase system. Discontinuous point of O/M distribution ξ is located in the surface for t=0, where Phase 1=the lower O/M phase and Phase 2=the higher O/M phase.

CONCLUSION

The oxidation of $(U_{0.7}Pu_{0.3})O_{2-x}$ with two fcc phases was evaluated at temperatures up to 150ºC and the curve of the isothermal oxidation was analyzed by the model of diffusion in a system consisting of two phases. The diffusion model could represent the oxidation curve as a function of time and temperature. The oxidation of the $(U_{0.7}Pu_{0.3})O_{2-x}$ proceeded by diffusion of the phase with O/M≈2.00 which was formed on the sample surface.

REFERENCES

1. R. E. Woodley and R. L. Gibby, HEDL-SA-592 (1973)
2. R. Eicher, *et al.*, J. Nuclear Materials, 124, (1984) 9
3. C. Sari, U. Benedict and H. Blank, J. Nuclear Materials, 35, (1970) 267
4. M. Kato, *et al*., Proceedings of Actinides 2005, Manchester, 4P04, (2004), 108
5. M. Kato, *et al*, J. Nuclear Materials 344, (2005) 235
6. W. Jost, Diffusion in solids, liquids and gases, Academic Press, Inc., (1960), 69

A New Method of Describing Uranium Oxidation in Water Vapor

V.K. Orlov, A.A. Karnozov, T.B. Karnozova

The Federal State Unitarian Enterprise A.A. Bochvar All-Russian Scientific Research Institute of Inorganic Materials (VNIINM), P/Box 369 Moscow, 123060 Russia

It is shown that uranium oxidation rate in water vapor depends on water evaporation rate from glassy capillary vessels (moisture bearer).

A new method of describing gaseous products accumulation kinetics is offered. The method is based on an assumption that dynamic equilibrium between water vapor consumption rate during uranium oxidation and water evaporation rate from moisture source can be achieved in the studied system by providing constant temperature.

The figure 1 shows dependence rate of water evaporation and rate of water vapor consumption during Uranium oxidation on water vapor pressure. With water vapor pressure dropping below the pressure of saturated water vapor the rate of metallic Uranium oxidation decreases (blue arrow), while the rate of water evaporation from the source increases (red arrow).

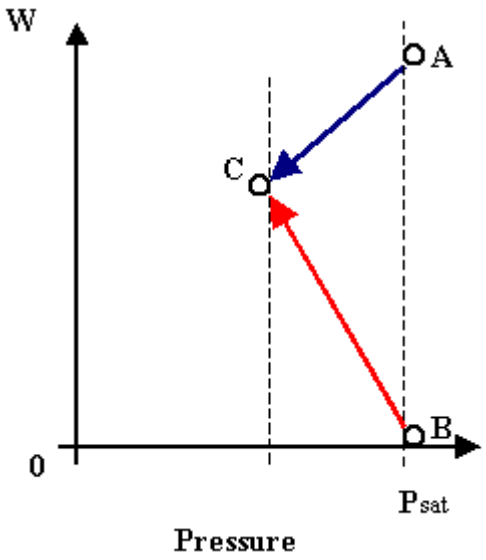

Fig.1: The dependence of water evaporation rate and water vapor consumption rate during Uranium oxidation on water vapor pressure.

The process of uranium oxidation in water vapor can be relatively shared in two parts: transitional one and stationary one. In the first part (transitional) water vapor pressure is decreased by saturated water vapor pressure to stationary pressure, which is accompanied by gaseous products accumulation rate increase in the reaction vessel.

In the second part (stationary) water vapor pressure keeps constant (stationary) up to complete evaporation of liquid water from capillary vessel (moisture bearer); gaseous products accumulation rate keeps constant in the reaction vessel.

Physical-Chemical and Radiation-Chemical Processes in the PuO_2 - Sorbed Water System

M.V. Vladimirova, A.A. Karnozov

The Federal State Unitarian Enterprise A.A. Bochvar All-Russian Scientific Research Institute of Inorganic Materials (VNIINM), P/Box 369 Moscow, 123060 Russia

Turning weapons-grade plutonium into dioxide and its further use for MOX -fuel is one of major activities on conversion of excessive plutonium stocks. PuO_2 is a hygroscopic substance. When exposed to plutonium's alpha-radiation, the sorbed water is decomposed resulting in the formation of hydrogen and oxygen, to constitute a potential hazard associated with a possible detonating mixture formation and a buildup of pressure inside sealed vessels. The special containers will be created to ensure safe storage and handling of plutonium dioxide. With this aim in view, it is necessary to have the data on kinetics of H_2 and O_2 formation, and a mathematical model to calculate amounts of the evolved gases and their pressure in a container for any initial data.

The presentation generalizes the experimental data on kinetics of hydrogen and oxygen formation depending on water content, a technique of water sorption onto PuO_2 (from a liquid or gas phase), specific surface area of powder, radiation dose rate, time and temperature of plutonium dioxide storage.

As for the system including the water sorbed from the liquid phase, it has been shown that the H_2 and O_2 formation rates increase with increasing radiation dose rate and H_2O amount. On long storage of PuO_2, the gas-phase hydrogen amount reaches the steady-state value that is equal in moles to the initial amount of sorbed water. It has been concluded that kinetic characteristics of formation of the water radiolysis products depend on water content, and the rates of the H_2 and O_2 formation reaction have the first order relevant to the sorbed water amount.

Based on this and on the results of comparison of calculated and experimental data, there has been created a mathematical model of sorbed water radiolysis, including the reactions of radiolysis product formation, the reaction of PuO_2 with H_2O_2 resulting in formation of water and overstoichiometric plutonium oxide, and the reaction of H_2 and O_2 recombination to form water. The mathematical model was used to calculate the amounts of H_2 and O_2 for various initial conditions. Good agreement has been shown between the calculated and experimental data obtained for the water sorbed onto PuO_2 from the liquid phase.

Outlined have been the main lines of the experimental and calculation activities required to obtain full quantitative information on radiolysis of the water sorbed onto PuO_2 from the gas phase.

Alteration of U(VI)-Phases Under Oxidizing Conditions

A.P. Deditius[†], S. Utsunomiya[†], R.C. Ewing[†]

[†] Department of Geological Sciences, University of Michigan, Ann Arbor, Michigan 48109-1005

INTRODUCTION

Uranium-(VI) phases are the primary alteration products of the UO_2 in spent nuclear fuel and the UO_{2+x} in natural uranium deposits. The U(VI)-phases generally form sheet structures of edge-sharing UO_2^{2+} polyhedra. The complexity of these structures offers numerous possibilities for coupled-substitutions of trace metals and radionuclides. The incorporation of radionuclides into U(VI)-structures provides a potential barrier to their release and transport in a geologic repository that experiences oxidizing conditions. In this study, we have used natural samples of UO_{2+x}, to study the U(VI)-phases that form during alteration and to determine the fate of the associated trace elements.

SAMPLE AND ANALYTICAL METHODS

Samples were obtained from the Marshall Pass deposit, Colorado, a unique locality because of the presence of Cu minerals; thus, this is also a potential analogue to canister interactions with spent nuclear fuel (SNF)[1] for programs considering such waste package materials. The uranium ore deposit is located close to the surface and has reacted both with ground and meteoritic waters. Primary uraninite formed under reducing conditions in veins controlled by faulting. The UO_{2+x} is intergrown with Cu, Zn, Pb, Sb, Ag, As sulfides and sulfosalts, such as tetrahedrite, covellite, chalcocite, chalcopyrite, galena and sphalerite[2]. Five samples of different degrees of alteration were analysed by optical petrography, scanning electron microscopy/energy dispersive X-ray spectrometry (SEM/EDS), electron microprobe analysis (EMPA) and transmission electron microscopy (TEM).

RESULTS AND DISCUSSION

The chemical composition of the uraninite by EMPA is 75.1-77.6 wt% U, 1.2-2.0 wt.% Ca 1.0-2.1 wt.% Pb, 0.98-1.7 wt.% W, 0.16-1.0 wt.% As, with minor amounts (<1 wt.%) of Zr, Ti, REE, Mo, Si, P and Fe.

The first stage of alteration was caused by penetration of oxidizing fluids with W and Mo. The oxidation of U may have caused the reduction in the uraninite unit cell parameter, creating microfractures, and providing additional pathways for the fluids. Uraninite grains show grain spallation, finally resulting in lost of cohesion and subsequent separation. Sulfides and sulfosalts are unstable under these conditions, liberating Pb, As, S, Cu, Zn, Sb, Ag. The presence of Mo in the fluids with liberated Pb resulted in precipitation of wulfenite ($PbMoO_4$). Acidic solutions derived from the dissolution of the sulfides caused the oxidation and dissolution of uraninite. In general, the sequence of uraninite alteration is consistent with that previously reported from the Nopal I deposit (Mexico) and the laboratory experiments: uraninite, uranyl oxide hydrates, uranyl silicates, and finally, alkali + alkali earth uranyl silicates[3,4].

In the present samples, the sequence of formation began with ianthinite, $U^{4+}(UO_2)O_4(OH)_6(H_2O)_9$, followed by schoepite-type minerals, e.g., $(UO_2)_8O_2(OH)_{12}(H_2O)_{12}$,

with mainly preserved “dehydrated schoepite”. Subsequently, two phases formed: (*i*) a rare Pb-uranyl oxide hydrate and (*ii*) mats of fine-grained platy crystals of a Ba-Mo-W uranyl phase with the composition of: 47.4-55.2 wt.% of U, 7.27-14.8 wt.% of W, 5.73-10.9 wt.% of Mo, 3.62-4.54 wt.% of Ba, 1.25-1.65 wt.% of Ti, 0.65-1.32 wt.% of Fe, and 0.26-0.61 wt.% of Ce. The latter phase is a uranotungstite-type[5] mineral, $(Ba,Pb,Fe^{2+})(UO_2)_2(WO_4)(OH)_4(H_2O)_{12}$, with possible substitution of Mo for W. A similar, but previously unknown, Cs-Ba-Mo uranyl oxide hydrate has been reported in the SNF corrosion experiments[6]. At the next stage of paragenesis, fluids with Si and Ca entered into the system leading to supersaturation for uranophane, $Ca(UO_2)_2(SiO_3OH)_2(H_2O)_5$, and then uranyl arsenates, (trogerite, $(UO_2)_3(AsO_4)_2(H_2O)_{12}$; metazeunerite, $Cu[(UO_2)(AsO_4)]_2(H_2O)_8$), precipitated partially replacing the previously formed phases.

A different alteration sequence was observed in the areas where uraninite is intergrown with sulfides and sulfosalts. The Cu-bearing minerals (tetrahedrite, covellite, chalcocite, chalcopyrite) show evidence of dissolution, such as corrosion rinds. The paragenesis of uranyl-minerals including Cu in the system may be applicable to the corrosion of Cu-based SNF containers[1]. In veinlets, (meta)zeunerite precipitated replacing uraninite and the Cu-minerals, as well. A thin layer (2-5μm) of a fine-grained unknown phase enriched in U (44.6-49.2 wt.%) and Sb (22.4-26.1 wt%) was found between uraninite, U-arsenate and tetrahedrite. This may be a new U-Sb mineral, a mixture of uranyl oxide hydrate and Sb oxide or antimonite containing U, which has been proposed as a phase that forms in the fission-product waste stream that results from the reprocessing of SNF, especially $^{90}Sr^{2+}$ and REE^{3+} in acidic waste streams[7].

The last stage of alteration is most likely caused by reaction with meteoric water of low ionic strength. U-arsenates and silicates were replaced by “dehydrated schoepite” (II). Finally, uranyl minerals were altered to swamboite, $U^{6+}(UO_2)_6(SiO_3OH)_6(H_2O)_{30}$.

CONCLUSIONS

In Marshall Pass, Colorado, oxidizing fluids of various compositions resulted in a complex sequence of alteration phases. The most common trace element is As, forming uranyl arsenates as a major phase. In case of supersaturation with W and Mo, an unknown U-W-Mo phase precipitated. Additionally, crystallization of a U-Sb phase reflects substantial local variability in Sb-concentration. This occurrence provides a good example of the complexity one may expect in anticipating the results of the corrosion of SNF in an open system under oxidizing conditions.

Acknowledgements

This work was supported by the Office of Science and Technology and International (OST&I) of the Office of Civilian Radioactive Waste Management (DE-FE28-04RW12254). The views, opinions, findings and conclusions or recommendations of the authors expressed herein do not necessarily state or reflect those of DOE/OCRWM/OSTI.

1 T. Hedmann, *et al.*, C. R. Physique. **3,** (2002).
2 D. Zhao and R.C. Ewing, Radiochim. Acta. **88,** (2000).
3 D.J. Wronkiewicz, *et al.*, J. Nucl. Mater. **238,** (1996).
4 E.C. Pearcy, *et al.*, Appl. Geochem. **9,** (1994).
5 K. Walenta, Tschermaks Mineral. Petrol. Mitt. **34,** (1985).
6 E.C. Buck, *et al.*, J. Nucl. Mater., **249,** (1997).
7 M.V. Siviaiah, *et al.*, Radiochim. Acta. **92,** (2004).

Enthalpy of Formation of $Pu_{(1-x)}Zr_xO_2$ Fluorite and $CaPuTi_2O_7$ Pyrochlore

T. Lee [*], J. Mitchell[*], A. Navrotsky[†], B. Ebbinghaus[¥]

[*]Los Alamos National Laboratory, Los Alamos, NM, USA 87545 USA
[†]University of California at Davis, Davis, CA 95646 USA
[¥]Lawrence Livermore National Laboratory, Livermore CA 94552 USA

ABSTRACT

The total inventory of high-level radioactive nuclear waste in the US alone is projected to exceed 100,000 metric tons by the year 2035. Oxides with the fluorite and pyrochlore structures, are chemically and thermally durable, radiation tolerant, and proliferation resistant, and, thus, are of great interest as nuclear waste forms suitable for burial.[1] These properties also make oxides with the fluorite structure attractive as potential inert matrix nuclear fuels.[2] Such nuclear waste forms or nuclear fuels, however, must also be thermodynamically stable. For example, recent studies have suggested that the $CaPuTi_2O_7$ pyrochlore could be thermodynamically unstable with respect to an oxide-perovskite phase assemblage.[3] We will use high temperature high temperature oxide melt drop solution calorimetry to investigate the thermodynamic stability of the $Pu_{(1-x)}Zr_xO_2$ fluorite phase and the $CaPuTi_2O_7$ pyrochlore phase. Our preliminary results show that mixing in the analogous $Ce_{(1-x)}Zr_xO_2$ fluorite phase is ideal. That is, unlike in other fluorite oxide systems, there is no thermodynamic driving force to order, and the inherent disorder in this and the $Pu_{(1-x)}Zr_xO_2$ fluorite solid solutions should result in exceptional tolerance to radiation damage.

This work supported in part by the Seaborg Institute Postdoctoral Fellowship.

1 R. C. Ewing, Canadian Mineralogist **39**, (2001).
2 G. Ledergerber, *et al*., Progress in Nuclear Energy **38**, (2001).
3 K. B. Helean, *et al*., Journal of Nuclear Materials **303**, (2002).

An Experimental Investigation on Phase Relation of Americium-doped PuO_2

S. Miwa[*], M. Osaka[*], H. Yoshimochi[*], K. Tanaka[*], K. Kurosaki[†], M. Uno[†], S. Yamanaka[†]

[*]Oarai Research and Development Center, Japan Atomic Energy Agency, Oarai-machi, Higashi-ibaraki-gun, Ibaraki, 311-1393, Japan. E-mail: miwa.shuhei@jaea.go.jp
[†]Department of Nuclear Engineering, Graduate School of Engineering, Osaka University, Yamadaoka 2-1, Suita-shi, Osaka 565-0871, Japan

INTRODUCTION

Japan Atomic Energy Agency (JAEA) is promoting R&D programs for future nuclear cycle technology based on fast reactors, which is essential to a reduced environmental burden and a sustainable energy supply [1]. Development of the mixed oxide (MOX) fuel and target containing minor actinides (MAs), which are considered as promising candidates for the future fast reactor, is underway [1,2]. The target is composed of actinide oxides and non-radioactive support materials such as MgO [2].

Among MAs, americium (Am) is of special concern because of its high and lasting radiotoxicity, together with several noticeable properties such as its effect on oxygen potential [3-5]. It was revealed through these studies that only a small amount of Am addition to oxides had significant effects on various properties [3-5]. Am-doped PuO_2, $(Pu,Am)O_{2-x}$, is considered as a candidate form for MAs-including oxide of the target [2]. Since phase relation is one of the most fundamental properties especially for the evaluation of irradiation behaviour, an experimental investigation on phase relation of $(Pu,Am)O_{2-x}$ is carried out in this study. In particular, effects of Am addition to PuO_{2-x} on the phase relation are focused on.

EXPERIMENTAL

The $(Pu_{0.91}Am_{0.09})O_{2-x}$ solid solutions were prepared by a conventional powder metallurgical route; i.e., ball-milling of $(^{241}Am,Pu)O_{2-x}$ powder, uni-axial pressing into pellets, followed by sintering in moisture added Ar containing 5 % H_2 for 3 h at 1973 K. Density of the stoichiometric $(Pu_{0.91}Am_{0.09})O_2$ was about 79 % of theoretical. There were no cracks in the sintered body.

The sintered pellets were then thermally treated under moisture added Ar/H_2 at different oxygen potentials to adjust the O/M ratio from 1.90 to 2.00 [4]. The O/M ratios at various oxygen potentials were calculated from the weight change relative to the stoichiometry. X-ray diffraction (XRD) analysis was carried out for the $(Pu_{0.91}Am_{0.09})O_{2-x}$ having different O/M ratios at room temperature. Phase transition temperatures of $(Pu_{0.91}Am_{0.09})O_{2-x}$ at the O/M range mentioned above were investigated by Differential Thermal Analysis (DTA).

RESULTS AND DISCUSSION

XRD patterns showed a single phase of the fluorite structure for $(Pu_{0.91}Am_{0.09})O_{2.00}$. Figure 1 shows lattice parameter dependence of $(Pu_{0.91}Am_{0.09})O_{2-x}$ solid solution on O/M ratio. It is seen

that the lattice parameter decreases with decrease of O/M ratio. The lattice parameters of $(Pu_{0.91}Am_{0.09})O_{2.00}$ and $(Pu_{0.91}Am_{0.09})O_{1.92}$ agreed with those of calculated by using Vegard's law, in which assumes $(Pu_{0.91}Am_{0.09})O_{2-x}$ as an ideal solid solution of PuO_2, $PuO_{1.62}$, AmO_2 and $AmO_{1.61}$.

Figure 2 shows peak locations observed in the DTA plotted on the phase diagram of temperature versus O/M ratio for $(Pu_{0.91}Am_{0.09})O_{2-x}$. DTA peaks were observed on both increasing and lowering the temperature at constant O/M ratios. The DTA peaks were so small that they should be derived from quasi-stable phase transition. It is seen that there are phase transition temperatures at about 1000°C and 300°C through the investigated O/M ratio, while there are also indications of the phase transitions at about 600°C below O/M =1.95. It is considered that phase relation of $(Pu_{0.91}Am_{0.09})O_{2-x}$ has different aspects which can be divided by around O/M =1.95.

Osaka et al. [4] adopted following hypothesis for the interpretation of oxygen potential isotherms of $(Pu_{0.91}Am_{0.09})O_{2-x}$: i.e., Am is reduced prior to Pu in $(Pu,Am)O_{2-x}$. This hypothesis is also used for the discussion of the present aspects of phase relation in this study. With this hypothesis, the boundary O/M ratio, at which all Am in $(Pu_{0.91}Am_{0.09})O_{2-x}$ is trivalent, is 1.955. This O/M ratio is close to what divides the different phases mentioned above.

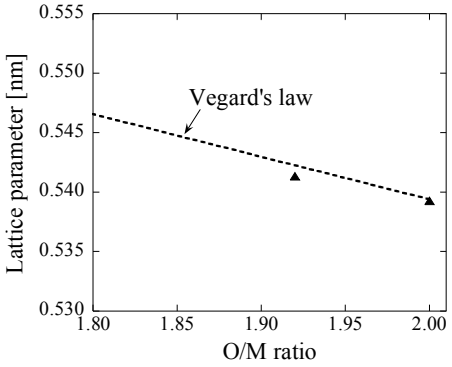

Fig. 1 Dependence of lattice parameter of $(Pu_{0.91}Am_{0.09})O_{2-x}$ on O/M ratio.

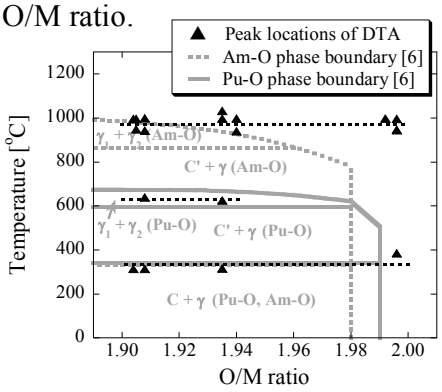

Fig. 2 Peak locations observed in the DTA for $(Pu_{0.91}Am_{0.09})O_{2-x}$.

It is known that the profile of phase diagram for Am-O system is similar to that of Pu-O system [6]. However, phase transition temperatures of Am-O system are higher than those corresponding to Pu-O system, as superimposed on Fig. 2 [6]. Of note is that there are phase transition temperatures corresponding only to Am-O system above the boundary O/M ratio, while there are phase transition temperatures corresponding to those of Pu-O and Am-O systems below the boundary O/M ratio. These results suggest that the Am-O system and Pu-O system are predominant in the respective phases of $(Pu,Am)O_{2-x}$ above and below the boundary O/M ratio.

1 K. Aizawa, Proc. Int. Conf. on Back-End of the Fuel Cycle, Paris, France, Sept. 9-13, 2001, p.50 (2001)
2 M. Osaka, H. Serizawa, M. Kato, M. Inoue, K. Nakajima, Y. Tachi, R. Kitamura, S. Ohki, S. Miwa, T. Iwai, K. Tanaka, S. Ukai, Y. Arai, Proc. GLOBAL 2005, Japan, Oct. 10-13, 2005, No. 240 (2005)
3 M. Osaka, I. Sato, T. Namekawa, K. Kurosaki and S. Yamanaka, J. Alloys and Comp. 2005, **397**, 110.
4 M. Osaka, K. Kurosaki and S. Yamanaka, submitted to J. Nucl. Mater..
5 M. Osaka, S. Miwa, H. Yoshimochi, K. Tanaka, K. Kurosaki and S. Yamanaka, Proc. Actinides 2005, England, July 4-8, 2005, 4P13 (2005)
6 C. Sari and E. Zamorani, J. Nucl. Mater., **37** (1970) 324.

Speciation of Pu in Aged Wastes and Wasteforms

Alayna Rodriguez, Juan Lezama-Pacheco, Steven D. Conradson
Los Alamos National Laboratory, Los Alamos NM 87544 USA

In the original discovery (or confirmation) of PuO_{2+x} the contention was made that it increased the environmental hazard of Pu because it should increase the solubility of PuO_2. Subsequent XAFS measurements showed that, whereas the adventitious O was incorporated as Pu(V) oxo groups analogous to the mononuclear solution chemistry of Pu, the Pu(V) was not necessarily preferentially leached from PuO_{2+x} compounds but was present at times even in colloids prepared by both hydrolytic and reductive precipitation from aqueous solution as well as in materials prepared by oxidation with H_2O vapor at both elevated and ambient temperature. An additional type of disorder was also identified in these measurements; a multisite O distribution even in compounds without the oxo groups that most likely originates in the incorporation of H_2O as OH^- in the PuO_2 lattice. This moiety also occurred in PuO_2 samples prepared at both ambient and elevated temperatures including, surprisingly, materials that had been fired at temperature in excess of 1000^oC where sorbed H_2O should be eliminated. These laboratory experiments raise the question of whether long term equilibration with the environment, whether the natural environment for Pu in soils or other more extreme ones for certain kinds of Pu wastes, will affect Pu speciation. For example, although curve-fit results of the EXAFS of PuO_{2+x} samples are very similar for both types of preparation methods, the white line amplitudes in the XANES of those prepared from aqueous solution are always higher than in the XANES of those that have been exposed to elevated temperatures. Similarly, the Fourier transformed spectra of aqueous-based materials exhibit broader features.

We are fortunate in having obtained XAFS spectra of some Pu wastes that have been subjected to long term exposure to various conditions, including size fractionated particles from the Pu cribs at Hanford and from an ion exchange resin used in Pu purification. The PuO_2 from the cribs was the insoluble fraction following HF extraction of Pu that had been air oxidized at high temperature. As expected, the Pu XAFS from the large particles resembles those ofO materials prepared at elevated temperatures. The spectra of the smaller fraction is very similar to those prepared by aqueous methods, indicating that exposure to H_2O over long periods actually can slowly modify the Pu speciation of the solid, converting it to the form that is equilibrated with liquid H_2O. The XAFS of the purification stream waste shows a Pu-O bond length that, while previously unobserved in the PuO_{2+x} system, is close to that expected for Pu(IV) coordination complexes with H_2O or NO_3^-. The formation and aging of colloidal PuO_2 in the presence of chelators – either the resin or the HNO_3 in the system – may therefore cause the surface Pu ions on the particles to remain coordinated to these ligands, resulting in a unique kind of PuO_2 structure.

Additional results on other systems will also be presented.

This work was supported by the Heavy Element Chemistry Program, Chemical Sciences, Biosciences, and Geosciences Division, Office of Basic Energy Sciences, U.S. Department of Energy under contract W-7405. XAFS measurements were performed at SSRL (Stanford Linear

Accelerator Center), which is operated by the US Department of Energy, Office of Basic Energy Sciences. Health Physics operations at SSRL and APS were supported by the Seaborg Institute for Transactinium Science at LANL.

Moisture Content of Impure Plutonium Oxide in Long-Term Storage

J. M. Berg

Los Alamos National Laboratory, Los Alamos NM 87544 USA

INTRODUCTION

Extensive campaigns to stabilize and package excess plutonium holdings in sealed stainless steel containers for long-term storage have recently been completed at several United States Department of Energy facilities. These activities were governed by the criteria in the US DOE Standard "Stabilization, Packaging, and Storage of Plutonium-bearing Materials".[1] A few thousand such packages containing plutonium metal or plutonium oxides have been created and are now being monitored under formal surveillance programs in several storage facilities.

The surveillance is designed in part to look for any indications of internal pressurization or container degradation. Pressurization, if it occurs, is expected to be highly correlated with residual moisture content on impure oxides. Therefore the packaging protocols specifically required that moisture content of oxides be measured prior to packaging. A maximum moisture threshold of 0.5 mass % of the package contents assures that the design pressure of the container will not be exceeded in storage under a set of worst-case assumptions.

As a result of these required moisture measurements, there is now a wealth of data on the moisture content of a wide variety of impure plutonium oxides following controlled treatment and handling protocols. This paper will summarize those data, discuss their limitations, and illustrate trends based on impurities, processing history and handling conditions.

DISCUSSION

It was recognized before these packaging campaigns began that some pre-treatment of plutonium oxide feed materials would be necessary to assure that potential chemical and radiolysis reactions associated with impurities would not over-pressurize and/or corrode the containers. Water was identified the common reactant in the pressure generating and corrosion reactions of greatest potential concern. Therefore the specified pre-treatment for oxides, calcination in air at either 950 °C or 750 °C, was selected principally as a simple means to reduce the moisture content. Calcination was presumed to also decompose residual organics, nitrates and carbonates.[1] Substantial quantities of halide salts were presumed to remain in the materials.

Packaging protocols required measurement of the final moisture content of each batch after calcination. If the measurement did not show conclusively that the moisture content was below 0.5 mass %, further pre-treatment was performed and the measurement was repeated. The 0.5 % threshold was chosen to assure that even if complete conversion of the hydrogen content of the water to $H_2(g)$ occurred, the resulting total gas pressure would be below the design limit of the container in all cases.

Several analytical techniques of varying specificity were employed to measure moisture content depending on the facility and the type of material. The most common technique employed for plutonium oxides was thermo-gravimetric analysis (TGA). Mass changes of

samples (~ 3 grams) from each batch were measured as a function of time during a temperature ramp to 1000 °C under a flowing stream of argon. For the purposes of certifying that a container met the 0.5 % criterion, all mass loss in the TGA data was assumed to be due to H_2O. This interpretation of the TGA data made it a conservative technique with considerable bias toward over-estimating moisture for some materials due to evaporation of NaCl and KCl at high temperature. In approximately 20% of the cases FTIR spectroscopy or mass spectrometry were performed on the effluent gas from the TGA to obtain more specific measurements of moisture.

The different techniques gave reported moisture content values that are quite diverse in their uncertainties and inherent biases. This was acceptable for certification that storage criteria were being met because a conservative measure of moisture was more important than an accurate measure. However, there are other potential uses for moisture content that would benefit from greater accuracy. Among these is the identification of the containers in storage with the highest moisture content for more frequent surveillance. There is also potentially useful information in the correlations between moisture content and the major impurities, the origin and processing history of the material, and the different handling protocols that were employed in the packaging campaigns.

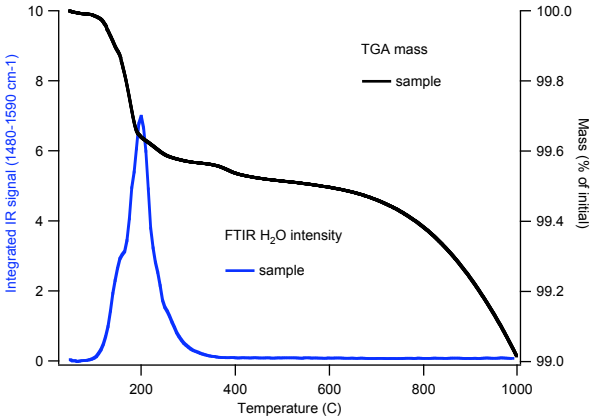

Fig.1: TGA and H_2O-specific FTIR data from a sample containing alkali halide impurities and approximately 0.4 % moisture.

Fortunately, the raw data from all the techniques were retained and could be analyzed later in greater depth to obtain more accurate moisture estimates. As expected, the results show that true moisture content is substantially lower in general than values estimated from total TGA mass loss. The handling atmosphere had the largest effect on residual moisture content. Where material was stabilized and packaged in a dried air atmosphere (~1000 ppm H_2O), residual moisture had a median below 0.02 mass % and rarely exceeded 0.05 mass %. Batches handled in humid air had a median moisture content between 0.05 and 0.1 % with a few as high as 0.4 mass %. To the extent that impurity contents are known, there appear to be correlations with moisture content, though we are have not completed those analyses as of this writing.

Though too numerous to list here, we acknowledge the many people who developed the moisture measurement methods and who collected the data. We specifically thank Ted Venetz and G. Scott Barney for providing the raw data from the Hanford campaign and Mark Brugh for providing the raw data from the Rocky Flats campaign. This work was supported by the United States Department of Energy under the Surveillance and Monitoring Program, Materials Identification and Surveillance Project.

1 DOE-STD-3013-2004 "Stabilization, Packaging, and Storage of Plutonium-bearing Materials", United States Department of Energy, 2004.

Reaction mechanisms of the thermal conversion of Pu(IV) oxalate into plutonium oxide

N. Vigier[1], S. Grandjean[1], B. Arab-Chapelet[1], F. Abraham[2]

[1] CEA Valrhô Marcoule, DRCP/SCPS/LCA, Bât 399, BP 17171, 30207 Bagnols-sur-Cèze, FRANCE
[2] UMR CNRS 8012, ENSCL-USTL, LCPS, B.P. 108, 59652 Villeneuve d'Ascq Cedex, France

INTRODUCTION

During the oxalic conversion of plutonium into oxide at the end of the PUREX process, the thermal transition of Pu(IV) oxalate into oxide plays a significant role leading to the main properties of the oxide. The structure of the solid intermediates is often speculating and the reaction mechanisms are quite misunderstood and divergent from a study to another [1-7]. This work deals with a detailed structural investigation on the main solid intermediates encountered when calcining Pu(IV) oxalate into oxide under air or argon.

EXPERIMENTAL METHODS

The Pu(IV) oxalate precipitate, $Pu^{IV}(C_2O_4)_2,6H_2O$, was prepared by mixing an acid Pu(IV) nitrate solution and a concentrated $H_2C_2O_4$ solution in a vortex effect reactor with a slight excess of $H_2C_2O_4$. The resulting crystallized powder was filtered off and dried at room temperature.
Thermogravimetric analyses (TG) were carried out with a NETZSCH STA 409C thermal analyzer using alumina crucibles, under argon or air flow at a gradient of 2°C min^{-1} up to 700°C.
Solid intermediates were isolated at specific temperatures for structural investigations.
X-ray powder diffraction data were acquired with an INEL CPS 120 diffractometer (curved position sensitive detector) using Cu-$K_{\alpha 1}$ radiation isolated by a germanium monochromator. Silicon or gold was used as an internal standard. Each solid sample was mixed to an epoxy resin in order to fix up the contamination.
UV-visible spectra of the solid intermediates and products were acquired between 400 and 800 nm with a HITACHI U-3000 analyzer equipped with an integration sphere.
Infrared (IR) spectra of all samples were recorded with the NICOLET MAGNA IR 550 series II. A spectral range from 400 to 4000 cm^{-1} was typically investigated.

RESULTS

A typical TG plot is shown on figure 2 (static air). Each intermediate was identified by extrapolating the molecular formula from the mass loss, or by structural analyses (XRD, UV-Visible, IR) of the isolated solid after stopping the heating at the corresponding temperature. Only two isolated intermediates were not strictly identified due to their particular instability: $Pu^{IV}(C_2O_4)_2,H_2O$ and $Pu^{IV}(C_2O_4)_2$. Both compounds reacts quasi-instantaneously with trace amounts of water to form again $Pu^{IV}(C_2O_4)_2,2H_2O$. Under air, the transitory reduction of Pu(IV) into Pu(III) is for the first time established directly by structural analysis of the solid intermediates: the Pu(III) intermediates are mixed oxalate-carbonate structures and not anhydrous Pu(III) oxalate as previously stated [1, 5-7].
The same investigations were led using Ar atmosphere instead of air. If transitory plutonium reduction is observed using both atmospheres, the nature of the corresponding Pu(III) solid intermediate(s) was found significantly different.

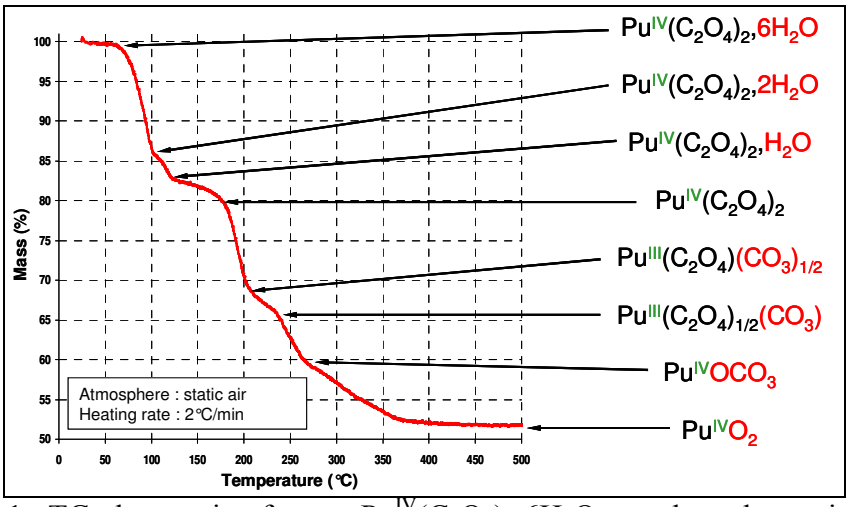

Fig. 1 : TG plot starting from a $Pu^{IV}(C_2O_4)_2,6H_2O$ sample under static air.

The proposed reaction mechanism leading to plutonium oxide under air is detailed in figure 2. This schematic path differs very significantly from that obtained under argon stream.

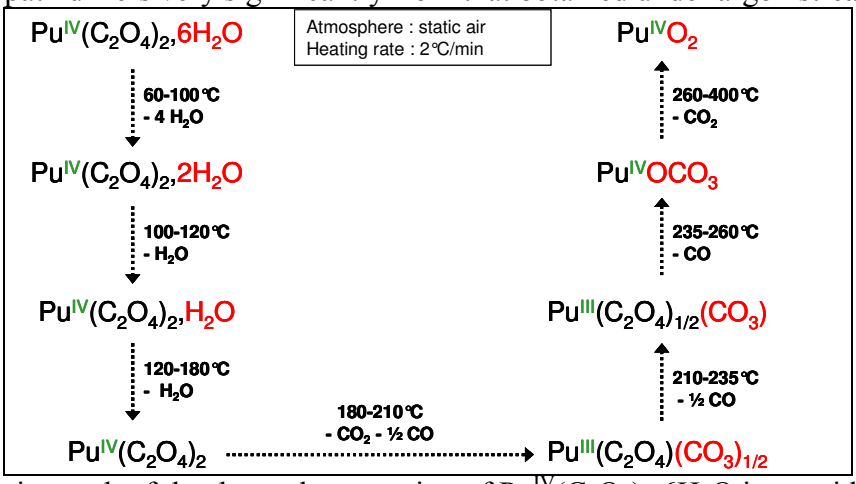

Fig. 2 : reaction path of the thermal conversion of $Pu^{IV}(C_2O_4)_2,6H_2O$ into oxide under air.

CONCLUSION

The reaction mechanism of the thermal treatment of $Pu^{IV}(C_2O_4)_2,6H_2O$ into oxide under air or argon was thoroughly investigated using TG analysis and structural analysis of the solid intermediates. Distinct reaction paths were established depending on the atmosphere used.

REFERENCES

[1] M.N. Myers, U.S.A.E.C, document HW 45128 (1956).
[2] G.S. Rao, M.S. Subramanian, G.A. Welch, J. Inorg. Nucl. Chem. 25 (1963) 1293-1295.
[3] I.L. Jenkins, M.J. Waterman, J. Inorg. Nucl. Chem. 26 (1964) 131-137.
[4] A. Glasner, J. Inorg. Nucl. Chem. 26 (1964) 1475-1476.
[5] D.A. Nissen, J. Therm. Anal. 18 (1980) 99-109
[6] R.D. Kozlova, A.I. Karelin, O.P. Lobas, V.A. Matyukha, Radiokhimiya, 26 (3) (1984) 311-316.
[7] A.I. Karelin, N.N. Krot, R.D. Kozlova, O.P. Lobas, V.A. Matyukha, J. Radioanal. Nucl. Chem. 143 (1) (1990) 241-252.

Pu association with Corroded Magnox Sludge: Relevance to Storage Pond Management, Future Remediation Strategy and Effluent Treatment

S.A. Parry[*], F.R. Livens[*], L. O'Brien[†]

[*]Centre for Radiochemistry Research, School of Chemistry, University of Manchester, Oxford Road, Manchester, M13 9PL.
[†]Nexia Solutions, Sellafield, Seascale, Cumbria, CA20 1PG, UK.

Background: Managing Pu-contaminated Corroded Magnox Sludge

"Magnox" fuel elements were developed for use in the UK's first generation reactors, and comprise a natural uranium core supported by a magnesium-rich alloy cladding. Spent fuel rods are stored in water-filled storage ponds, mostly at the Sellafield site (Windscale, Cumbria), under carefully controlled conditions to minimise corrosion of the Magnox cladding. However, the Magnox alloy cladding corrodes readily in water, and over the last 50 years, some 12000 m^3 of contaminated sludge has accumulated at UK facilities.

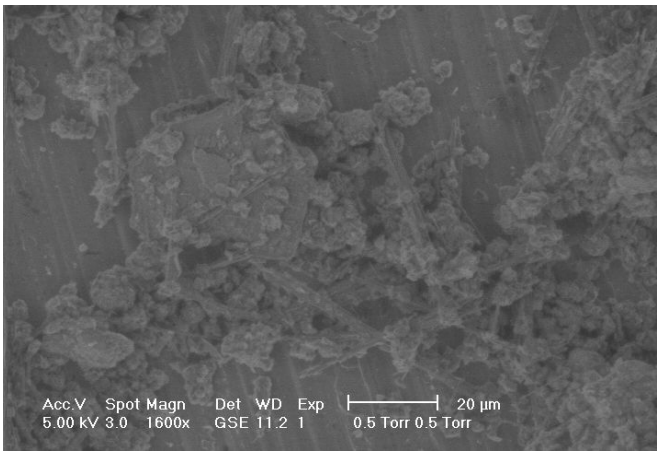

Fig. 1: Environmental scanning electron microscope (ESEM) image of CMS sludge illustrating platy brucite crystals and needle-like artinite crystals.

Corroded Magnox sludge (CMS) is generally believed to compromise brucite, $Mg(OH)_2$, which is very soluble at neutral and acid pH. As a result, the storage ponds are maintained at pH>10, conditions which facilitate carbonation through reaction with atmospheric CO_2.

CMS is contaminated with highly radioactive isotopes from the spent fuel, in particular Pu, which is difficult to manage in these high pH, aqueous systems, since the most stable oxidation state, Pu (IV), is very susceptible to a complex series of hydrolysis reactions leading to the formation of colloidal and/or surface reactive species, depending on conditions. In addition, Pu (IV) solubility will be further affected by the presence of carbonate, since soluble ions such as $[Pu(CO_3)_5]^{6-}$ can be formed.

Because the highly radioactive, Pu-contaminated CMS dissolves easily, it is amongst the highest priority wastes for immobilisation prior to disposal. However, the nature of the waste is not well understood, indeed our current work has shown that the evolution of the CMS is more complex than originally thought. Therefore, before a remediation strategy can be developed, knowledge of the composition and evolution of the aging CMS, and the behaviour of the association of Pu with the sludge must be acquired.

Experimental Assessment of Factors Controlling Pu Mobility

At present the discharge from the storage ponds passes through an effluent treatment plant prior to release into the environment. However, the complex chemistry of Pu and CMS make Pu mobility and discharge difficult to predict. Therefore, we have performed a full-factorial experiment to assess quantitatively the control a range of factors (reagents, particulate, and solution pH) have on the solubility of Pu prior to, and during effluent treatment.

Our experimental approach in addressing this problem has taken a second line to investigate the nature of the fine particulate, CMS and identify the phases present. Our initial characterisation of inactive CMS simulant has shown it to consist of brucite and additionally the mineral artinite, $Mg_2CO_3(OH)_2.3H_2O$ (Fig. 1), likely formed through reaction of the highly alkaline waste sludge with atmospheric CO_2.

To assess the factors controlling Pu solubility we have used filtration experiments to identify the conditions/reagents that yield hold-up of Pu on a 0.2 μm filtration membrane, either as Pu-colloid or Pu associated with particulate. The 0.2 μm molecular size cut-off prevents a conclusive assessment if the Pu remains truly in solution but provides a valuable first approximation, and an insight as to which factors may be significant in controlling Pu solubility during effluent treatment.

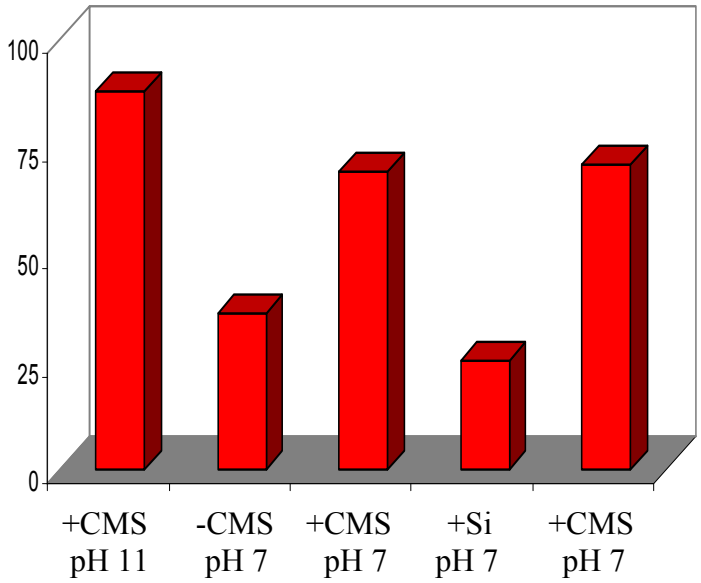

Fig. 2: % of Pu (IV) retained on a 0.2 μm filter

The results (Fig. 2) show that the presence of CMS and Si, likely to generate particulate and/or colloidal particles in aqueous solution results in filtration of Pu. The results also indicate dissolution of Pu following a reduction in pH, from pH 11 to pH 7.

Self-irradiation damage in zirconolite for minor actinides immobilization

X. Deschanels, V. Broudic, S. Peuget, C. Jegou, D. Roudil

CEA Valrhô Marcoule, BP17171, 30207 Bagnols-sur-Cèze, France

INTRODUCTION

Zirconolite is a potential host phase for the conditioning of the minor actinides arising from the reprocessing of the spent fuel [1-4]. In order to study the consequences of the self-irradiation damage on this structure, samples doped with 10wt.% of $^{238}PuO_2$ were fabricated. This article reports the result obtained on the evolution of macroscopic properties (initial alteration rate, swelling, hardness) of this material up to an integrated dose of $5\times10^{18}\alpha.g^{-1}$.

EXPERIMENTAL

Forty ^{238}Pu doped pellets were fabricated in hot cells by natural sintering. The relative density of all these pellets exceeded 91%. Polished cross sections of these samples were examined by scanning electron microscopy (SEM) coupled with X-ray microanalysis (EDX) and X-ray diffraction analysis to check their homogeneity. The macroscopic swelling was determined from sample density measurement by hydrostatic weighing in water. The ceramic hardness was measured in air by Vickers micro-indentation on polished specimens, with indenter loads of 100 g maintained for 5 s.

The dissolution characteristics of the ceramics were determined by Soxhlet-mode dynamic leach testing at 100°C during 55 days. The mean alteration rate of the ceramics was measured by analysing the release of plutonium at the end of the test and by measuring the sample weight loss.

Some pellets were annealed continuously at 250 and 500°C in order to evaluate the evolution of their macroscopic swelling and the recovery of their crystallographic structure under these conditions.

RESULTS

The ^{238}Pu-doped pellets fabricated for this study become X-rays amorphous for a dose close to $5\times10^{18}\alpha.g^{-1}$ at room temperature. This result is in good agreement with others published earlier [3-4].

The figure 1 shows the measured macroscopic swelling versus the integrated dose. This swelling was about 6% at room temperature for an integrated dose of 5×10^{18} g^{-1}. Up to an integrated dose of $10^{18}\alpha.g^{-1}$, the microscopic swelling estimated from X-ray diffraction analysis is close to the macroscopic one. This result suggests that both phenomena have the same origin, i.e. the production of point defects in the structure. The swelling also generates microscopic cracks within ceramics. The pellets annealed at 500°C recovered their initial density and their crystalline structure (Fig. 2).

The hardness of the samples decreases by approximately 25% compared to its initial value, when the integrated dose reached $3\times10^{18}\alpha.g^{-1}$. Similar behaviour has also been reported by Weber [5].

The results of leaching test indicate a good behaviour of this matrix which has an initial leaching rate lower than 10^{-2} g.m^{-2}.j^{-1} if it is calculated on the variation of mass, and about 10^{-4} g.m^{-2}.j^{-1} if it is based on the release of plutonium in the leachate.

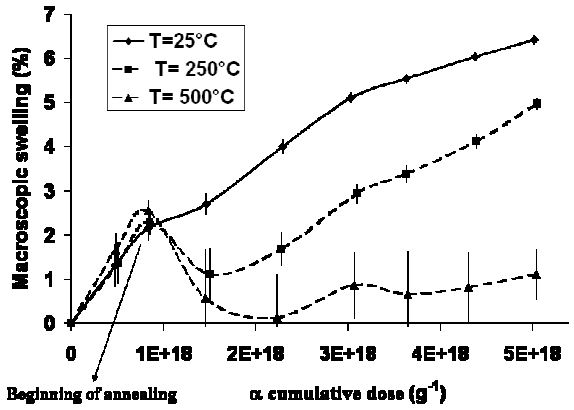

Fig. 1 : Macroscopic swelling vs. Integrated dose for samples stored at room temperature, at 250 and 500°C.

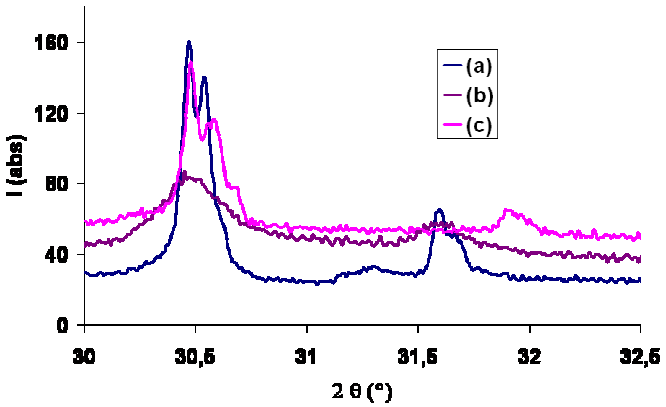

Fig. 2 : Recovery of the structure for peaks corresponding to planes [221] 2θ=30,5° and [-402]: (a) sample after annealing at 500°C (α dose = 2,4 10^{18} α g^{-1}); (b) sample stored at room temperature (α dose = 2,2 10^{18} α g^{-1}); (c) initial state (α dose = 8 10^{17} α g^{-1}).

The consequences of the production of helium were not evaluated in this work. The available data on helium thermal diffusion [1] indicate that this is a relatively slow process (10 micrometers traversed in 100 years at 300°C). It is reasonable to think that a part at least of helium will remain occluded in material and that it will be able to have a long-term impact on the swelling of the pellets. Complementary work will have to be undertaken to evaluate this point.

CONCLUSION

Doping zirconolite with ^{238}Pu allows us to obtain after only 4 years interesting results on the long term behaviour of this structure. At integrated dose below 5 10^{18} α.g^{-1} the ceramic exhibits satisfactory resistance to self-irradiation and good defect healing behaviour at relatively low temperature. The consequence of helium production at higher concentration approaching 2 10^{19} He.g^{-1} (or 0.1 at.%) have to be investigated soon.

The authors thank T. Advocat and F. Jorion for their contribution to this study.

1 F. Jorion, *et al.* , *accepted in Nucl. Sci. Eng*., (2006).
2 X. Deschanels, *et al., accepted in J. Nucl. Mat.*, (2006).
3 D.M. Strachan, *et al.,* J. Nucl. Mat., **345**, (2005).
4 F.W. Clinard, Am. Ceram. Soc. Bull., **65** (1986).
5 W.J. Weber, J.W. Wald, Hj. Matzke, J. Nucl. Mat. **138,** (1986).

SHS method for immobilization of plutonium-containing waste

Levakov Eu.V., Postnikov A.Yu.

(RFNC - VNIIEF, Russia, Sarov)

Glagovskyi E.M., Kuprin A.V., Bogdanov A.I., Pelevin L.P.

(VNIINM, Russia, Moscow)

The main results of work in the area of technology development for immobilization of highly active waste (HAW) and, in particular plutonium-containing ones into mineral-like array compounds using the method of self-spreading high-temperature synthesis (SHS) are presented.

The choice of mineral-like arrays for HAW immobilization is proved. According to the results of thermodynamic calculations the availability of systems' formation based on zirconolite, pyrochlorine and other mineral-like compounds under SHS mode has been shown. The conditions influencing on both characteristics of SHS systems combustion and quality of obtained materials have been studied to optimize the technological parameters of SHS mineral-like arrays.

Base technological modes for SHS compacting of arrays based on pyrochlorine containing HAW simulators have been tested.

It is shown that the parameters of hydrothermal stability of arrays formed by SHS methods are similar to the same ones in arrays got by the method of cold compacting- sintering. Based on the experimentally got results the stands for immobilization of HAW simulators by SHS have been created.

Glass Fabrication and Product Consistency Testing of Lanthanide Borosilicate Glass for Plutonium Disposition

C. Crawford, J. Marra, N. Bibler

Savannah River National Laboratory, Aiken SC 298008 USA

INTRODUCTION AND BACKGROUND

The Department of Energy Office of Environmental Management (DOE/EM) plans to conduct the Plutonium Disposition Project (PDP) at the Savannah River Site (SRS) to disposition excess plutonium.[1] A plutonium glass waste form is the leading candidate for immobilization of the plutonium for subsequent disposition in a geological repository. Reference Lanthanide Borosilicate (LaBS) glasses, developed during the former Plutonium Immobilization Program (PIP), were originally studied in 1995/96. Current FY06 PDP research and testing being conducted at the Savannah River National Laboratory (SRNL) addresses several near term data needs identified by DOE/EM and the Yucca Mountain Repository. Our initial phase studies have examined the LaBS glass dissolution and subsequent fate of plutonium and the neutron absorbers during the dissolution processes, and the degree of macroscopic cracking that occurs during processing of the Pu glass waste form and subsequent pouring of High-Level Waste (HLW) in the Defense Waste Processing Facility (DWPF). We have also investigated frit formulations to improve durability and processability of the Pu-LaBS glass. This presentation will focus on the durability testing of a baseline Frit B LaBS glass containing 9.5 wt% PuO_2. The Frit B LaBS formulation resulted from earlier PIP testing.[2]

RESULTS

This study was performed with the baseline Frit B LaBS glass with frit composition shown in Table 1. A Frit X formulation is also shown in Table 1 that includes increased rare earth elements and decreased aluminum and silicon. The Frit X formulation should have improved qualities for PuO_2 immobilization and has recently been used to successfully vitrify a 9.5 wt% PuO_2 LaBS glass that will be tested in upcoming studies in the SRNL. For the tests in the current program, plutonium LaBS glass was fabricated at SRNL using Frit B material that was vitrified from reagent grade chemicals in Pt/Rh crucibles at 1500 ºC melt temperature for 2 hours, followed by quench-pouring. This cullet frit was ground to -325 mesh and mixed with PuO_2 powder in the SRNL shielded cells facility via remote handling. The PuO_2 LaBS glass was fabricated in Pt/Rh crucibles at 1500 ºC for 4 hours, followed by water quenching. The resulting PuO_2 glass was crushed, mixed and remelted to enhance

Table 1. LaBS Glass Frit Compositions

Oxide	Frit B (wt%)	Frit X (wt%)
Al_2O_3	21.3	9.0
B_2O_3	11.6	11.7
Gd_2O_3	12.8	12.15
HfO_2	6.6	6.3
La_2O_3	8.1	17.1
Nd_2O_3	8.2	13.5
SiO_2	28.9	18.0
SrO	2.5	2.25

homogenization of the glass. The glass density measured by water displacement using > 100 mesh glass powder in a pycnometer was determined to be 3.57 g/cm^3. A significant finding from XRD and SEM characterization of the washed and dried powdered PuO_2 LaBS glass is the presence of trace, perhaps 1 vol%, amounts of undissolved PuO_2 in the glass. It could be that this undissolved PuO_2 in the glass is result of incomplete mixing of the glass precursors (PuO_2 powders mixed with the -325 mesh Frit B powders in a polybottle via remote handling) before fabrication. Future studies could examine other means of mixing such as mechanical mixing to better blend the PuO_2 powder in with the frit precursor powder.

The Product Consistency Test (PCT) is an ASTM standard Test (ASTM 1285-02) for leaching nuclear waste forms. This is the leach test used for the Frit B Pu-glass at SRNL discussed in this paper. As part of this SRNL program, other corrosion testing is planned at Argonne National Laboratory (ANL) involving monolithic leach tests and vapor hydration testing (VHT), as well as at the Pacific Northwest National Laboratory (PNNL) involving flow methods (Single-Pass Flow-Through (SPFT) and Pressurized Unsaturated Flow (PUF). Our PCT results performed from 7 to 56 days at 90ºC, using varying surface area to volume (SA/V) ratios of 1500 m^{-1} to 20,000 m^{-1}, indicate that normalized release of all Pu Frit B glass components including Pu are in the range of 10-100X lower than normalized release of Al, B and Si from the reference Environmental Assessment (EA) glass.[3] The PCT testing was carried out in both steel and Teflon® vessels using ultrapure water (ASTM Type 1) as lechant. The leachates were filtered and vessels acid-stripped.

Colloidal plutonium species have been observed in previous Pu-glass corrosion studies involving the accelerated dissolution associated with the PUF test.[4] The PCT leachates from this current study were examined after both syringe-filtration with 0.45 µm filters, and 30,000 nominal molecular weight limit (NMWL) ultrafilters capable of excluding colloids. Comparison of the different filtered leachate solutions indicates no significant differences in the plutonium concentrations (determined by ICP-MS), indicating that plutonium colloid formation does not occur under these PCT test conditions. Alteration secondary phases can form on the surface of glass powders used in long term, e.g. 120-240 day PCT's, and in PUF corrosion tests.[4] The leached glass from our 28-day and 56-day PCT's performed in Teflon® at 90 ºC and 20,000 m^{-1} SA/V were thus characterized by SEM to examine the glass powder surfaces after leaching. No evidence of any alteration phases were observed from these leached glasses using SEM imaging capable of 1 to 100 µm resolution. Further details on the LaBS frit development, Pu glass fabrication, and Pu glass dissolution testing results will be presented in this paper and compared to previous published data.

REFERENCES

1. US Federal Budget, FY2006, Fissile Materials Disposition, 10 Million $ Appropriation for Conceptual Design Activities for the Plutonium Immobilization Facility at the SRS, DOE/EM (http://thomas.loc.gov/).
2. N. E. Bibler, *et al*., Mat. Res. Soc. Symp. Proc., Vol. 412, Materials Research Society, Pittsburgh, PA, (1996).
3. C. M. Jantzen, *et al*., Ceramic Transactions, Env. And Waste Management Issues in the Ceramic Industry, Vol. 39, American Ceramic Society, Westerville, OH, (1994).
4. B. P. McGrail, *et al.*, PNNL-11834, UC-2030, Pacific Northwest National Laboratory, Richland, WA, October (1998) (and references cited therein).

Diffuse reflectance spectroscopy of actinide ions in polycrystalline ceramics designed for immobilisation of HLW

Y. Zhang, E. R. Vance, B. D. Begg

Australian Nuclear Science and Technology Organisation, PMB 1, Menai 2234, Australia

INTRODUCTION

Diffuse reflectance spectroscopy (DRS) is a useful tool for deriving information about actinide speciation in the solid state and has been used to probe uranium valences in polycrystalline brannerite[1] on which a number of intraconfigurational *f-f* electronic absorption bands for $U^{4+}(5f^2)$ and $U^{5+}(5f^1)$ ions have been observed over the near infrared (NIR) range (4000-12000 cm^{-1}), and plutonium valences in zirconolite[2]. It is of interest in the nuclear waste form application to study systematically the DRS spectra of actinide ions in other actinide-bearing ceramic phases, e.g. perovskite, zirconolite, pyrochlore and monazite.

EXPERIMENTAL

Samples doped with various amounts of U/Np/Pu were made by the standard alkoxide/nitrate route[3] and sintered at around 1400°C for 16-20 hrs under air/argon/H_2-N_2 atmospheres as appropriate. X-ray diffraction and scanning electron microscopy confirmed that the samples were essentially single-phase.

Roughly polished (200 grit SiC) disc samples were used for DRS measurements at ambient temperatures over the NIR range (4000-12000 cm^{-1}) using a Cary 500 spectrophotometer equipped with a Labsphere Biconical Accessory. Spectra were converted into Kubelka-Munk units, $F(R)=(1-R)^2/2R$, by reference to the spectrum of a Labsphere certified standard (Spectralon).

RESULTS AND DISCUSSION

U^{4+}/U^{5+}

Like U^{4+} ions in $ThTi_2O_6$[1], U^{4+} ions in perovskite, zirconolite, pyrochlore-rich ceramic and zirconolite glass-ceramic show weak bands in the visible and NIR regions and show rather similar spectral features. In contrast to the DRS spectra of U^{4+}, DRS spectra of U^{5+} are much simpler with only a small number of intraconfigurational *f-f* transition bands in the NIR region and they are fairly similar for different ceramics. The U^{5+} bands slightly shift to the IR direction when the U coordination numbers increase, from 6-fold for brannerite to 8 and/or 7 for pyrochlore and zirconolite. Compared to the free ion energy levels[4], the observed band shifts, splittings, intensities and additional bands are related to the actual U ion site symmetries in the ceramic crystal structures.

Np^{3+}/Np^{4+}

Sintering samples in air or argon always gives rise to the formation of Np^{4+}. Np^{3+} can be formed at reducing conditions in perovskite and in monazite but not in zirconolite under reducing conditions. Reduction of perovskite samples by heating in 3.5% H_2/N_2 atmosphere to produce Np^{3+} generally led to increased absorption (with the samples turning black in color) and broadly

featureless spectra, obliterating any weak Np^{3+} absorptions. However, for samples containing 0.1 formula units (f.u.) of Np, characteristic absorption peaks for Np^{3+} at around 4100 cm^{-1} could be detected for both samples with or without Al on the Ti-site as charge compensators, and distinctly different from Np^{4+} spectra.

The DR spectrum of a zirconolite sample sintered in air with 0.01 f.u. of Np^{4+} on the Ca site is similar to that of a perovskite except an additional sharp and strong transition band at around 7000 cm^{-1} due to the lower Np site symmetry in zirconolite. There appeared to be little difference in the electronic spectra between Np^{4+} in the Ca vs the Zr site of zirconolite as the crystal field splittings in the two kinds of sites cannot be distinguished at ambient temperature due to the band broadening and overlapping.

Pu^{3+}/Pu^{4+}

The DR spectra of Pu ions give rise to a number of unresolved intraconfigurational f-f electronic absorption bands of a few hundred cm^{-1} bandwidth. No clear spectral differences were evident when Pu^{4+} was targeted to Ca or Zr sites in zirconolite. Samples prepared in reducing atmospheres with a view to producing Pu^{3+} were strongly absorbing, leading to suppression of Pu transitions. Evidence for Pu^{3+} in perovskite and zirconolite under reducing conditions has been obtained previously by XANES[5].

In general, there was approximate agreement of the Kubelka-Munk absorption intensities with Beer's Law for the different actinide ions at low concentrations (0.001-0.03 f.u.) in most of the ceramics studied. It would appear that U spectra are most sensitive to valence change (U^{4+}/U^{5+}) and site symmetry whilst Np (Pu^{3+}/Pu^{4+}) and Pu (Pu^{3+}/Pu^{4+}) are not.

We would like to thank Alan Brownscombe and Terry McLeod for sample preparations.

1 K. Finnie, Z. Zhang, E. R. Vance and M. L. Carter, *J. Nucl. Mater.*, **317** (2003) 46-53.
2 E.R. Vance, K.S. Finnie, Y. Zhang and B.D. Begg, "Diffuse Reflectance Spectroscopy of Pu Ions in Zirconolite", *Scientific Basis for Nuclear Waste Management* XXVIII, Eds. J. M. Hanchar, S. Stroes-Gascoyne and L. Browning, Materials Research Society, Warrendale, PA, USA, pp. 261-6.
3 E.R. Vance, Materials Research Society, MRS Bulletin, Vol. **VIX**, **12** (1994) 28-32.
4 W.T. Carnall and H.M. Crosswhite, ANL-84-90, Argonne National Laboratory, USA.
5 B.D. Begg, E.R. Vance and S.D. Conradson, *J. Alloys Compds.*, 271-273 (1998) 221-226.

Plutonium Oxide Polishing for MOX Fuel Fabrication

F. Coriz[1], J. Danis[1], D. Gray[1], D. Martinez[1], J. Martinez[1], C. Martinez[1], Y. Martinez[1], D. Garcia[1], J. Royba[1]l, B. Griego[1], M. Saba[1], J. Valdez[1], K. Ramsey[2], J. Alwin[1], D. Costa[2]

[1]Actinide Process Chemistry Group, NMT-2, Nuclear Materials Technology Division, Los Alamos National Laboratory, Los Alamos, NM 87545 USA
[2] Pit Disposition Science & Technology Group, NMT-15, Nuclear Materials Technology Division, Los Alamos National Laboratory, Los Alamos, NM 87545 USA

Los Alamos National Laboratory (LANL) was successful in polishing 120 kg of plutonium as highly purified PuO_2 for the European Mixed Oxide (MOX) Lead Test Assembly (LTA) managed by Duke, COGEMA, and Stone & Webster (DCS). The purified oxide has been successfully fabricated into fuel pellets that went into making the lead test assembles (LTAs). The LTAs have been inserted into the Catawba nuclear reactor located in South Carolina which is presently generating electricity, using MOX fuel produced from surplus nuclear weapons.

This project has been recognized as representing the first plutonium oxide for LANL that was polished under the quality requirement of the Nuclear Regulatory Commission (NRC). In addition, the project has been credited as one of the "largest single nonproliferation project in history" by US Ambassador Linton Brooks (9/23/04). The process flow sheet for PuO_2 purification was based on aqueous recovery that included several unit operations (dissolution, ion exchange, oxalate precipitation, and calcination). Data from the chemical and physical test will be presented to show product quality and consistency in the production phase of this project. In addition, upcoming optimization experiments will be presented in preparation to polish an additional 330 kg of PuO_2 for the Fuel Pellet Fabrication Facility in Savanna River. For example, during the production phase of this project in early 2003, it was determined that the ion exchange unit operation was a waste-intensive and inefficient process that needed improvement. In order to meet the stringent impurity specification for the MOX PuO_2 Polishing Project, approximately 500 L of 7 M nitric acid was used for washing impurities from the plutonium. Yearly production capacity is projected to be at 90 kg of purified PuO_2, which would generate 30,855 L of Transuranic Waste (TRU) liquid waste to be dispositioned using an evaporation process. Currently, the distillates from the evaporation process are sent to the LANL Radioactive Liquid Waste Treatment Facility (TA-50) for further treatment.

In order to reduce or eliminate the waste stream dependency on sending the distillate to an external treatment facility and advancing the Laboratory's mission on reducing waste generation, LANL has identified an avenue to recycle the processed distillate (7M HNO_3) back into the aqueous polishing process (ion exchange). To ensure quality assurance and control, LANL will first test the recycled acid to ensure that no additional contaminates are introduced into the ion exchange process, inadvertently causing the product oxide to fail specification requirements. The qualification exercise will include running a series of ion exchange

experiments using the recycled acid and analyzing the product oxides impurity levels. Based upon a successful qualification exercise, aqueous polishing has estimated using 24,375 L of recycled nitric acid out of the 30,855 L of effluent sent to the evaporation process. NMT-2 projects recycling 79% of the effluent as 7M acid back into the anion exchange process, reducing the nitric acid waste sent to LANL's Radioactive Liquid Waste Treatment Facility.

The role of magnesium chloride in gas generation and corrosion during storage of impure plutonium oxides

Eduardo Garcia[*], Patricia Bielenberg[†], Kirk Veirs[*], John Berg[*], Adam Montoya[*], Max Martinez[*]

[*]Los Alamos National Laboratory, Los Alamos NM 87545 USA
[†]ExxonMobile, Baton Rouge LA

INTRODUCTION

Of the 3322 containers packaged under DOE's 3013 Standard[1] at Hanford, Rocky Flats, and Livermore, 1290 (39%) have been identified as potentially susceptible to pressurization or corrosion.[2] The vast majority of these containers have chloride salt impurities. Initial studies of materials representative of this class of stored material have shown unexpectedly high rates of hydrogen generation and corrosion.[3] Corrosion occurs in 304L stainless steel and in heat affected zones of welds in 316L stainless steel as shown in Fig. 1. Pure plutonium oxide with the same amount of moisture generates hydrogen at lower rates with no observable corrosion.

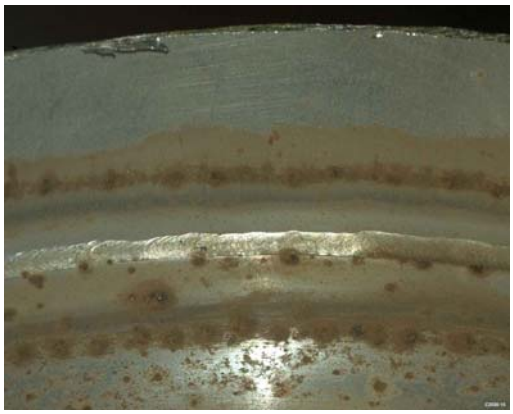

Fig 1: Pitting corrosion formed on the interior surface of a container filled with a stabilized material of 80% PuO_2 and 20% salt with 0.2wt% water. The weld joins 316L (above) to 304L (below).

Electrorefining processing salts contain equimolar mixtures of NaCl and KCl with added anhydrous $MgCl_2$. Stabilization of these salts by calcining was thought to destroy the $MgCl_2$ component by hydrolysis resulting in MgO. These materials pickup moisture rapidly at low relative humidities (RH), indicating that some of the $MgCl_2$ survives calcination because NaCl and KCl do not pickup moisture until their deliquescent point, which is above 70% RH. Thermal gravimetric analysis of materials after calcination with FTIR identification of the evolved gases show HCl being evolved at low temperatures, ~ 200°C, which is consistent with thermal hydrolysis of hydrated $MgCl_2$. In order to identify the role $MgCl_2$ plays in these observations, we have (1) conducted x-ray diffraction studies of salt mixtures to identify the $MgCl_2$ containing component, (2) identified the soluble constituents of calcined salts to see if Mg is present, and (3) conducted hydrogen gas generation studies to see if $MgCl_2$ containing salts generate gas at sufficient rates.

X-RAY DIFFRACTION STUDIES

Magnesium chloride is known to form double salts with alkali metal chlorides of formula $XMgCl_3$ and X_2MgCl_4, where X is Na or K. These salts are hygroscopic but their hydration behavior has not been quantitatively characterized. However, the $XMgCl_3$ salts have been shown to adsorb water and form the hexahydrate just as $MgCl_2$ does. In the equimolar NaCl/KCl

mixture with small amounts of added $MgCl_2$, the magnesium component appears to be a $Na_yK_{2-y}MgCl_4$ salt where y is less than one. This salt appears to pickup water at low RH to form a hydrate in a manner very similar to $MgCl_2$.

SOLUBLE MAGNESIUM AND GAS GENERATION STUDIES

One gram samples of twelve calcined materials representative of materials in 3013 containers were dissolved in 100 ml of water and then filtered to remove the insoluble oxides, which were mainly PuO_2. The soluble components were measured using ion selective electrodes for Na, K, Cl and F and ICP/AES for Ca, Cr, Fe, Ni, Mg, Mn, and Mo. The pH and conductivity were also measured. Chemical analysis of the starting material was also available. The fraction of the total magnesium that was soluble varied from less than 1% to 27%. The correlation between soluble magnesium and hydrogen gas generation is given in Table I. Two materials, 520610020 and 053038, have high gas generation rates for the amount of soluble magnesium. These materials have high soluble calcium content. Calcium chloride also adsorbs water and will hydrolyse thermally, but at much higher temperatures than $MgCl_2$.

Table 1 The soluble Mg and Ca content of salt bearing MIS representative materials and the hydrogen gas generation rate.

Material	Soluble Mg (wt%)	Total Mg (wt%)	Soluble Ca (wt%)	H_2 rate (kPa/day)
520610020	0.001%	8.50%	5.526%	0.27
TS707001	0.002%	0.01%	0.024%	0.03
PMAXBS	0.016%	0.24%	0.006%	0.15
07242201A	0.023%	0.17%	0.274%	0.13
053038	0.038%	0.79%	1.583%	0.61
ARF-102-85-365	0.050%	0.56%	0.000%	0.40
CLLANL025	0.062%	0.38%	0.000%	0.52
011589A	0.086%	2.26%	0.251%	0.68
ARF-102-85-295	0.157%	4.04%	0.064%	0.60
ARF-102-85-223	0.157%	0.59%	0.002%	0.78
C00695	0.174%	0.95%	0.014%	1.37
C06032A	0.218%	2.15%	0.000%	1.29

CONCLUSION

Magnesium chloride present in plutonium processing salts survives calcination and adsorbs water from the atmosphere. The resulting hydrated salt will radiolysis producing hydrogen gas. Corrosive gases are also produced with the most likely candidate being HCl.

1 DOE-STD-3013-2000, “Stabilization, packaging, and storage of plutonium-bearing materials”, U.S. Department of Energy, Washington, D.C. 20585.

2 E. Kelly, L. Peppers, K. Veirs, and J. Berg, LA-UR-05-2193.

3 Veirs, D. K.; Worl, L. A.; Harradine, D. M.; Martinez, M. A.; Lillard, S.; Schwartz, D. S.; Puglisi, C. V.; Padilla, D. D.; Carrillo, A.; McInroy, R. E.; Montoya, A. R., LA-14148.

Recent Studies of Uranium and Plutonium Chemistry in Highly Alkaline Radioactive Wastes

W. King[*], D. Hobbs[*], and W. Wilmarth[*]

[*]Savannah River National Laboratory, Aiken, SC 29808 USA

INTRODUCTION

Operation of the Department of Energy facilities at the Savannah River Site (SRS) has generated millions of gallons of highly radioactive wastes that are stored in large underground storage tanks comprised of carbon steel. The highly alkaline wastes consist of three forms: Sludge produced when acidic wastes from purification of irradiated nuclear fuels and targets are neutralized and consists of transition metal hydroxides and oxy-hydroxides along with similar compounds of aluminum; Supernate containing soluble components of the neutralized reprocessing solutions and largely a mixture of dissolved salts, predominantly sodium hydroxide, sodium nitrate and sodium nitrite; and Saltcake produced upon evaporation of the supernate and is largely sodium salts of nitrate and nitrite. Small quantities of uranium and plutonium are partitioned in the three waste types.

Retrieval of sludge began in the 1990s and is currently being vitrified at the Defense Waste Processing Facility (DWPF) in a borosilicate glass matrix for disposal in the federal repository for High-Level Waste. The alpha component of the other two waste classes (saltcake and supernate) must be reduced prior to shallow land burial at SRS. The alpha removal technology is a batch contact with monosodium Titanate and has been well tested.[1] The waste processing strategy calls for the saltcake to be dissolved with water and batched through the alpha removal process along with the supernate wastes. These operations will require numerous waste transfers and will result in the mixing of these streams.

The chemistry of uranium and plutonium is of interest in these processing steps to ensure that their concentrations due not exceed solubility limits, resulting in the precipitation of the actinides. Even though their concentrations are low, the volumes involved (millions of gallons) can lead to criticality concerns. The actinide solubilities have been previously studied. Allard compiled measured and estimated complex formation quotients for the actinides as a function of oxidation state in the pH range of 7 to 11.[2] Hobbs and Karraker[3] have measured the uranium and plutonium solubility in simulated SRS waste solutions and have developed solubility models as a linear function of a number of anion concentrations. Additionally, the mixing of various process solutions can result in the precipitation of various compounds like aluminosilicates. Aluminosilicates have been shown to occlude actinides.[4] As a result of these concerns, SRNL has been examining the chemistry of uranium and plutonium in these possible mixing scenarios.

RESULTS

Several supernate samples have been retrieved from selected waste tanks and characterized for actinide content. The uranium and plutonium solubilities were measured using

a technique modified from that used by Addai-Mensah, et al.[5] The method includes the spiking of supernate solutions with small volumes of acidic uranyl nitrate and plutonium oxide solutions, and the direct addition of preformed uranium and plutonium solids to fresh supernate. Initial results revealed that a DWPF recycle stream was supersaturated in uranium, but not plutonium. Solubility test results for several other tank supernate samples reveal that Pu solubility is typically < 5 mg/L, while U solubility limits can approach 50 mg/L. The solubilities are believed to vary with the concentrations of the primary anions in solution, including hydroxide, nitrate, nitrite, carbonate, and sulfate. Statistical models have been developed to predict solubility as a function of composition and temperature.

The chemistry of uranium was also examined under the conditions whereby sodium aluminosilicate was forming. In this study, the degree of uranium supersaturation was tested as to whether it influenced the participation of uranium in the aluminosilicate reaction. Figure 1 shows the fate of uranium when highly supersaturated. In these experiments, uranium was spiked into the waste solution and held at temperature (50 °C) for 50h. Samples were taken very shortly after uranium addition and at 50 h to determine if the uranium had precipitated. An aliquot of sodium metasilicate was added to the waste solution and a second sample was taken following the dissolution of the metasilicate and periodically over approximately 200 h. Figure 1 shows the results for the test conducted with a uranium solution at a degree of supersaturation of 2.7. At the time that the second sample was collected, during the 50th hour, a concomitant reduction in the aluminum concentration occurred, indicating that formation of aluminosilicate had commenced. Evident from the silicon and aluminum data, aluminosilicate formation continued over the duration of the test.

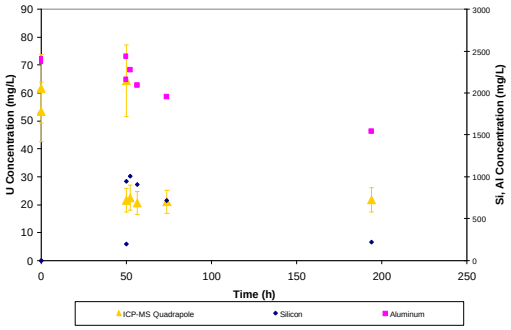

Figure 1. Uranium Concentrations during Aluminosilicate Formation.

The successful processing of High-Level Waste requires a fundamental understanding of the fate of uranium and plutonium under highly alkaline conditions. The importance of this work will assist in the successful retrieval and processing of the stored wastes at the Savannah River Site. These results along with others will be reviewed.

---

[1] F.F. Fondeur, D. T. Hobbs, M. J. Barnes, S. D. Fink, *Separation Science and Techology*, **2005**, 40(1-3), 571-592.
[2] R. Allard, "Solubilities of the Actinides in Neutral and Basic Solutions," Actinides in Perspective, Edited by N. M. Edelstein, Pergamon Press, 1982.
[3] D. T. Hobbs and D. G. Karraker, Nucl. Tech., *114*, 318, 1996.
[4] W. R. Wilmarth, S. W. Rosencrance, D. T. Hobbs, C. M. Jantzen, J. E. Laurinat, W. B. Van Pelt, W. L. Tamosaitis, A. J. Mattus, M. Z. Hu, D. W. DePaoli, C. F. Weber, C. P. McGinnis, S. Mattigod, "Aluminosilicate Formation in High Level Waste Evaporators: A Mechanism for Uranium Accumulation" Proceedings of Waste Management '02.
[5] J. Addai-Mensah, J. Li, M. Zbik, and W. R. Wilmarth, "Uranium Sorption on Solid Aluminosilicate Phases under Caustic Conditions", J. of Sep. Sci. and Tech., 40, 267, 2005

DOE's Technical Requirements for Packaging of Nuclear Material Stored Outside of a Glove Box

G. D. Roberson[*], D. Kirk Veirs[†]

[*]Department of Energy, Albuquerque NM USA
[†]Los Alamos National Laboratory, Los Alamos, NM 87545

INTRODUCTION

The storage of nuclear materials by the U.S. Department of Energy has been the subject of concern and much expense recently. The U.S. Defense Nuclear Facilities Safety Board's concern about materials left in process after production work stopped as a result of the end of the Cold War resulted in DNFSB Recommendation 94-1. In response to 94-1, DOE issued a stabilization, packaging, and storage Standard in 1994 with updates in 1996, 1999, 2000, and 2004, the 3013 Standard. Since that time over 4000 containers packaged to the 3013 Standard have been prepared and are in storage at Hanford, Savannah River Site, and Lawrence Livermore National Laboratory. Since 1994 there have been a number of events that led the DNFSB to issue recommendation 2005-1. The DNFSB cited in particular an August 5, 2003, event at Los Alamos National Laboratory's (LANL) Plutonium Facility that resulted in multiple workers receiving plutonium-238 uptakes as a result of the degradation of a package stored longer than planned and an October 6, 2004 incident at LLNL that involved the accidental drop of a package containing salt-bearing plutonium oxide. The DOE is developing a Manual to ensure all packages containing Special Nuclear Materials (including U, Np, Pu, Am, Co, Sr, Sc Th, Bk, CF, or Cm) outside of a glove box meet minimum standards of design, construction, procurement, and testing. This presentation will present the new requirements and their technical basis.

SCOPE

The Manual, scheduled to be issued by December 30, 2006, will applicable to all DOE facilities. Establishing packaging requirements for nuclear materials within the DOE complex requires consideration of a diverse population of material types for storage for uncertain periods of time. From a safety standpoint, nuclear material packaging must protect against a number of challenges that could breach the container and release radioactive material. Many of the materials of concern generate gases that result in container pressurization and may be pyrophoric or highly reactive. The container design must take into account corrosion, oxidative expansion of stored metal, effects of radiolysis, diurnal pumping and damage due to impacts from drops and tooling during handling. The DOE sites have not fully considered these issues for all packages within their inventories. For this reason, a consistent set of packaging requirements was found to be necessary for interim storage of Nuclear Materials outside of an approved engineered contamination barrier in order to protect workers.

This presentation will cover the limits on materials, the criteria that must be met for package design, allowable packaging configurations, and the requirements of a surveillance program.

1. U.S. Defense Nuclear Facility Safety Board Recommendation 1994-1.
2. U.S. Defense Nuclear Facility Safety Board Recommendation 2005-1.
3. DOE-STD-3013-2004.
4. HQ-EH-2004-1, OAK--LLNL-LLNL-2004-0046

The Legacy of Bolas Grande Spheres at Los Alamos National Laboratory: A Responsible Management and Disposition Plan [1]

J. Kohler , W. Crooks, W. Partain, R. Villarreal, D. Martinez, E. Flores, P. Pittman, T. Harden, L. Field

Los Alamos National Laboratory, Los Alamos, NM 87545 USA

THE LEGACY

There are 14 Bolas Grande Spheres that reside at the Los Alamos National Laboratory in outdoor, above ground, un-covered storage. They were manufactured during the Cold War.

Fig 1: Bolas Grande Spheres in outdoor storage at Los Alamos National Laboratory

The instrumented Spheres, each used only once, provided the containment that confined the fall-out from a small-scale internal plutonium detonation.

The steel Spheres are 6 feet in diameter, weigh up to 14,000 pounds, and have a wall thickness of 1-2 inches.

Fig 2: Inside a Bolas Grande Sphere

Bolas Grande Spheres contain SNM consisting of plutonium-239 (^{239}Pu) in the form of actinide metals and oxides, mixed in a matrix of metal, powdered silica, graphite, electrical wires and other hardware. Each sphere is estimated to contain approximately 400 pounds of radioactive debris. The debris is settled below that level of the 20-inch port.

The primary radioactive component of the material in these spheres is americium -241 (^{241}Am) created from the decay of plutonium-241 (^{241}Pu). ^{241}Am emits a highly energetic 60 keV gamma ray. The gamma ray flux increases over time as the ^{241}Pu is decaying to ^{241}Am with time. Gamma flux reaches a maximum dose at 60 years.

While the steel containment sphere significantly attenuates the flux from this material, several of the spheres, in their outdoor storage locations, have contact dose measurements of 3mR/hr.

THE PROBLEM

The spheres cannot reside outdoors forever, yet currently there is no clear-cut disposition path. Their outdoor storage location subjects them to uncertain environmental conditions and natural phenomenon. The two Category II nuclear facilities on the lab site that could process these spheres, Plutonium Facility-4 (PF-4) and the Chemical and Metallurgical Research Facility (CMR), each have design and engineering limitations in light of advances in safety and radiation protection standards/regulations. While several spheres were emptied in the late '90s in PF-4, that process was neither ALARA engineered nor worker friendly and, absent an emergency, could not be restarted without significant re-engineering. Space in the CMR Facility could be redesigned for sphere processing, but the facility itself does not meet modern seismic criteria.

THE CHALLENGE

Introducing new nuclear processes into aging nuclear facilities presents challenges to the regulator, the engineer, and the safety analyst. Complying with the constraints and limitations of modern regulations can present mutually exclusive alternatives. Yet doing nothing, maintaining the status quo, or postponing action to an unspecified future date is neither environmentally nor socially responsible.

THE SOLUTION

The paper will introduce the Bolas Grande Project at Los Alamos. It will describe how the Project Team plans to meet the challenge of sphere processing in a safe and expeditious manner, in light of new regulations and their impact on aging nuclear facilities.

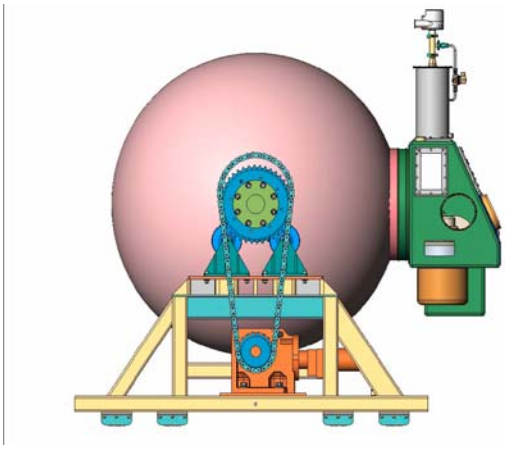

Figure 3: Bolas Grande Sphere mounted on the Sphere Support Stand with attached Dry Work Station

The Bolas Grande Project is developing a set of ALARA compliant, uniquely designed and engineered Bolas Grande structures, systems, and components (SSCs) to remediate the spheres. Central elements of the design are the Sphere Support Stand, the Dry Work Station, and the Wet Chemical acid etch decontamination process using a mixture of Nitric and Fluoboric acid. The functional safety requirements called out by the Bolas Grande Preliminary Documented Safety Analysis (PDSA) and compliance with DOE Order 420.1, "Facility Safety", directly impact the design of the SSCs.

[1] J. Kohler, *et al.,* Bolas Grande Project Critical Decision (CD)-1 Package, Title 1 Design Report and Design Package

Influence of H_2O content in test atmosphere on creep properties of (U, Pu)O_2 materials

V. Basini*, F. Bruguier*,

*CEA Cadarache, DEC/SPUA/LMPC, Bat 315, 13108 St Paul lez Durance, France

INTRODUCTION

MOX fuel tested under transient conditions behaves particularly well from the pellet-cladding interaction point of view and can undergo power variations above the current standard UO_2 threshold.

To complete understanding on the specific mechanical properties of MOX fuel, experimental programs have been undertaken within the framework of the cooperation between EDF, FRAMATOME-ANP and CEA. Since the MOX benefit is largely attributed to its higher fuel creep, the influent parameters on the thermo-mechanical behaviour of MOX fuels are studied and compare to the behaviour of UO_2. Among them, influence of oxygen potential variations have been studied via creep tests under different atmospheres (dry and damp) and seem to be one of the most influent.

EXPERIMENTAL PROCEDURE

Cylindrical pellets of (U,Pu)O_2 had elaborated by classical powder metallurgy route : UO_2 and PuO_2 powders are mechanically mixed to obtain a plutonium content of about 7 %, mixed powders are shaped by uniaxial pressing and sintering under Ar+5%H_2+1000ppmH_2O atmosphere at 1700 °C, thereby ensuring the material stoichiometry. After sintering, the pellets were thermally treated under the same atmosphere during 245 h to obtain a solid solution of (U, Pu)O_2. The samples are of PWR geometry, 13 mm high and 8.2 mm diameter. Their characteristics are given on table 1. Compressive tests were conducted in a suitable adapted furnace on a screw-type Instron machine placed in glove box (Figure 1). Creep tests were performed at 1500 °C under different atmosphere : vacuum, Ar+5%H_2 and Ar+5%H_2+ x ppm H_2O (x ranges from 500 to 3000 ppm).

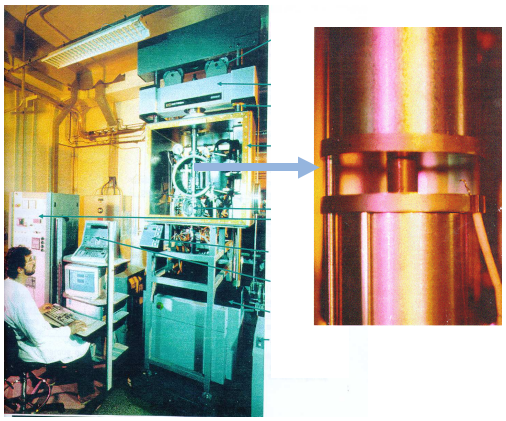

Fig 1: Mechanical test device

Pu Content (%)	Grain size (µm)	Porosity (%)	O/M Ratio[a]
7	6,5	2	2.001 ± 0.003

Table 1 : characteristics of (U, Pu)O_2 pellets

[a] : obtain by thermogravimetry measurements

EXPERIMENTAL RESULTS

Creep tests have been performed at 80 MPa under varied atmospheres : vacuum, Ar/H2 and Ar/H2 + 1000 ppm H_2O. Creep curves, exhibit a classical primary regime followed by a stationary strain rate regime in which the creep parameters were determined. No difference is observed between vacuum and Ar/H_2 atmosphere, the stationary creep rate is about 0,6 %/h. One test was started first under Ar/H_2 atmosphere, and then, when the stationary strain rate regime was reached, vapour water was introduced in the furnace. The stationary creep rates increase rapidly with the humidification of the atmosphere, about almost 10 times the creep rate under dry atmosphere. The same rate is obtained when the test is directly performed under damp atmosphere.

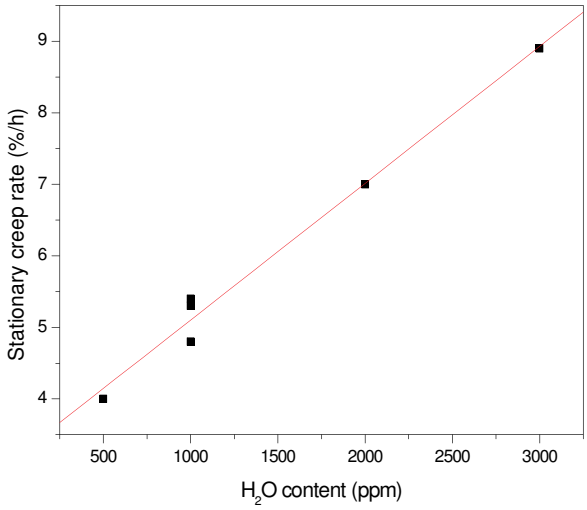

Fig 2 : Influence of H_2O content on stationary creep rate of $(U,Pu)O_2$

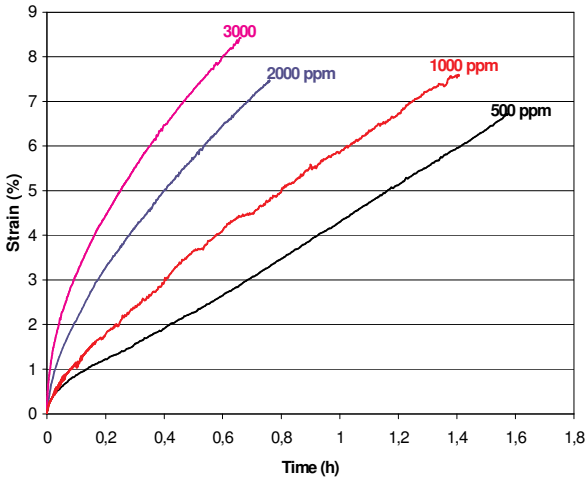

Fig 3 : Variation of primary creep under different atmospheres

Linear increasing of the stationary creep rate is observed with H_2O content from 0 to 3000 ppm (Figure 2). The primary creep strain is also increased with the H_2O content (Figure 3). For instance, after 20 minutes, a primary creep strain less than 2 % is measured for 500 ppm H_2O content, instead of about 7% for 3000 ppm H_2O content. Same tests have been performed on UO_2 pellets and showed a low influence of the humidification of the atmosphere (stationary creep rate increase by a factor 4 from dry atmosphere to Ar/H_2 +1000 ppm H_2O) and no influence of the H_2O content from 0 to 2000 ppm is observed.

CONCLUSION

This study showed the important influence of the oxygen potential on the creep behaviour of $(U, Pu)O_2$ materials. Primary creep strain and stationary creep rate increase with increasing of the H_2O content. The influence is different in the case of UO_2 material and then allow us to make the assumption that it could be one of the influent factor of the better in pile behaviour of MOX fuels. Relation between oxygen potential and creep parameters on UO_2 and $(U,Pu)O_2$ will have to be evaluated.

Determination of elastic moduli at high temperatures for alpha-Plutonium and Uranium-Vanadium alloy with an ultrasonic method

L. Bourgeois, M.-H. Nadal, F. Clement, G. Ravel-Chapuis

CEA-Centre de Valduc, Département de Recherches sur les Matériaux Nucléaires,
21120 IS-SUR-TILLE, FRANCE

INTRODUCTION

The knowledge of the elastic moduli[1] is necessary in calculations with classical mechanical computer codes, both in the elastic and in the elastoplastic regimes. When a structure is stressed versus temperature other than room temperature, these elastic moduli must be known across the whole range of temperature investigated. For materials which are submitted to high temperatures, most of the conventional measurement methods, such as mechanical testings, are unsuitable. An alternative solution is an ultrasonic method which has the advantage to determine the elastic moduli[2] for a very weak strength to deformation ratio. A contact delay-line ultrasonic device[3] has been developed to measure the shear and compression waves velocities up to 1000K on cylindrical specimens.

EXPERIMENTAL SET UP

The determination of the shear modulus $\mu(T)$ depends on the acoustic velocities, in particularly on the shear velocity, which variation versus the temperature θ can be measured. The principle of the experiment consists in measuring the time of flight of the acoustic wave through the sample as described on the figures 1.a and 1.b. The elastic-wave velocities determination requires the accurate knowledge of the distance of propagation through the solid versus temperature l(θ). This is obtained using the thermal expansion of the material. A furnace is used so that the main heating region is located on the sample. This latter (cylindrical sample of 4.5 mm to 10 mm width and 23 mm diameter) is placed between two wave-guides. At the end of each one, two transducers are connected with the same ultrasonic characteristics. The two wave-guides are used to ensure the propagation of the waves through the sample and also to undergo the temperature gradient. Therefore, the thermal resistance of the wave-guides is sufficient to keep the transducers near the room temperature.

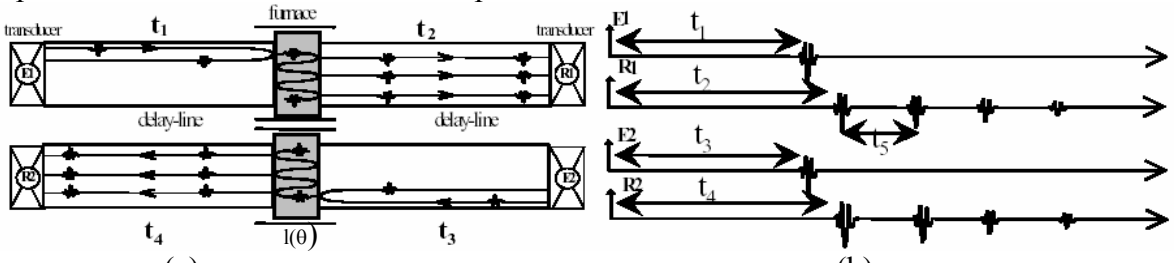

(a) (b)

Fig 1: (a) Propagation of the ultrasonic waves in the delay-line/material/delay-line structure, (b) Echograms acquired by each transducer.

EXPERIMENTAL RESULTS

Experimental results are presented for plutonium and uranium-vanadium samples.

Figure 2 presents the evolution of the shear modulus of the uranium-vanadium alloy. The measures have been realized in the temperature range ($0.2 < T/Tm < 0.7$). The melting point of uranium-vanadium alloy is $Tm = 1400K$. The evolution of $\mu(T)$ keeps a monotonous decrease up to the first shift $\alpha \rightarrow \beta$ at 938K where the decrease is more important. We have developed a model including phase jumps and change of state to obtain a continuous description of $\mu(T)$ up to the melting point considering the second phase shift $\beta \rightarrow \gamma$ at 1040K. $\mu(T)$ results seem to exhibit enforced phase jumps comparing to Young modulus.

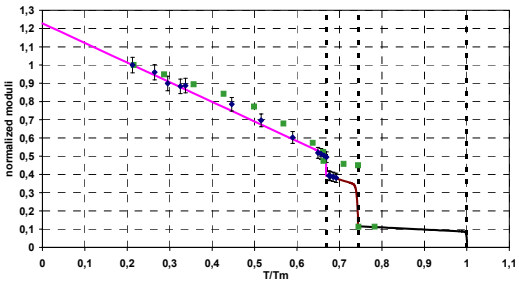

Fig 2: Normalized shear modulus variation of the U-V (●) versus temperature with the associated modelling (-). Comparison to normalized Young modulus (■).

Figure 3 shows the latest results obtained at the end of 2005 for α-Pu. The evolution of the normalized time of flight of the longitudinal wave and the normalized variation length are compared up to $T/Tm = 0.74$. It can be seen that the time of flight variation versus temperature is the same for the two samples. Theses changes are coherent with the curve of variation length but the amplitudes are different which means that there are probably problems on the experimental set up. Indeed, with this contact device, the samples are under strains and their dimensions are not kept, especially because of the important thermal expansion of the material.

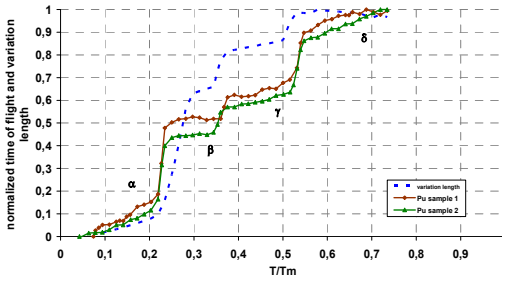

Fig 3: Normalized time of flight of longitudinal wave and variation length versus temperature for α-Pu.

CONCLUSION

Our next goal is to improve the contact device by reducing the strain on the samples, especially to improve characterization of materials having an important thermal expansion coefficient. Our measurements have to be completed by longitudinal and shear wave velocity measurements to determine all the elastic moduli of U-V alloy and α-Pu. For this latter, dilatometric measurements have to be realized with respect to the temperature kinetic of ultrasonic measurements and the material composition.

REFERENCES

1. M.-H. Nadal and P. Le Poac, J. Applied Physics 93, 5, 2472-2480, (2003).
2. M. Fukuhara, A. Sanpei, J. of Mat. Sci. Let., 12, (1993).
3. M.-H. Nadal, C. Hermerel, C. Gondard and L. Paradis, 14th World Conference on NDT & INTEXT NDT, New Delhi (Inde) (1996).

Determination of single crystal elastic constants from polycristalline material using X-ray diffraction: prospects for plutonium

B. Ravat[*], N. Baclet[*], E. Lépine[†], C. Valot[◇], Ch. Valot[◇], K. Inal[†]

[*]CEA Centre de Valduc, Is sur Tille F-21120, France
[†]MECASURF, ENSAM, 2 cours des Arts et Métiers, 13617 Aix en Provence, France
[◇]CEA, Centre de Cadarache, 13108 St Paul les Durances, France

INTRODUCTION

The knowledge of the single crystal rigidity tensor is fundamental to define interatomic potentials used for the modelling of self-irradiation in plutonium alloys. Ultrasonic technique allows the determination of the elastic tensor components, but it requires single crystal, which is very difficult or even impossible to obtain for materials such as plutonium alloys. Thus, X-Ray diffraction (XRD) has been revealed to be an interesting technique since it allows to determine the X-ray Elastic Constants (XEC) which, combined with a polycristalline model (self-consistent model[1,2]), can be used to determine Single Crystal Elastic Constants (SCEC) from a polycrystalline material.
However, due to the difficulties in handling plutonium, the method has been first tested on copper, which has a face centred cubic structure and a high mechanical anisotropy, properties similar to those of δ-Pu.

ANALYTICAL AND EXPERIMENTAL APPROACHES

The SCEC are determined by applying a uniaxial stress to the polycrystalline sample thanks to a small 4-points bending device and measuring by using XRD the lattice planes spacing which is used as an internal strain gauge. The XEC corresponding to the *{hkl}* lattice planes can then be determined. A scale transition relationship remains necessary to link the mesoscopic strains (scale of the crystallites) to the macroscopic stresses. First, a relationship between strains at different scales can be written with an equation of localisation:
$\varepsilon^{II}(\Omega) = A(\Omega)..\varepsilon^{I}$, where ε^{I} and ε^{II} are the macro and mesoscopic strains, Ω is the crystallites orientation and A(Ω) is the localisation tensor of the self-consistent model defined as:
$A(\Omega) = \left[E..\left(c(\Omega) - C\right) + I\right]^{-1}$ where E is the Morris tensor, c is the single crystal rigidity tensor, C is the macroscopic stiffness tensor and I is the identity matrix. This form for the localisation tensor takes into account the nature, orientation and shape (spheroidal grains) of crystallites. Moreover, the elastic behaviour within the limits of the anisotropic Hooke's law for the single crystal is expressed by: $\sigma^{I} = C..\varepsilon^{I}$. Considering that the material is elastically isotropic at the macroscopic scale (not textured), neglecting the strain of second order and performing XRD experiments for $\phi = 0°$ (which is the direction of the applied uniaxial stress), the following relationship, called "sin²Ψ", is obtained: $\varepsilon_{\phi\psi\{hkl\}} = [½S_{2\{hkl\}}.\sin^2\psi + S_{1\{hkl\}}.]\sigma^{I}_{11}$ where ½S_2 and S_1 are the XEC, σ^{I}_{11} is the applied stress and (Φ,Ψ) are the XRD measurement directions. An analytical expression of the self-consistent model, which takes into account the mechanical interactions between each grain and the elastic polycrystalline matrix, is then obtained. It allows to deduce the SCEC from the components of the macroscopic stiffness tensor C_{ij} (determined by

ultrasonic method) and the XEC: $\frac{1}{2}S_{2\{h00\}}$.and $\frac{1}{2}S_{2\{hhh\}}$. For cubic materials, the latter are calculated from the XEC experimentally determined for two *{hkl}* lattice planes.

RESULTS

In order to validate the analytical and experimental approaches described above as well as the bending device accuracy, a first experiment has been performed on a rolled copper sample which ultimate tensile strength is 160 MPa. A second experiment has then been performed on annealed copper to reduce its ultimate tensile strength down to 50 MPa, closer to the one for the δ-PuGa alloys, which limited the range of applied stress. XRD experiments have also been performed to control that the sample was not textured since this can not be taken into account in the analytical expression of the self-consistent model. The components C_{ij} of the stiffness tensor have also been determined on the annealed sample. Since the diffractometer is out of glove box, the XRD experiments on plutonium alloys will have to be performed on samples confined in a 80µm thick polymer Rilsan sealed film. The last experiment on copper has been performed on a confined sample to check that the Rilsan film did not modify the applied stresses. All the results (values of c_{ij}) for the different experiments are presented in the figure 1. The values have been compared to those obtained from ultrasonic technique on a copper single crystal[3]. The results show a good agreement with a dispersal of values less than 10%, which validates both the analytical and experimental approach.

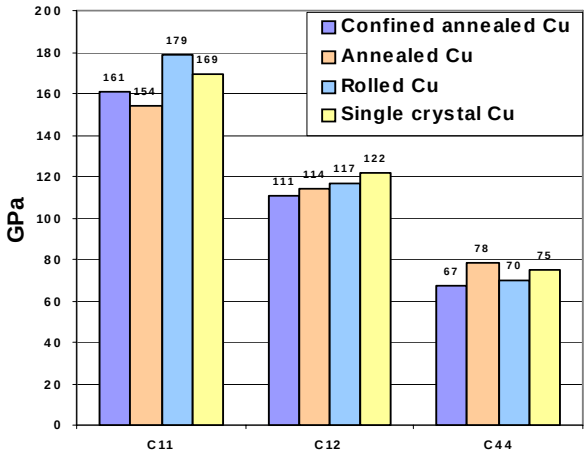

Fig 1: Copper single crystal elastic constants.

CONCLUSION

XRD experiments combined with an analytical expression of the self-consistent model have been revealed to be very satisfying for the determination of Single Crystal Elastic Constants from a polycrystalline material. The next step of this work, in progress, is to perform this experiment on radioactive materials and especially on δ-PuGa alloys.

1 Morris P.R., Int. J. Eng. Sci., **8**, 1970, 49
2 E. Kröner, Acta Metall.,**9** ,1961, 155
3 Landolt-Börnstein, New Series, 18 Springer Verlag, Berlin, 1984

Shear modulus determination versus temperature up to the melting point using a laser-ultrasonic device

M.-H. Nadal, C. Hubert

CEA-Centre de Valduc, Département de Recherches sur les Matériaux Nucléaires
21120 IS-SUR-TILLE, FRANCE

INTRODUCTION

The shear modulus μ is one of the parameters needed to implement the constitutive laws. These mechanical properties can be measured for a solid or a liquid with different ultrasonic methods [1, 2]. This paper deals with the determination of μ(T) especially during the solid-liquid phase transition. Elastic wave velocity determination is performed by an original laser-ultrasonics device [3]. Indeed, owing to its non-contact characteristic, this technique has demonstrated its potential for high temperature measurement [4]. The present work focuses on Tin and proposes the simultaneous determination of the longitudinal and the shear velocities from the room temperature T_0 up to the melting point T_m. Indeed, a special effort was made to measure shear-wave velocity despite a strong attenuation function of the temperature. A continuous function μ(T) from T_0 to T_m is proposed, taking into account the drastic jump of the shear modulus at T_m, validated by experimental measurements.

EXPERIMENTAL SET UP

This study is devoted to the characterization of white Tin samples obtained by cold rolling (T_m = 505 K) in the temperature range [300 – 600] K. The samples have a parallelepiped shape with a square surface (15×15 mm^2) and their thicknesses range from 1 mm to 5 mm. The experimental setup is composed of three main components: a Q-switched Nd:YAG laser operating at the wavelength of 1.064 μm to generate ultrasounds; a Mach-Zehnder heterodyne interferometer [3] to measure the normal component of the mechanical displacement; a furnace with infrared lamps to control the temperature of the sample (1-10 K/min - temperature level better than 1/10 K). A sample is introduced inside a quartz cell located in a greater quartz tank filled by inert gas (Ar) to avoid oxidation effects, especially around the melting point.

EXPERIMENTAL RESULTS

The experiment principle is to determine the times of flight respectively of the longitudinal and shear waves in the solid, and of the longitudinal waves in the liquid. Measurements are performed in a transmission configuration at the epicenter. Correcting the thickness for thermal expansion, velocity is then determined versus temperature (V_{SL} longitudinal wave velocity in the solid; V_{LL} longitudinal wave velocity in the liquid; V_{SS} the shear waves velocity in the solid) (figure 1). These values of V_{SL} are in good agreement with the results of Nakano *et al* [**5**], even if a difference exists around the melting point because of a shift in the measurement of the temperature (in the quartz cell and not in the sample). The shear-wave attenuation, due to the approach of the melting, leads to a crucial difficulty of the shear velocity measurement. The elastic moduli are deduced from the previous results by using the well known following equations given for an isotropic solid. Furthermore, the density of the liquid Tin is given by a linear function versus temperature.

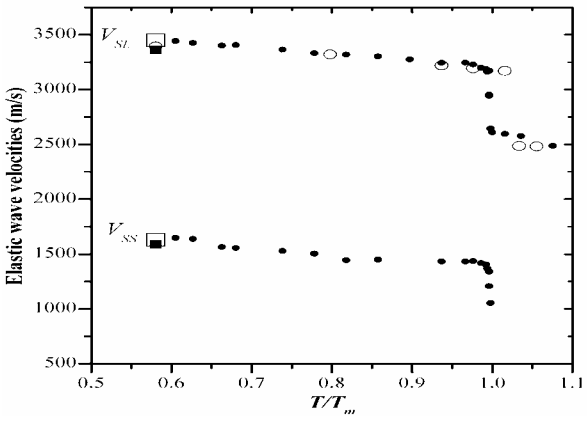

Figure 1: Elastic velocities of Tin versus temperature up to the melting point, (●) this study, (❍) [5].

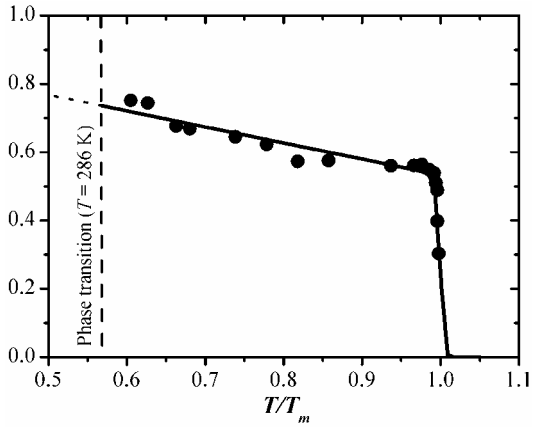

Figure 2: Evolution of the shear modulus μ/μ_0 of Tin versus T/T_m up to the melting point: (●) experiment and (—) the model.

For pure polycrystal metals, a μ(T) modeling [6] is proposed made of a continuous analytical expression over a large temperature range, from the absolute temperature to the melting point leading to:

$$T/T_m \in [0;1+\varepsilon] \quad \mu(T) = \frac{\mu_0\left[1-a\ (T/T_m)\right]}{\Im(T/T_m)}, \quad \Im(T/T_m) = 1 + \exp\left[\frac{T/T_m - 1}{\varepsilon\left\{1-\frac{T}{T_m(1+\varepsilon)}\right\}}\right] \quad (1)$$

where a is a positive factor, μ_0 is the shear modulus at 0 K. According to the intrinsic characteristics of the material, the model [Eq. (1)] becomes a full consistent model to describe the μ(T) evolution versus the complete temperature range of our study ($T/T_m \in [286/T_m;1+\varepsilon]$). Figure 2 shows the comparison between some experimental data of the shear modulus versus temperature and the modeling. The fall of μ(T) around $T/T_m = 1$ is described rather well by the modeling. The results show $\varepsilon = 0.05$. It can be noted that the drastic fall of μ(T) around the melting point can be described by a function falling down to zero in a weak temperature range.

CONCLUSION

This paper shows the high potential of Laser-Ultrasonics to study the solid to liquid transition. Applied to Tin, this work succeeded in the determination of both longitudinal and shear wave velocities and the elastic moduli from ambient to the liquid. An analytical and continuous description of μ(T) is proposed and validated by the experimental data. The drastic fall of μ(T) at T_m is then described. Future projects deal with an innovating ultrasonic device to measure accurately surface-wave velocities connected to μ(T).

REFERENCES

[1] H.J. McSkimin, Physical Acoustics, E. P. Mason, New York, Vol. 1A, Chap. 4, p.271, 1964.
[2] D. J. Steinberg, S.G. Cochran, and M.W. Guinan, J. Appl. Phys. 51, 1498, 1980.
[3] D. Royer and E. Dieulesaint, Appl. Phys. Lett. 49, 1056, 1986.
[4] M. Paul, B. Haberer, and W. Arnold, Mater. Sci. Eng. A168, 87, 1993.
[5] H. Nakano, Y. Matsuda, and S. Nagai, Meas. Sci. Technol. 9, 217, 1998.
[6] E. Fraizier, M.-H. Nadal, R. Oltra, J. Appl. Phys., Vol 93, No 1, pp. 649-654, 2003.

The Effect Of Pressure On Phase Stability In The Pu-Ga Alloy System

D.R. Harbur

Los Alamos National Laboratory, Los Alamos NM 87544 USA

Abstract

In examining and analyzing over three decades of research on the transformations involved in the Pu-Ga alloy system, it has become evident that the data is comprised of many seeming incongruities and contradictions. Plutonium is not the easiest material to generate data on, and because of the complexities in its phase relationships, and its sensitivities to alloying, temperature and pressure, the analysis of the data is not always straightforward. The best technique that the metallurgy community has for identifying the different phases in Pu is x-ray diffraction, and many capable scientists have well developed the art as it is applied to Pu and its alloys. X-ray diffraction, however, is not a very good tool for studying non-diffracting disordered materials. In this paper we have shown that under certain processing methods large amounts of a non-diffracting disordered-state are formed in Pu-Ga alloys, which we call the amorphous-state. The amorphous-state is certainly not an equilibrium-state, but it nevertheless can be formed under certain pressure-states, and more surprisingly once formed can persist for extended times and temperatures at ambient pressures. Being a physical-state, the amorphous-state has distinct physical properties, meta-stability and sensitivities to Ga content.

When Pu is alloyed with small amounts of Ga and homogenized, the δ-phase can be stabilized over a reasonable temperature and pressure range. At low temperatures, the δ-phase will begin to transform to the α'-phase, with the transformation temperature being dependent upon the amount of Ga. At very low Ga contents near 1 at. % Ga the δ-phase will begin to transform very near room temperature and the transformation products are a mixture of the α'-phase and the amorphous-state. At 0.68 at. % Ga all of the δ-phase transforms into the α'-phase and the amorphous-state upon cooling to room temperature.

The δ-phase also becomes unstable at high hydrostatic-pressures, and this instability is also strongly related to the Ga content. The higher the Ga content, the higher the pressure before the δ-phase transforms to a denser-state. The transformation path is dependent upon the overall Ga content of the δ-phase.

At a Ga content of 1.0 at. % Ga the transformation begins by forming a mixture of the α'-phase and the amorphous-state. For this alloy, the α'-phase and amorphous-state mixture is stable upon pressure release even after small incremental pressure cycles just above the initiation of the transformation. It is believed that the large amount of amorphous-state formed early in the transformation cycle for this alloy disrupts the crystallographic alignment between the martensitic α'-phase and the parent δ-phase and is responsible for the martensitic α'-phase not transforming back to the δ-phase upon pressure release.

At a Ga content of 1.7 at. % the δ-phase first transforms directly to the α'-phase. After about 50% α'-phase is formed, the transformation changes to a δ→amorphous-state transformation with a little more α'-phase forming either from the δ-phase or the amorphous-state. The amorphous-state in this mixture begins to transform to the α'-phase at pressures of 5-7 kbars. Pressure release at low pressures, where little of the amorphous-state has formed, results in the martensitic α'-phase transforming back to the δ-phase. The amorphous-state in these two lower Ga alloys slowly crystallizes into the δ-phase upon heating. When the α'-phase transforms into the β-phase, near the normal α→β transformation temperature, the rejected Ga moves into the amorphous-state causing it to spontaneously crystallize into the δ-phase. This behavior shows that the relative stability of the amorphous-state to that of the δ-phase is dependent upon the Ga content.

At 2.5 at. % Ga the δ-phase initially transforms to the α'-phase. Only as the pressure approaches 10 kbars and the amount of α'-phase approach 60 % does any significant amount of the amorphous-state form in this alloy, and only after a 10 kbar pressure cycle does the phase-mixture remain stable upon pressure release. Even after a 10 kbar pressure-cycle the martensitic α'-phase transforms directly back to the δ-phase when heated. It appears that at this alloy content enough amorphous-state forms at 10 kbars to disrupt the α'→ δ transformation on pressure release, but not enough forms to disrupt the α'→ δ transformation during the heating cycle. The small amount of amorphous-state that forms in this alloy crystallizes into the δ-phase over a wide temperature range extending even into the normal β-phase temperature range.

In addition to the transformation start pressure being dependent upon the Ga content, the rate at which the δ-phase transforms to a denser material is also dependent upon the Ga content. As one would expect, the δ-phase in the lower Ga content alloys transforms faster than in the higher Ga content alloys. As pointed out above the rate at which the δ-phase transforms does not necessarily relate to the rate of formation of the products of that transformation. The δ-phase is transforming to two products in the lowest Ga alloy, but is only transforming to the α'-phase early on in the transformations of the two higher Ga alloys.

The existence of the amorphous-state requires innovative new tools for identification and analysis. The density/compressibility data presented in this paper is one such tool for analyzing the amorphous-state, but it requires other knowledge of the material for proper analysis. Disordered states are common in irradiated materials. In the on-going studies of aging effects in Pu, the existence of radiation damage, and irradiation particles and effects requires careful examination for the possibilities of amorphous-state development.

LA-UR-06-1109

Strong Electron-Phonon Coupling in δ–Phase Stabilized Pu

Matthias J. Graf, Turab Lookmann, John M. Wills, Duane C. Wallace, Jason C. Lashley

Los Alamos National Laboratory, NM 87545 USA

ABSTRACT

Heat capacity measurements of the δ-phase stabilized alloy $Pu_{0.95}Al_{0.05}$ suggest that strong electron-phonon coupling is required to explain the moderate renormalization of the electronic density of states near the Fermi energy. We calculate the contributions of the heat capacity from the lattice and electronic degrees of freedom, as well as from the electron-lattice coupling term, and find good overall agreement between experiment and theory assuming a dimensionless electron-phonon coupling parameter of order unity, $\lambda \sim 0.8$. This large electron-phonon coupling parameter is comparable to reported values in superconducting metals with face-centered cubic crystal structure, for example, Pd ($\lambda \sim 0.7$) and Pb ($\lambda \sim 1.5$). In addition, our analysis shows evidence of a sizable residual low-temperature entropy contribution, $S_{res} \sim 0.4\ k_B$ (per atom), which can be fit by a two-level system. Therefore, we speculate that the observed residual entropy originates from crystal field effects of the Pu atoms or from self-irradiation induced defects frozen in at low temperatures.

The actinide metal plutonium (Pu) exhibits six unique crystal structures in the solid state at ambient pressure between absolute zero and its melting temperature. The phases range in symmetry from simple monoclinic (sm) to body-centered cubic. The easily worked face-centered cubic (fcc) phase, denoted by δ, is thermodynamically stable in pure plutonium from 592 K to 736 K, and can be stabilized down to room temperature by small additions of trivalent elements such as gallium or aluminum. The effects of alloying have a profound impact on the electronic structure. Specifically, the low-temperature α phase (sm) of pure Pu has an enhanced Sommerfeld coefficient of γ_S=17 mJ/(mol K^2) compared to a simple metal with typically $\gamma_S \sim 1$ mJ/(mol K^2), while the stabilized δ phase exhibits a moderately heavy electron mass with an enhanced Sommerfeld coefficient γ_S=50-70 mJ/(mol K^2). It is believed that the high-volume δ phase has localized, nonbinding electrons, while in the low-volume α phase the electrons are itinerant and binding. This behavior resembles the Mott transition in correlated electron systems. In a recent calorimetry study, Lashley and coworkers [1] pointed out that the low-temperature data of the heat capacity of $Pu_{0.95}Al_{0.05}$ exhibit a moderately enhanced Sommerfeld coefficient, γ_S=64 mJ/(mol K^2), and a λ-shaped anomaly around 60 K in *C/T*. These observations were suggestive to those authors to describe $Pu_{0.95}Al_{0.05}$ as an incipient heavy-fermion system.

The purpose of this study [2] is to give a quantitative description of the electron-phonon interaction on the conduction electrons in a plutonium alloy and whether the observed low-temperature λ-shaped anomaly in *C/T* is associated with a martensitic phase transformation. From this study we conclude that the observed anomaly is unlikely due to a full or partial martensitic phase transformation from the high-temperature δ phase into the low-temperature α' phase (note the substitutional binary alloy α' and α have the same crystal structure). Because on

cooling this transformation finishes around 130-180 K and is completely reversed on heating around 380 K. Instead of a structural transformation, we speculate that crystal field effects or self-irradiation induced defects and vacancies, for example, Frenkel pairs, are responsible for the reported excess entropy.

A direct consequence of our analysis is that the relatively strong electron-phonon coupling of order unity, necessary for describing the measured specific heat data, would suggest that the alloy PuAl should become superconducting below a few Kelvin. So far no evidence of superconductivity has been observed down to roughly 3 K.

We divide the calculation of the total heat capacity of a metal into a vibrational, electronic, electron-phonon coupling, and residual (everything else) term, $C = C_{ph}+C_e+C_{ep}+C_{res}$. One by one, we calculate their contributions and importance. Furthermore, we assume that the thermodynamic properties are dominated by the fcc δ-Pu crystal structure and any possible admixture of α' is negligible.

In Figure 1 we are comparing the combined total theoretical heat capacity with experiment. The agreement is excellent. Here we combine the individual contributions to the heat capacity, assuming an electron-phonon coupling parameter λ~0.8 with Eliashberg's $\alpha^2F(\omega)$ function that has an Einstein mode at 2.8 THz, a two-level system (TLS) with an occupation factor $n \approx 0.5$ and level splitting $T_{TLS} \approx 120$ K, as well as an electronic density of states peaked at the Fermi level.

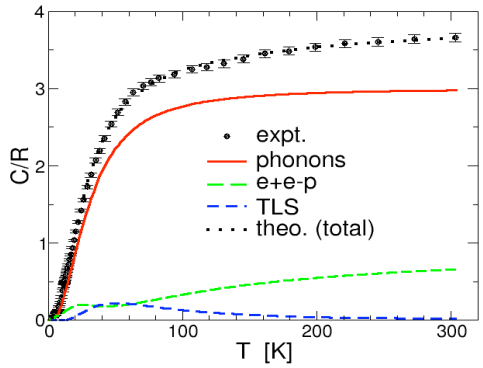

Figure 1: Comparison between experiment and theory. Specific heat is decomposed into phonon, electron-phonon renormalized electronic and two-level system contributions.

In conclusion, we studied heat capacity measurements of a δ-phase stabilized PuAl alloy and calculated the vibrational, electronic, electron-phonon, anharmonic, crystal field, and structural transformation contributions. Thereby, we found several important aspects: (1) electron-phonon coupling is strong and cannot be neglected at low temperatures; (2) a residual excess entropy of order S_{res}~0.4 k_B (per atom) can be understood in terms of an additional internal degree of freedom, for example, crystal field effects or self-irradiation induced defects at plutonium sites; (3) a structural transformation from $\delta \rightarrow \alpha'$ occurs at temperatures too high, and is too small in magnitude, to account for the low-temperature excess entropy.

Acknowledgements

This work was supported by the U. S. Department of Energy at Los Alamos National Laboratory under contract No. W-7405-ENG-36.

1 J. C. Lashley et al., Phys. Rev. Lett. **91**, 205901 (2003).

2 M. J. Graf, T. Lookman, J. M. Wills, D. C. Wallace, J. C. Lashley, Phys. Rev. B **72**, 045135 (2005).

Bulk and Shear Modulus of Polycrystal Plutonium through the (α-β) and (β-γ) Phase Transitions [1]

I. Mihut, J. B. Betts, H. Ledbetter, D. Dooley, D.A. Miller, A. Migliori

We used resonant-ultrasound spectroscopy to measure simultaneously the bulk and shear moduli of pure polycrystal Pu from 295K to 475K. Our measurements span the α-β and β-γ phase transitions. We used the known volume changes to obtain absolute values for the moduli of β and γ. When we add these measurements to our previous work, we obtain the behavior of the bulk modulus and the polycrystal shear modulus of pure Pu from 18K to 475K.

[1]This work was supported by the National Nuclear Security Administration, The State of Florida, and the National Science Foundation.

LAUR 06-0985

Cerium Isomorphism and the δ-α Transformation in Plutonium

Andrew C. Lawson*, Jason C. Lashley* and Peter S. Riseborough†
*Los Alamos National Laboratory, Los Alamos NM 87545 USA
†Physics Department, Temple University, Philadelphia, PA 19122-6082 USA

MODEL

Aptekar' and Ponyatovskiy (A-P) gave a model for the isomorphous γ-α transformation in cerium metal that is based on a putative binary phase equilibrium between the α and γ phases with energy difference ΔE, entropy difference ΔS, volume difference ΔV and energy of mixing U, all of which are materials parameters to be found from experiment. The difference in free energies of the two phases is

$$\Delta G(p,T,\Delta E,\Delta S,\Delta V,U) = RT[Cln(C)+(1-C)\ln(1-C)]+[\Delta E-T\Delta S+p\Delta V]C+UC(1-C)$$

The phase diagram is determined by minimizing the Gibbs free energy with respect to C, the relative concentration of the phases. Excellent agreement with experiment is found for the choices ΔE = 505 Cal/mole, ΔS = 3.69 Cal/mole-K, ΔV = 3.4 cm^3/mole and U = 2200 Cal/mole, as shown in the calculated phase diagram of Figure 1.

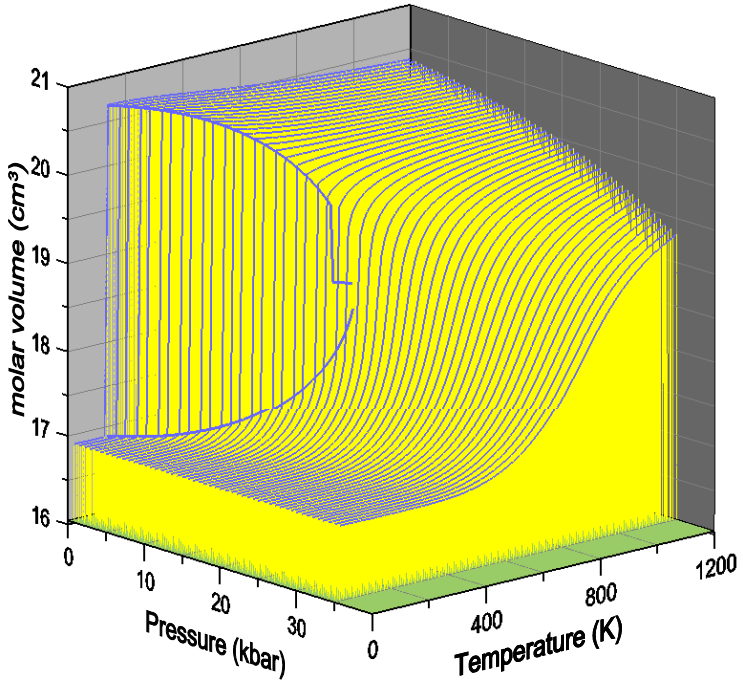

Fig.1. Phase diagram of cerium metal calculated with the A-P model.[1]

PU-GA LATTICE CONSTANTS

Chemical periodicity indicates the possibility of describing the extreme properties of plutonium with a cerium model. We used the Aptekar'-Ponyatovskiy model to describe the δ-α transformation in plutonium metal. The α-phase is not isomorphous with δ, but it is nearly so, and the volume change is comparable with that observed for cerium. For appropriate choices of the parameters we can fit the lattice constant versus temperature curves of Pu-Ga alloys, where the parameters ΔE etc. are now assumed to depend on gallium concentration. The discontinuity in the lattice constant of unalloyed Pu is a consequence of the model.

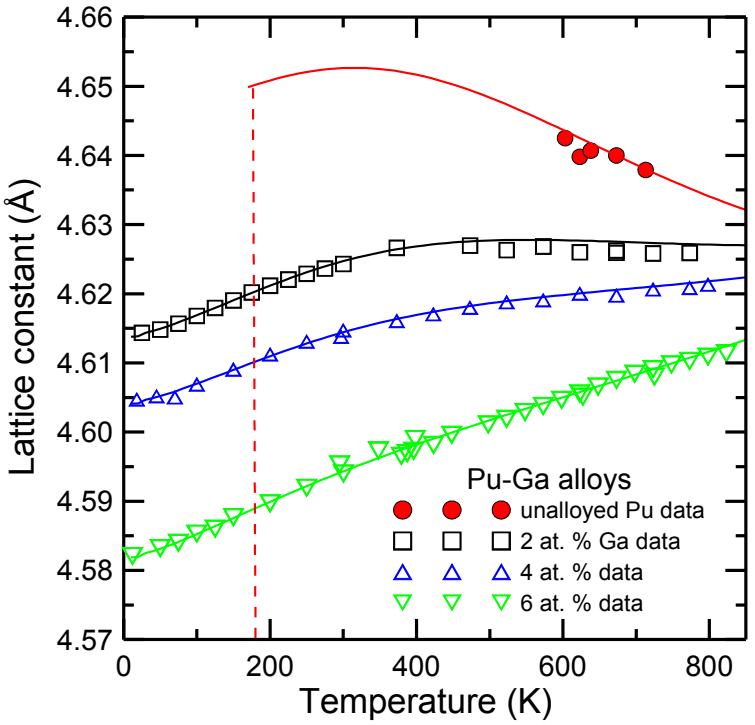

Fig.2. Lattice constants of δ-phase Pu-Ga alloys measured by neutron diffraction[2] (points) and their fit with the A-P model[1] (lines).

The energy of mixing, U is found to be ~2600 Cal/mole, equivalent to the energy of 1300K used in the invar model[2] of the lattice constants. We will give further details on the application of the A-P model to the problem of δ-phase stabilization.

This research was conducted under the auspices of the United States Department of Energy.

1. I. L. Aptekar' and Ye. G. Ponyatovskiy, Fiz. metal. metalloved. **25** 777 (1968) and Fiz. metal. metalloved. **25** 1049 (1968).
2. A. C. Lawson, J. A. Roberts, B. Martinez and J. W. Richardson, Jr., Phil. Mag. B **82** 1837 (2002).

Crystallographic anisotropy in the compression of some f-electron metals

Jagan Akella, Reed Patterson, Chantel Aracne-Ruddle
Lawrence Livermore National Laboratory, Livermore, CA 94550

The complex crystal and electronic structures of the f-electron metals give rise to interesting behavior when these materials are subjected to high pressures and temperatures. Several of these metals show a symmetry lowering transition, which is attributed to delocalization of the f-electrons. In recent high-pressure experiments on low symmetry α-Uranium, we have observed anisotropic compression. Although condensed matter physics theory has predicted Uranium should undergo a phase transition, there is to date no experimental evidence for this from studies up to 1 Mbar. We will present a detailed study of the metal, showing interesting variation in both axial ratios b/a and c/a with increasing pressure. This observation is in accord with the proposal made by Akella et al., (1990) that the orthorhombic axes in Uranium show "differential" compression. In addition, we will compare our data with that from Behan etal., 2003,.It is evident from our study that more detailed and careful studies are needed to ascertain whether other lighter actinides show similar anisotropic compression.

THE ASSESSMENT OF PHASE DIAGRAM OF THE U-ZR SYSTEM

A.L.Udovsky [*], D.A.Vasyliev[*], H.A.J. Oonk[†]

[*] A.A. Baikov Institute of Metallurgy and Material Sciences RAS, Moscow, Russia
[†] Chemical Thermodynamics Group, Faculty of Chemistry, Utrecht University, CD Utrecht, The Netherlands

In [1] we have calculated preliminarily different parts of phase diagram of the uranium - zirconium system, which have not included phase equilibria with $U_{0,333}Zr_{0,667}$ – base solid solution (δ – phase). In [2] we have calculated stabilities parameters for metastable ω–phases, which is isomorphic with δ – phase, for pure Zr and U as well as calculated phase diagram of the U-Zr system into 850 – 2100 K. It is necessary note that calculated stability parameters for metastable ω– and HCP-phase of the pure uranium to put in difficulties, since the δ – phase become metastable at temperature interval below 800 K. These calculated results were contradicted with experimental phase diagram.
In present report we have assessed stability parameters for metastable HCP – phase of pure uranium by using ab-initio pseudopotential calculated results for cohesive energies and bulk modulus for different phases of uranium at 0 K. We have obtained differences enthalpy and entropy (only vibrational part) between HCP- and BCC-phases of uranium as well as re-calculated interaction parameters for different phases of the U-Zr system.
We have applied a new minimization algorithm with the goal function (the generalized χ^2 – method [4]) to calculate phase diagrams and thermodynamic properties of binary system for solution of indirect task (calculation interaction parameters for BCC- phase, β–U – base solid solution, δ – phase solid solution, α–U – base solid solution, HCP-Zr – base solid solution) for the uranium - zirconium system. We have compared calculated as thermodynamic properties as function of composition and temperature for as phase diagram with experimental data obtained by different scientists, which have been assessment in the review [5].
As a result we have calculated phase diagram of the U-Zr system in temperature interval from 600 up to 2123 K, at that δ – phase become thermodynamic stable in temperature interval from temperature of peritectoid reaction up to 600 K and below.
As test we have compared predicted temperature dependencies of thermodynamic properties of alloys different compositions for the uranium - zirconium system [6], which we have not used in optimisation procedure, with experimental data.

Acknowledgements
The work supported by Dutch-Russian Program NWO-RFBR (Project № 047.011.2001.011) and Russian Federation Target Program "Integration" (Project B0056)

1 A.L.Udovsky, D.A.Vasilyev, M.Jacobs, H.A.J.Oonk. Program & Abstracts of CALPHAD XXXII, La Malbaie, Quebec, Canada, May 25-30, 2003, p. 122.(2003)
2 A.L.Udovsky, D.A.Vasilyev, H.A.J.Oonk. CALPHAD XXXIV, May 22-27, 2005, Maastricht, The Netherlands. Programme and Abstracts. Univ.Utrecht, p.77. (2005).
3 M.Freyss, Th.Petit, J.-P. Crocombette. J.of Nucl. Mater. V.347 p.44-51 (2005).
4. A.L.Udovsky. Russian Metally, № 2, p.136-157 (1990).
5. R.I. Sheldon, D.E. Peterson. The U-Zr (Uranium-Zirconium) System. Los Alamos National Laboratory. Bulletin of Alloys Phase Diagrams. Vol.10, № 2, 165-181 (1989).
6. Y.Takahashi, K.Yamamoto, T.Ohsato, H.Shimada, T. Terai. J. Nuclear Materials, v.167, p.147-151 (1989).

Lattice dynamics and thermodynamics of light actinides

J. Bouchet and G. Jomard

CEA-DAM, DPTA, Bruyères-le-Châtel, France

INTRODUCTION

Despite the general interest in *f*-electron elements, details about their phonon-dispersion relationships are very limited. Experimentally, this fact is due to the great difficulty of realizing such experiments. The most developed technique for the study of phonons, based on neutrons scattering, needs crystals large enough and isotopes with a small neutron absorption cross section. Lanthanides and actinides hardly satisfy these two conditions, not to mention the radioactivity of some of them. But recently, a new hope has emerged with several works, using inelastic x-ray scattering, mostly on U[1,2] and Pu[3]. Nevertheless all this experimental issues show that theoretical works are needed to tackle the *f* electrons systems elastic properties. Unfortunately these calculations are far from straightforward. The most important problem comes from the difficulty to treat correctly the *f*-electrons and the relativistic effects, as the spin-orbit coupling, needed in such heavy materials. To our knowledge there is only one *ab-initio* spectrum for a *f* element, which was obtained by Dai[4] on fcc plutonium.

Density functional perturbation theory (DFPT) is a well established tool for calculating the vibrational properties from first principles in the framework of the harmonic approximation. The crystal free energy is easily built by adding to the phonon contributions the 0 K isotherm, accessible to standard density functional theory (DFT) calculations. A step beyond the harmonic approximation can be made by allowing phonon frequencies to depend on crystal volume, the so-called quasiharmonic approximation. This approach has been shown to give an accurate description of the thermodynamic quantities of many bulk materials below the melting point. Taking into account the anharmonic effects through the volume dependence gives access to thermal expansion, phase transition and crystal stability.

RESULTS AND DISCUSSION

Here we apply the quasiharmonic approximation to the study of the thermal properties of Th metal, such as thermal expansion, bulk modulus or Debye temperature. In Fig.1 we display the phonon dispersion curves as calculated along several symmetry directions at zero pressure conditions (equilibrium volume). Our results[5] are in very good agreement with neutron-scattering data at ambient condition[6]. We have also calculated the phonons spectrum of Th in the bct structure. The results are presented in Fig.2., and compared to the phonon dispersions of fcc. The T_1 branch strongly softens during the phase transition in fcc and becomes imaginary near the Γ point, in contrary, the frequencies of this branch increase with pressure in bct. This observation indicates that the fcc structure at this pressure is dynamically unstable. The soft phonon mode near the zone center is expected for the second order transition between fcc and bct since both

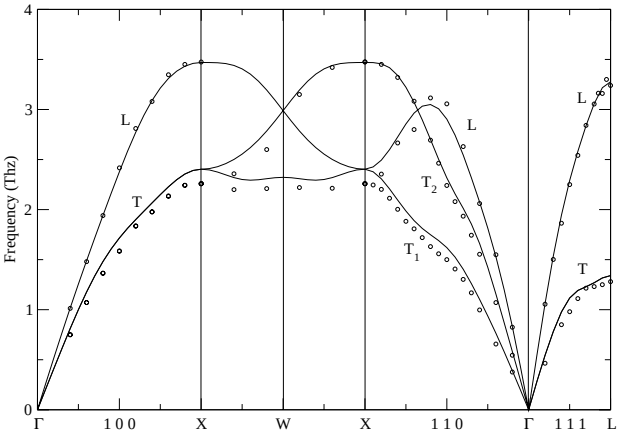

Fig 1: Calculated phonon dispersion curves for fcc Th at the lattice parameter corresponding to static equilibrium. Experimental neutron-scattering data are denoted by circles.

structures have one atom in their respective unit cell. We have also calculated thermodynamic properties of Th, as the linear thermal expansion or specific heats.

Using DFPT we have studied the pressure dependence of the elastic constants of the light actinides (Th, Pa, U, Np and Pu), the results help to understand the stability of the complex structures adopt by these metals. The phonons spectrum of U has also been calculated, this will shed light on the origin of charge density waves in this material and the nature of vibrational softening observed experimentally[1]. Phonons spectrum for fcc Pu obtained in GGA are compared to the DMFT results[4].

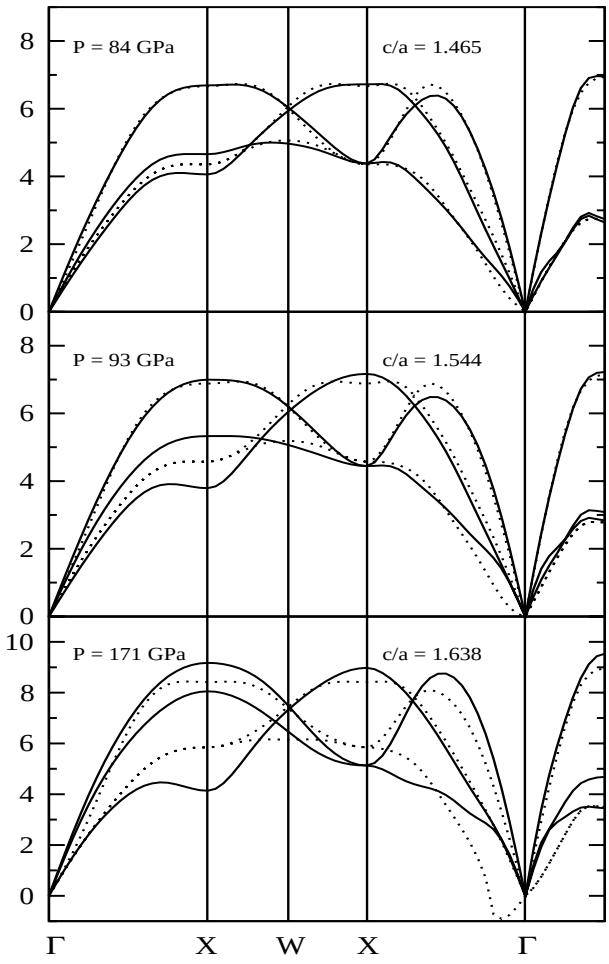

Calculated phonon dispersion curves for bct (solid lines) and fcc (dashed lines) Th for pressure and *c/a* ratios in the transition region. The symmetry directions are those of fcc.

This work will help to understand the effect of electronic structure on lattice dynamics in *f*-electron metals.

1 M. E. Manley, *et al.*, Phys Rev Lett **86**, (2001).
2 M. E. Manley, *et al.*, Phys Rev B **67**, (2003).
3 J. Wong , *et al.*, Science **301**, (2003).
4 X. Dai *et al.*, Science **300**, (2003).
5 J. Bouchet, F. Jollet and G. Zerah, submitted to Phys Rev B, cond-mat.
6 R.A. Reese, S.K. Sinha and D.T. Peterson, Phys Rev B **8**, (1973).

Contribution to the U-Ga Phase Diagram

Shai Salhov[a], Giora Kimmel[a], and M P. Dariel[b]

[a]Nuclear Research Centre - Negev, P O Box 9001, IL-84190 Beer-Sheva, Israel
[b]Department of Materials Engineering, Ben-Gurion University of the Negev,
P O Box 653, IL-84105 Beer-Sheva, Israel.

INTRODUCTION

Three Ga-rich intermetallic compounds, namely UGa_3, UGa_2 and U_2Ga_3 were reported by Buschow[1] in the U-Ga binary system. No information was provided regarding the U-rich side of the diagram, in particular, regarding the solubility of Ga in the three allotropic phases of uranium. Dariel et al.[2] have shown that the compound with the highest uranium content was actually U_3Ga_5, space group Cmcm, Pu_3Pd_5-type, and not the previously reported U_2Ga_3. In a series of studies, Dayan et al.[3-6] reported that U(Ga) β-phase alloys can be retained at room temperature where they eventually transform via a shear-like transformation into a mixture of α'-U(Ga), a monoclinic variant of orthorhombic α-U[3], and the U_3Ga_5 compound. In the present communication we provide further information regarding the uranium-rich side of the U-Ga diagram.

EXPERIMENTAL

Uranium metal lumps with 300 ppm metallic impurities and Ga, 99.95% pure were melted on the water cooled copper hearth of an arc furnace under a0.4 bar, gettered argon atmosphere and cast into split copper crucibles. The U(Ga) alloy samples, wrapped in thin Ta foils underwent various heat treatments in evacuated pyrex ampoules. The samples were characterized using conventional optical microscopy, XRD, SEM, DTA techniques.

The solubility limit of Ga in the high temperature γ and β-phases of uranium was determined by electron microprobe measurements on a U15at.%Ga sample. Since the U_5Ga_3 compound has the highest U content in the phase diagram, the U15at.%Ga samples were in all instances two-phase alloys containing some U_5Ga_3 compound and a U-rich solid solution. As had been shown previously[3-6], β-phase alloys can be retained at ambient temperature by quenching; moreover, γ-phase alloys also transform by fast quenching into β-phase alloys retained at room temperature. Lengthy anneal in the U-γ temperature range leads to segregation of the U_5Ga_3 compound particles at the grain boundaries of the Ga-saturated U_γ grains, as shown in Fig.1. Upon quenching from this γ-range, the interior of the well and clearly delineated U_γ grains undergoes a transformation into Ga-saturated U_β as shown unambiguously by x-ray diffraction. Composition measurements of the Ga content, using WDS, at the interior of these grains quenched from different temperatures in the U_γ range, allows determining the temperature dependence of solubility limit of Ga in U_γ phase.

After aging treatments carried out in the U_β temperature range, using a similar procedure as the above-described one, it was possible to determine the solubility limit of Ga in the U_β phase. The solubility of Ga in U_β and in U_γ is reported in Table I. Clearly the solubility in in U_β is much lower than in U_γ, nevertheless the latter when quenched to ambient temperature retains a greatly supersaturated in U_β structure. The rapid transformation of the U_γ solid solution into the in U_β solid solution during quenching suggests that it proceeds via a massive

transformation mechanism. The resulting 2-phase, $U_\beta + U_3Ga_5$, microstructure, shown in Fig. 1, is retained at room temperature and allows determining the composition dependence of the in U_β lattice parameters well beyond the solubility limit of Ga in the U_β phase, shown in Fig.2.

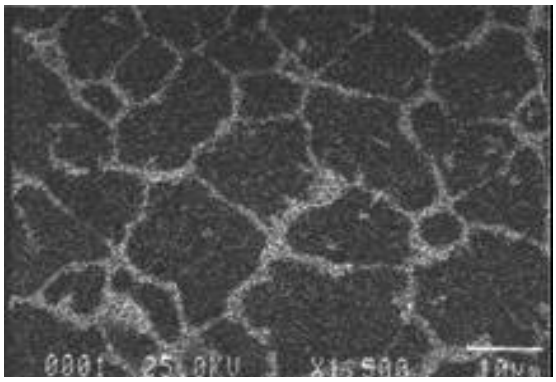

Fig.1. Ga distribution by $Ga_{K\alpha}$ mapping in a U-10at%Ga alloy annealed at 900°C and quenched to room temperature. The grain boundaries of the U_γ phase are clearly delineated by segregation of the U_3Ga_5 compound.

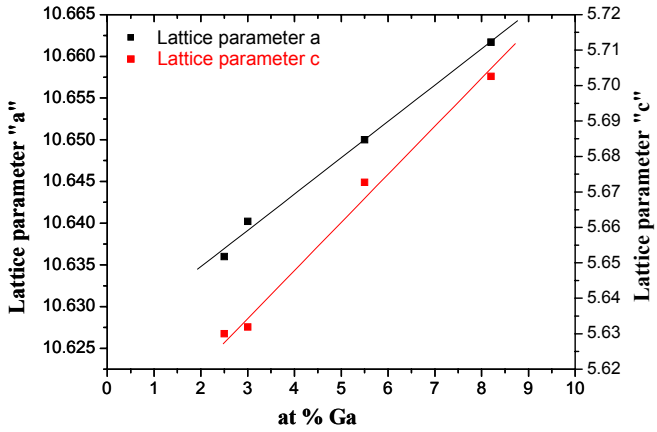

Fig.2. Composition dependence of the lattice parameters of the metastable U_β(Ga) phase at ambient temperature.

The kinetics of the greatly supersaturated U_β phase, quenched from the U_β temperature range are currently under investigation.

Table I.
Solubility limit of Ga in U_β and U_γ

matrix	Temp.	Solubility limit
γ-U	1000°C	8.5±0.1 at%
	900°C	5.7±0.1 at%
	800°C	2.5±0.4 at%
β-U	710°C	1.8±0.2 at%
	680°C	1.2±0.4 at%

REFERENCES

1. K. H. J. Buschow, J. Less-Common Met. 31, (1973) 165.
2. D. Dayan, G. Kimmel and M. P. Dariel, J. of Nuclear Materials 135 (1985) 40.
3. D. Dayan, M.P. Dariel and M. Dapht, J. Less-Common Metals 121, 399 (1986).
4. D. Dayan, H. Klimker and M.P. Dariel, Met. Trans. 19A, 909 (1988).
5. D. Dayan, M. Talianker and M.P. Dariel, Met. Trans. 20A, 1163 (1989).
6. D. Dayan, H. Klimker, M. Talianker and M.P. Dariel, Met. Trans. 21A, 2125 (1990).

Formation of Higher Chloride Complexes of Np(IV) and Pu(IV) in Water Stable Room Temperature Ionic Liquid [BuMeIm][Tf_2N]

S.I. Nikitenko[1], P. Moisy[2]

[1] CNAB - UMR5084, BP 120 Le Haut Vigneau, 33175 Gradignan Cedex, France,
[2] CEA Valrho, DEN/DRCP/SCPS, Bat.399, BP 17171, 30207 Bagnols sur Cèze Cedex, France

A UV/VIS/NIR spectroscopic study shows that in [BuMeIm][$(CF_3SO_2)_2N$] hydrophobic room-temperature ionic liquid solutions, $[BuMeIm]_2[AnCl_6]$ complexes, where $BuMeIm^+$ is 1-*n*-butyl-3-methylimidazolium and An(IV) is Np(IV) or Pu(IV), have an octahedral An(IV) environment similar to that observed in solid complexes.

Water has no influence on the absorption spectra of $AnCl_6^{2-}$ complexes, indicating their stability to hydrolysis in ionic liquid. Adding [BuMeIm]Cl modifies the UV/VIS/NIR absorption spectra of An(IV) in the ionic liquid and causes solids to precipitate. The solid-state reflectance spectra of the precipitates reveal considerable differences from the corresponding An(IV) hexachloro complexes. A voltammetric study indicates that $AnCl_6^{2-}$ complexes are electrochemically inert in [BuMeIm][$(CF_3SO_2)_2N$] at the glassy carbon working electrode.

By contrast, quasi-reversible electrochemical reduction An(IV)/An(III) and An(IV) oxidation are observed in ionic liquids in the presence of [BuMeIm]Cl. The oxidation wave of noncoordinated chloride ions interferes with the An(IV) oxidation waves. The spectroscopic and voltammetric data clearly indicate the formation of nonoctahedral An(IV) chloride complexes with a Cl^-/An(IV) ratio exceeding 6/1 in [BuMeIm][$(CF_3SO_2)_2N$] in excess chloride ions.

Study of Np Speciation in Citrate Medium

L. Bonin[1], E. Ansoborlo[1], C. Den Auwer[1], G. Cote[2], Ph. Moisy[1]

[1]CEA Vlarhô - DEN/DRCP/SCPS; BP 17171 - 30207 Bagnols sur Cèze, France
[2]ENSCP, UMR 7575; 11, rue Pierre et Marie Curie 75231 Paris Cedex 05, France

In the framework of the French Environmental Nuclear Toxicology program, additional experiments related to the decorporation of actinides are planned. The lack of information on the neptunium behavior within blood and the inefficiency of therapeutic treatments, led us to study the complexation of this element with basic anions. Within this purpose, the *in vitro* behavior of Np(IV) and Np(V) in simple media simulating biological media was studied.

This study was more specifically focused on the behavior of neptunium with citrate ion. In order to determine the speciation of this system, spectrophotometry was more particularly used. Concerning the complexation phenomenon, the existence of several complexes of Np(V) with various acido-basic forms of the citrate anion was observed; regarding Np(IV), complexes with Cit^{3-} have been observed.

From the quantitative study of these equilibriums, the values of the absolute constants for the complexation of Np(IV) and Np(V) with citrate were determined: $\log K_{4,0,1}=16.3\pm0.3$ and $\log K_{4,0,2}=15.0\pm0.3$, $\{\log K_{5,0,1}=2.5\pm0.2$, $\log K_{5,1,1}=1.6\pm0.5$, $\log K_{5,2,1}=1.2\pm0.2\}$ and $\{\log K_{5,0,2}=1.5\pm0.3$, $\log K_{5,1,2}=0.9\pm0.5$, $\log K_{5.2.2}=0.5\pm0.3\}$. From those constants, E-pH diagrams were built, allowing thermodynamical predictions for the behavior of neptunium in citrate medium. Those predictions are in accordance with the experimental instability of Np(V) in presence of citrate, and lead to the conclusion that this instability is due to Np(V) disproportionation.

Given the pH and the citrate concentration in blood plasma, the state of a Np-Cit system at room temperature has been inferred, as well as the speciation of Np in citrate solution before *in vivo* injection.